Influence of hydrogen and methane addition in laminar ammonia premixed flame on burning velocity, Lewis number and Markstein length

S. Zitouni, Pierre Brequigny, C. Mouna m-Rousselle

Influence of Hydrogen and Methane Addition in Laminar Ammonia Premixed Flame on Burning Velocity, Lewis Number and Markstein Length

Authors: Zitouni, S. (*), Brequigny P., Mounaïm-Rousselle C.,

Université Orléans, INSA-CVL, EA 4229 – PRISME, F-45072, France

(*) Corresponding Author Email:

seif-eddine.zitouni@univ-orleans.fr

Abstract:

The use of Ammonia (NH_3) and blends with either Methane (CH_4) or Hydrogen (H_2) obtained by in-situ NH_3 cracking, seem to be promising solutions to partially or fully decarbonise our energy systems. To strengthen understanding of fundamental combustion characteristics of these NH_3 blends, the outwardly propagating spherical flame configuration was employed to determine the flame speeds and Markstein lengths. The air/fuel mixtures were varied across a large range of compositions and equivalence ratios. In general addition of CH_4 or H_2 results in a linear and exponential increase in measured laminar burning velocity, respectively. Of the appraised mechanisms, Stagni and Okafor kinetics mechanisms yielded best agreement with NH_3/H_2 and NH_3/CH_4 flame speed measurements. With respect to measured Markstein length, for a fixed equivalence ratio, addition of CH_4 to NH_3 resulted in a linear reduction in stretch sensitivity for the tested conditions. For lean NH_3/H_2 flames, an initial decrease in Markstein length is observed up to 30 – 40% H_2 addition, at which point any further addition of H_2 results in an increase in Markstein Length, with a non-linear behaviour accentuated as conditions get leaner. Above stoichiometry similar stretch behaviour is observed to that of NH_3/CH_4. Different theoretical relationships between the Markstein length and Lewis Number were explored alongside effective Lewis Number formulations. For lean NH_3/H_2 mixtures, a diffusional based Lewis Number formulation yielded a favourable correlation, whilst a heat release model resulted in better agreement at richer conditions. For NH_3/CH_4 mixtures, a volumetric based Lewis Number formulation displayed best agreement for all evaluated equivalence ratios. For NH_3/H_2, changes in measured Markstein Length were demonstrated to potentially be the result of competing hydrodynamic and thermo-diffusive instabilities, with the influence of the thermo-diffusional instabilities reducing as the equivalence ratio increases. On the other hand, the addition of CH_4 to NH_3 results in the propensity of moderating hydrodynamic instabilities, resulting in a stabilising influence on the flame, reflected by increasing positive Markstein number values. Finally, a systematic analysis of the flame speed enhancements effects (kinetic, thermal, diffusive) of CH_4 and H_2 addition to NH_3 was undertaken. Augmented flame propagation of NH_3/CH_4 and NH_3/H_2 was demonstrated to be principally an Arrhenius effect, predominantly through the reduction of the associated activation energy.

Keywords: Ammonia-hydrogen, ammonia-methane, Laminar flame Speed, Lewis Number, Markstein Length

1. Introduction

The historical prevalence of hydrocarbon fuel usage to sustain our power and transport needs, and the associated greenhouse gas emissions produced, have resulted in important environmental and ecological adversities [1]. As such, in order to attain zero-carbon targets, the large-scale employment of renewable and carbon-free fuels within our energy systems is required to maintain a balanced trajectory between human development, progress and cohesion with the environment. In light of this context, Ammonia (NH_3) has emerged in recent years as an efficient zero-carbon hydrogen (H_2) carrier. Liquid NH_3 offers higher H_2 content than for example, ethanol, methanol and gasoline, in conjunction with exhibiting a higher volumetric energy density than that of liquid H_2 [2]. Due to NH_3 prevalent use in the agricultural industry, considerable storage and distribution infrastructure is already established [2]. Although NH_3 offers several advantages, there remains several practical combustion challenges, notably the control and reduction of pollutant emissions (NO_x and N_2O). Moreover, NH_3 exhibits slow burning velocities, often associated to low burning efficiency in engines, a narrow flammable range and high ignition energy, potentially yielding poor flame stabilisation and extinction characteristics resulting in local or global extinctions. To improve NH_3's combustion properties, blending NH_3 with methane (CH_4) (for a partial decarbonisation) or H_2 (from the possible 'in situ' cracking of ammonia) has been proposed, and has gained considerable recent attention, with comprehensive reviews of NH_3 related work undertaken [2], [3]. Successful demonstrations in both gas turbines [4]–[6] and internal combustion engines [7], [8] have been achieved at high temperatures and pressures. Nevertheless, studies remain limited, as such there seems to be a practical necessity to develop and strengthen understanding of fundamental combustion characteristics of blends containing NH_3, ultimately leading to the development of combustors offering greater flame stability and reduced pollutant emissions.

The unstretched laminar burning velocity (S_L^0), is one main fundamental physio-chemical property of any premixed air-fuel mixture, reflecting both the combustion process and mixture reactivity. As such, S_L^0 is a key parameter helping understand premixed operational instabilities, notably flashback, blow-off or extinction, and a central step in turbulent flame modelling [9]. Variations in fuel composition inherently introduce changes in transport and chemical properties, in turn influencing witnessed burning and reactivity characteristics of the fuel mixture. The Lewis number (Le), defined as the ratio of thermal to mass diffusivity of the deficient reactant, details the transport mechanisms of various species across the flame front [9]. Early experimental investigations [10], [11] , supported by the development of asymptotic theories [12], [13], underline that preferential diffusion (i.e. Le deviating from unity), can strongly influence the burning rates of stretched flames – which undergo the combined effects of strain, curvature, and flame motion. Flames with Le > 1 exhibit greater relative thermal diffusivity, displaying a reduction in burning rate with increased stretch, due to heat loss to the unburned reactant. Conversely, flames with Le < 1 show a relative acceleration with increasing stretch [9]. The burnt gas Markstein length (L_b) is a measurable parameter which characterises the influence of Le on the flame response to the stretch rate. The Markstein number (Ma), defined as L_b divided by the laminar flame thickness (δ_L) – is an indicator of the propensity of a combustion system to be or not influenced by thermo-acoustic instability, and thus of interest to study [14].

Recent experimental studies have investigated S_L^0 and L_b characteristics of NH_3/air flames, notably by Hayakawa et al. [15], at atmospheric and 0.5 MPa of initial ambient pressure, and Kanoshima et al. [16], expanded on that work to include the influence of initial ambient temperature (400-500 K). Results from these studies underline that S_L^0 peaks at an equivalence ratio (ϕ) of ≈ 1.1, with an increase in pressure and temperature ensuing a decrease and increase

in S_L^0, respectively. With respect to L_b, NH_3/air flames display an increasing L_b with increasing ϕ, a similar trend to that of CH_4/air and H_2/air flames. It is noted that at normal temperature and pressure conditions (T=298K, P=0.1MPa) lean NH_3 flames exhibit negative L_b, with positive values recorded under rich conditions. Furthermore, L_b is observed to decrease with a rise in pressure and temperature, analogous behaviour to that of the flame thickness.

Okafor et al. [17], [18], investigated the influence of NH_3 on CH_4 based flames (up to ≈ 52% NH_3 by vol.%) across a wide range of ϕ and pressures (0.1 – 0.5 MPa), highlighting that S_L^0 decreases with increasing NH_3 fraction and pressure, developing a detailed and reduced kinetic mechanism. Experimental results of Shu et al. [19] on NH_3/CH_4 flames (298 K, 0.1 MPa), demonstrated similar tendency but with a uniform decrease in the flame flammability limits with NH_3 increase. They also highlighted the important role played by the H and OH radicals in NH_3/CH_4 flame propagation. In relation to flame stretch sensitivity of CH_4/NH_3 flames, Okafor et al. [17] emphasize the shift from a linear to a non-linear flame speed-stretch rate relationship exhibited with increasing ϕ and NH_3 fraction. It should be noted that this is unusual for fuels displaying Le values close to 1 (as is the case for pure CH_4 and NH_3), with this behaviour mainly attributed to an increase in the preheating zone thickness.

Lee et al. [20], [21] and more recently, Ichikawa et al. [22] and Lhuillier et al. [23] investigated the influence of H_2 upon NH_3 based flames. Ichikawa et al., demonstrated that at stoichiometric conditions (ϕ=1), S_L^0 increases non-linearly with increasing H_2 fraction, and decreases with increasing pressure. Lhuillier et al. reported an exponential increase in S_L^0 upon addition of H_2 at various initial conditions (298-473K, ϕ = 0.8 – 1.4, H_2 = 60% vol. max). With respect to the flame stretch sensitivity, Ichikawa et al.[22] reported a non-monotonic variation, with an initial substantial decrease in L_b with increasing H_2, prior to a minor increase in L_b upon further H_2 addition. Interestingly, this stretch behaviour dampens at higher pressures, with minimal variation in recorded L_b of NH_3 flames upon H_2 enrichment. Noteworthily, similar stretch-related non-monotonic trends have been observed for lean CH_4/H_2 flames [24].

The importance of flame stretch sensitivity and Le goes clearly beyond the laminar flame regime. Lipatnikov and Chomiak [25], in their extensive review of molecular transport effects on flame propagation, highlighted that preferential diffusional instabilities affect both weak and strong turbulent combustion. The influence of Le on turbulent flames has been reported in the course of experimental studies [26]–[28] as well as in direct numerical simulations [29], [30]. Although limited in scale, emerging studies focusing on turbulence-flame interaction for NH_3 and its blends with either H_2 and CH_4 underlined the potential role of preferential-diffusion and flame-stretch interaction upon turbulent flame characteristics. For example, Ichimura et al. [31] investigated NH_3/air flames at various turbulent intensities, underlining that although S_L^0 of NH_3/air is greatest at ϕ ≈ 1.1, lean mixtures exhibited better resistance to turbulence induced extinction than richer conditions, due to the potential thermo-diffusive accelerating effects of lean NH_3/air mixtures, displaying Le < 1. Similarly, Lhuillier et al. [8] investigated NH_3/H_2 and NH_3/CH_4 (15% vol. of H_2 or CH_4) turbulent flame propagation under engine related operating conditions (445K, 0.54 MPa). They reported a decreasing and increasing turbulent to laminar flame speed ratio upon CH_4 and H_2 addition, respectively, induced by the different thermo-diffusive properties and stretch-related behaviour of these ammonia blends.

Clearly, although emerging, the experimental study on the addition of H_2 or CH_4 to NH_3-based flames remains scarce. Furthermore, recent turbulent combustion experiments underlined the potential influence of preferential-diffusional instabilities upon NH_3-based flames [8], [31], [32], hence, the aim of this work is to investigate in detail the influence of Le change on flame behaviour. NH_3/CH_4 and NH_3/H_2 mixtures were varied across a large range of blend composition and

equivalence ratio, representative of the prospective demands of fuel-flexible combustors widely employed for power generation. The addition of either CH_4 or H_2 to a given NH_3/air mixture increases flame temperature, reactivity, mixture flame speed but changes the thermo-diffusive behaviour, which is studied in-detail throughout this work.

2. Experimental set-up and specifications

Laminar flame speed measurements were performed using a constant-volume spherical vessel. Details of the apparatus and post-processing techniques can be found in [33], updated for NH_3 specifications in [23], and thus only a brief summary is presented herein. The spherical vessel is equipped with four orthogonal 70 mm quartz viewing windows and has a nominal internal volume of 4.2 L. Thermal mass flow controllers (Brooks 5850S (± 1%)) were employed to introduce the reactants into the vessel. Mole fractions of all species were determined as a function of temperature (T), initial pressure (P) and fuel-air equivalence ratio. A piezo-electric pressure transducer and a type-K thermocouple were employed to check respectively the pressure and temperature prior to ignition. The maximum deviation between the effective initial pressure inside the chamber and the required initial pressure was no more than 1%. A vacuum-pump was used to empty the combustion chamber twice between tests ensuring a residual pressure of no more than 0.009 bar, with the remaining air compensated within the equivalence ratio calculation. Pre-mixing was achieved using an internal fan. A capacitor-discharge ignition was achieved via fine tungsten electrodes mounted at 90° to the measurement plane. After quiescence is attained, simultaneous TTL signal to the data-acquisition and ignition systems trigger the experiments. High speed Schlieren imaging of flame propagation was accomplished using a CMOS high speed camera (Phantom V1210) set to a suitable frame capture rate (3000 – 12000 fps), facilitating a spatial resolution of ~0.10 mm per pixel. Edge-detection algorithms written in a bespoke MATLAB script were employed to calculate flame propagation rates. A minimum of 3 to 5 repeats were conducted per experimental condition.

3. Experimental specifications and theory

Measurements were performed at initial conditions of 298 K (± 3 K) and 0.1 MPa (± 1 x 10^{-3} MPa), with high-purity fuels (NH_3 (99.95%), CH_4 (>99.995%) and H_2 (99.999%)) and dry-zero compressed air (AirLiquide, 20.9% O_2). To investigate the influence of CH_4 and H_2 on NH_3 flame speed and stretch-related behaviour, molar ratios were varied form 0 – 100% for CH_4; and 0 – 80% for H_2, in incremental steps across a wide range of equivalence ratios (ϕ= 0.7 – 1.2 and 0.6 – 1.4 respectively), with Table 1 summarising the experimental conditions.

Table 1: Experimental conditions ; T_u = 298 K (± 3 K), P_u = 0.1 MPa (± 1 x 10^{-3} MPa).

Equivalence Ratio (ϕ)	Percentage of Fuel in NH_3 (vol.%)	
	CH_4	H_2
0.6	/	20,30,40,50,60,80
0.7	20,30,40,50,60,80,100	/
0.8	0,10,20,30,40,50,60,80,100	0,10,20,30,40,50,60,80
0.9	0,10,20,30,40,50,60,80,100	0,10,20,30,40,50,60,80
1.0	0,10,20,30,40,50,60,80,100	0,10,20,30,40,50,60,80
1.1	0,10,20,30,40,50,60,80,100	0,10,20,30,40,50,60,80

1.2	0,10,20,30,40,50,60,80,100	0,10,20,30,40,50,60,80
1.4	/	20,30,40,50,60,80

Schlieren images were undertaken as in [17], [23], [34], with the shadowed edge considered as the burnt gas isotherm, which as discussed by Giannakopoulos et al. [35], is critical for characterising the influence of flame stretch. The laminar burning velocity and L_b relative to the burnt side were experimentally determined employing the same procedure as in previous studies [34], [36]. For an outwardly spherically propagating flame, the stretched flame speed (S_b) is expressed as the temporal derivative of the Schlieren flame radius (r_{sch}) as in Equation 1:

$$S_b = \frac{dr_{sch}}{dt} \quad (1)$$

The flame stretch rate (K) is defined as the change in flame area (A) gradient and calculated for a propagating spherical flame as shown in Equation 2:

$$K = \frac{1}{A} \cdot \frac{dA}{dt} = \frac{2}{r_{sch}} \cdot \frac{dr_{sch}}{dt} \quad (2)$$

Various correlations between S_b and K have been proposed, allowing the estimation of the unstretched flame speed (S_b^0). Two methodologies are employed in this study. The first model is based upon the assumption of large flame radii, considering both the effects of thermal expansion and Le, as in Equation 3 [37], which illustrates that the flame curvature ($\kappa_{curv}=2/r_f$) and S_b vary linearly, hence allowing the evaluation of S_b^0 and L_b from the linear extrapolation of S_b and K [38], [39]:

$$S_b = S_b^0 - L_b \cdot K = S_b^0 - S_b^0 \cdot L_b \cdot \frac{2}{r_f} \quad (3)$$

This methodology will be referenced herein as Linear Model based on Curvature (LMC). The second extrapolation method, attributed to Kelley and Law [40], is a non-linear model that allows for arbitrary Le and takes into account the deviations in adiabatic and planar assumptions, prominent in flames which are heavily influenced by stretch such as lean H_2-based flames. This non-linear model is expressed as in Equation 4:

$$\left(\frac{S_b}{S_b^0}\right) \cdot In\left(\frac{S_b}{S_b^0}\right)^2 = -\frac{2 \cdot L_b \cdot K}{S_b^0} \quad (4)$$

This model has been used frequently over the last decade, improving accuracy [39], [41], and will be referenced here as the Non-Linear Model based on Stretch (NMS).

Chen [38] underlined that the accuracy of different extrapolation techniques is related to the Le of the fuel-air mixture. Chen [38] demonstrated that it is preferable to employ LMC for mixtures exhibiting Le > 1 (i.e. positive L_b) and NMS for Le < 1 (i.e. negative L_b), due to the non-linear relationship between S_b and K; with these recommendations adopted in this study. Moreover, Wu et al. [39], quantified the uncertainty in extrapolation through the limitation of exploitable data range in relation to Markstein and Karlovitz numbers ($Ma_{lin}Ka_{mid}$); all data presented in this work fall within the recommended values of -0.05 – 0.15 range.

Irrespective of the extrapolation methodology employed, to obtain representative values of laminar flame speed, the burned gas expansion factor has to be used as $S_L^0 = S_b^0 \cdot (\rho_b/\rho_u)$ with equilibrium densities calculated using CHEMKIN-Pro, using Stagni et al. [42] and Okafor et al. [18]

kinetics reaction mechanisms, for NH_3/H_2 and NH_3/CH_4, respectively. The selection of these mechanisms is discussed later in section 5.2.

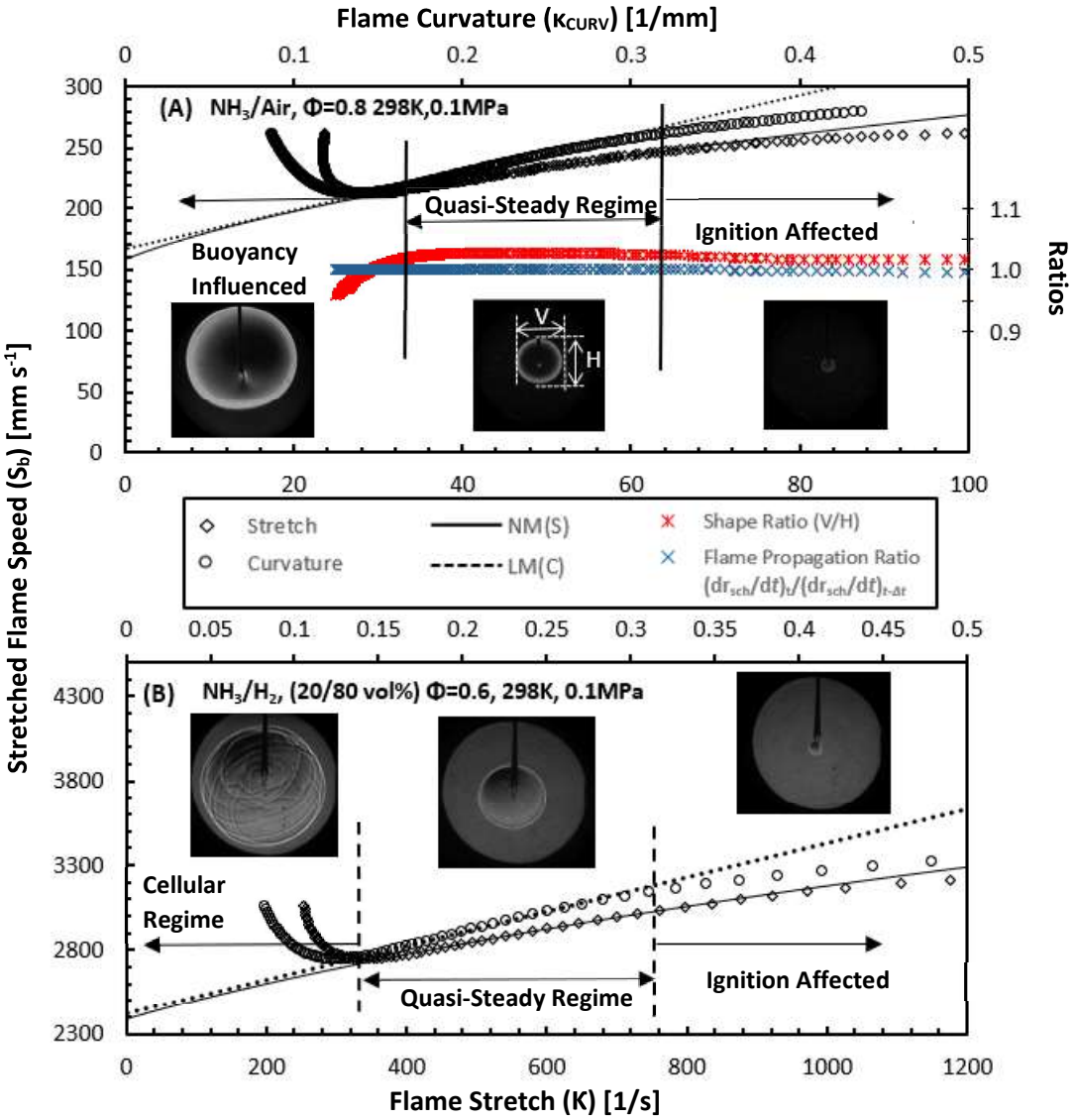

Fig. 1 – Stretched flame speed vs stretch rate (K) and curvature (κ_{CURV}) for (a) pure NH_3/air and (b) NH_3/H_2 (20/80 vol.%) (T_u – 298 K, P – 0.1 MPa)

Limits were set on the range of exploitable radii to minimise the influence of the spark, the buoyancy or the cellularity, and the confinement during the flame growth, ensuring measurements were restricted within the quasi-steady regime. Bradley et al. [43] suggest a spark affected radius up to 6 mm for CH_4/air flames, however Chen et al. [44] demonstrate this critical radius value to be dependent of Le. For all data presented here, 9 mm was chosen as the minimum radius, with preliminary investigation demonstrating minimal variation in results derived from data above 7 mm. To limit pressure effects a maximum radius of 25 mm was considered, within the 30% of chamber radius as proposed by Burke et al. [45] and satisfying $r_{sch}/(3V/4\pi)^{1/3} < 25\%$ as recommended by Chen [46]. Extrapolation methods used to yield flame speed and the corresponding L_b rely on a sufficiently large stable quasi-steady flame propagation regime. In the present study, pure NH_3/air flames, or blends containing less than 10% of CH_4 or H_2 (vol.%) at leanest and richest conditions were observed to be heavily influenced by the buoyancy, a consequence of their very low burning rate. As a result these flames were observed to lose sphericity, morphing in an ellipsoidal expanding flame, as noted

by Hayakawa et al. [15] and Chen et al. [47] for identical initial conditions (298 K, 0.1 MPa). For such flames, the methodology proposed by Hayakawa et al. [15] in delimiting the transition between ignition influenced, quasi-steady and buoyancy influenced propagation regimes was followed. The aforementioned regimes are determined based upon the flame shape and propagation ratio, defined as the vertical and horizontal radius of the flame ($r_{sch,V}/r_{sch,H}$) and $(dr_{sch}/dt)_t/(dr_{sch}/dt)_{t-\Delta t}$ (where dr_{sch}/dt denoting the flame propagation speed at time t), respectively. Figure 1.a illustrates the change in flame shape ratio and moving average of the flame propagation ratio against stretch for a lean NH_3/air flame (ϕ=0.80); with the relationship of stretched flame speed with stretch and curvature superimposed. As can be seen in Fig 1.a, a quasi-steady propagation regime is clearly identifiable, as such the point at which the flame shape ratio considerably changed was taken to represent the maximum flame radius limit. It should be noted that the upward motion of the growing flame kernel does not yield a significant influence upon the propagation speed, since change in the stretched flame speed still maintained proportionality to both flame-stretch and curvature until the transition point was attained. Under other conditions, minor modifications in useable flame radius selection were also required due to known instability issues associated with lean combustion of H_2-containing fuels. Lean H_2-based flames are particularly unstable with regard to diffusive effects, a consequence of their low Le (Le << 1), resulting in flame acceleration at low stretch and curvature rates [48], as illustrated in Figure 1.b, with an example case of a lean NH_3/H_2 (20/80 vol.%, ϕ=0.6) flame. Under the tested experimental conditions, it was noted that no flames developed a cellular surface composed of cells of comparable size. However, large cracks of a permanent nature appeared at leanest conditions (ϕ=0.60) for flames containing ≥ 40% H_2, with further H_2 enrichment enhancing surface cracking, as illustrated in Fig. 2. As underlined by Jomaas et al. [49], these large-scale cracks are most probably the result of large-amplitude initial disturbances, most probably triggered by the ignition event, and not a consequence of preferential diffusion. Nevertheless, using a suitably fast frame capture rate, a minimum of 30 acquired radii was obtained even for the fastest flames, from which flame speed data were estimated.

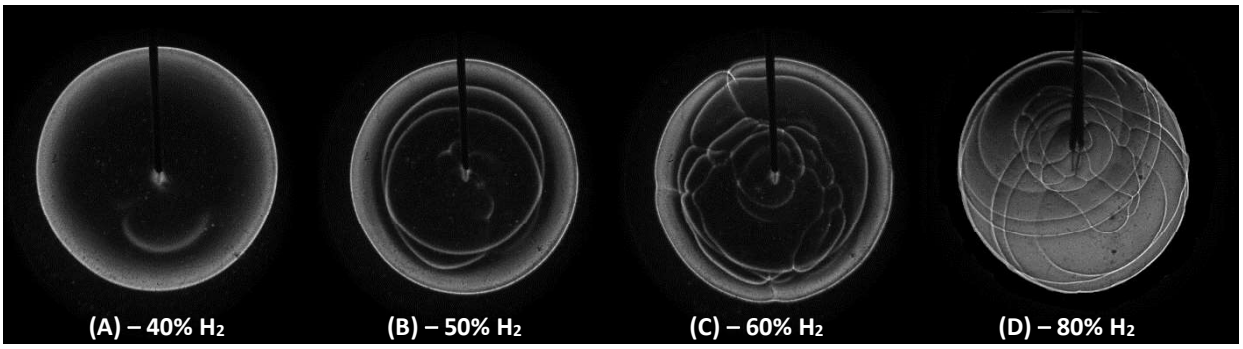

Figure 2 – Schlieren images illustrating the development of flame surface cracking as a function of H_2 fraction for NH_3/H_2 flames (T_u – 298 K, P – 0.1 MPa, ϕ=0.60)

The measurements of laminar flame speed are an essential step in order to improve the accuracy of reaction mechanisms [46]. Therefore, the quantification of the measurement uncertainties is required. For this study, uncertainty quantification relies upon the methods outlined by Moffat [50], employing a combination of the experimental facility specifications and accuracy of the processing techniques employed. It should be noted that the uncertainty is quantified for the unstretched flame speed (S_b^0), and not for S_L^0, since this is the parameter measured, here named as $U_{S_b^0}$.The total uncertainty estimate is given by Equation 5, where $B_{S_b^0}$ represents the total bias uncertainty, $t_{M\text{-}1.95}$ the student's value at 95% confidence interval and M-1 degrees of freedom, $\sigma_{S_b^0}$ the standard deviation of the repeated experiments, and M the number of experimental repeats at each condition;

$$U_{S_b^0} = \sqrt{B_{S_b^0}^2 + \left(\frac{t_{M-1,95}\sigma_{S_b^0}}{\sqrt{M}}\right)^2} \quad (5)$$

The total bias uncertainty, given by Equation 6, relating changes in S_b^0 with respect to an independent influential variable, (v_i, i.e. temperature, ambient pressure, ϕ, optical system, gas mixture quality) and the fixed error linked to that variable, y_i,

$$B_{S_b^0} = \sqrt{\sum_{i=1}^{n} \left(\frac{\partial S_b^0(v_i)}{\partial v_i} y_i\right)^2} \quad (6)$$

In order to determine $B_{S_b^0}$ by Equation 6, the relationships between S_b^0 and each independent variable must be established. As applied in [7], the potential changes in S_b^0 from several parameters are calculated as a function of ϕ; such as temperature (±3 K) and pressure (±1 x 10^{-3} MPa) by using data modelling with CHEMKIN-PRO. Uncertainty resulting from the optical system was evaluated from the summated fractional error of both the spatial resolution of the system (±0.05/25mm) and camera (± 1.5-7.5/3000-15000 fps). Losses due to radiation influence measured flame burning speed, through the combined effect on the flame propagation itself and the calculated density ratio, with radiation-induced uncertainty particularly significant for slow propagating flames (< 12 cm s^{-1}) [51]. Lhuillier et al. [7] investigated the dependence of errors resulting from radiation for NH_3/air flames, concluding that the correlation proposed by Yu et al. [51] was applicable, with this recommendation adopted for this study. Accordingly, error bars on all subsequent plots illustrating laminar flame speed measurements (S_L^0) are derived from Equation 5 and 6, with the error for $U_{S_b^0}$ scaled with respect to the density ratio.

4. Evaluation of Fundamental Parameters

Chen and Ju [38], [44] and Matalon and Bechtold [52], have proposed theoretical relationships relating the Markstein length (L_b) and Lewis Number (Le), requiring the evaluation of various fundamental flame parameters. The Zel'dovich number, was evaluated using the expression $Ze = (E_a/R_u) \cdot [(T_{ad} - T_u)/(T_{ad}^2)]$ with R_u the universal gas constant, T_u and T_{ad}, the temperature of the unburnt mixture and the adiabatic flame temperature, respectively. The activation energy, E_a, is defined as the slope of the mass burning flux (m^0) and the inverse adiabatic flame temperature at constant ϕ and pressure, empirically determined using the expression $E_a = -2R\partial[(m^0)]/[1/T_{ad}]$, where the mass burning flux can be replaced by $m^0 = (\rho_u \cdot S_L^0)$, as recommended by Egolfopoulos and Law [53]. It should be noted that this method is only valid for sufficiently off-stoichiometric conditions, with interpolation required for E_a values for mixtures near stoichiometry [54]. For the flame thickness, two definitions can be considered [9]. The first, commonly termed as the kinetic (or diffusion) flame thickness (δ_K), is defined as $\delta_K = \lambda/(\rho_u \cdot c_p \cdot S_L^0)$, where λ represents the thermal conductivity and c_p the specific heat at constant pressure. The second, referenced as the 'gradient' flame thickness (δ_G) can be expressed as $\delta_G = (T_{ad} - T_u)/(dT/dx)_{max}$. The 'kinetic' flame thickness is consistent with the approach detailed by Chen [38], [44] whilst the 'gradient' flame thickness is consistent with the method detailed by Bechtold and Matalon [52] and employed accordingly in the derivations Le and L_b as defined by the given authors.

4.1 Relationships of Le and L_b

For the purpose of this work, the relationships relating Le to L_b, proposed by Chen [38], [44] and Matalon and Bechtold [52] are considered. The first formulation based on spherically expanding flames is derived from the analytical developments done by Chen and Ju, and then used by Bouvet et al. [55], Lapalme et al. [56] and Zitouni et al. [34] in their studies on preferential-diffusion effects upon

multi-component fuels. This estimate of Le is referenced herein as Le_{CHEN} and can be expressed per Equation 7:

$$Le_{CHEN} = \left[\frac{L_b}{\sigma \cdot \delta_K} - \frac{Ze}{2}\right]^{-1}\left[1 - \frac{Ze}{2}\right] \quad (7)$$

With $\sigma = \rho_b/\rho_u$, the expansion ratio. From Equation 7, the retrieval of L_b is possible as in Equation (8).

$$L_{b-CHEN} = \left[\frac{1}{Le} - \left(\frac{Ze}{2}\right)\left(\frac{1}{Le} - 1\right)\right]\sigma \cdot \delta_L \quad (8)$$

A second formulation by Bechtold and Matalon, was derived from theoretical analysis on the dependence of L_b on stoichiometry. This formulation was considered by Jomaas et al. [49] in the case of acetylene (C_2H_2), Lapalme et al. [56] for H_2/CO and Zitouni et al. [34], for CH_4 blended with H_2 or C_3H_8. This estimate is denoted in following as Le_{BM}, and is expressed per Equation 9:

$$Le_{BM} = 1 + \left[\frac{L_b}{\delta_G} - \frac{2}{\sqrt{\sigma}+1}\right]\left[\frac{2 \cdot Ze}{\sigma - 1}\left\{\sqrt{\sigma} - 1 - In\left(\frac{1}{2}\left(\sqrt{\sigma}+1\right)\right)\right\}\right]^{-1} \quad (9)$$

Which provides $L_{b\text{-}BM}$ as per Equation 10:

$$L_{b-BM} = \delta_G\left[\frac{\gamma_1}{\sigma} - \left\{\frac{Ze}{2}(Le-1)\gamma_2\right\}\right] \quad (10)$$

where γ_1 and γ_2 are functions of the expansion ratio given in Equation 11:

$$\gamma_1 = \frac{2 \cdot \sigma}{\left(\sqrt{\sigma}+1\right)}\ ; \quad \gamma_2 = \left[\frac{4}{\sigma - 1}\right]\left[\sqrt{\sigma} - 1 - In\left(\frac{\sqrt{\sigma}+1}{2}\right)\right] \quad (11)$$

4.2 Lewis Number evaluation of multi-component fuels

Whilst the definition of the Lewis Number for single-fuel mixtures is relatively straightforward, no clear consensus on the correct formulation of Le for multi-fuel mixtures seems to exist [55]; the challenge arising from the fact that the diffusivity of each fuel must be considered. This is particularly applicable when the transport diffusion mechanisms are different as is the case for H_2, NH_3 or any alkanes. Bouvet et al. [55] identified three 'effective' Le formulations. The first formulation is based upon a volumetric fraction weighted average, resulting from Muppala et al. [26] computational study of turbulent $CH_4 - H_2/C_3H_8$ flames. At low-turbulence, this formulation results in reasonable agreement between modelled and experimental burning velocities; whilst at higher turbulent intensity modelled burning rates significantly underpredicted measurements. This volume weighted formulation will be referenced in this work as Le_V, and is expressed per Equation 12:

$$Le_V = \sum_{i=1}^{f} x_i \cdot Le_i \quad (12)$$

where x_i, is the fuel volumetric or mol fraction of the species i.

The second Le formulation is derived by Law et al. [57] from the asymptotic analysis of high pressure H_2/C_3H_8 laminar spherical flames. This formulation has been widely employed to discuss the thermo-diffusive behaviour of mostly binary and tertiary blends of hydrocarbons and hydrogen [27], [58]. This formulation is based upon the weighted average of the fuels' nondimensional heat release (q_i), referenced in this work as Le_H, and expressed as per Equation 13:

$$Le_H = 1 + \frac{\sum_{i=1}^{f} q_i (Le_i - 1)}{\sum_{i=1}^{f} q_i} \quad (13a)$$

where

$$q_i = \frac{Q \cdot Y_{i,unburnt}}{c_p \cdot T_u} \quad (13b)$$

with Q representing the overall heat of reaction, Y_i, the mass fraction of species i.

The third one is related to the work conducted by Dinkelacker et al. [27] on lean H_2/CH_4 flames. It is assumed that if the flame curvature is dominant, then the local enrichment of the most diffusive fuel at the flames leading edge can be expected. This overall reaction-rate enhancement is translated into a volumetric-weighted average of the fuel diffusivities. This diffusion weighted formulation will be referenced in this work as Le_D, and expressed per Equation 14:

$$Le_D = \frac{D_T}{\sum_{I=1}^{F} x_i \cdot D_{ij}} \quad (14)$$

where D_T is the mixture's thermal diffusivity and D_{ij} are the binary mass diffusion coefficients. Several methods have been proposed to estimate the binary mass diffusion coefficients at moderate ambient pressure (<10 bar), with empirical constants based upon experimental data [59]. The method of Wilke as well as that of Hirschfelder, Bird and Spot, detailed in [59], is used in this study. Once the binary coefficients for the combinations of gases are estimated, an effective formulation of the deficient species in the mixture must be designated. For lean fuel-air mixtures, the deficient reactant is scarce compared to the surrounding N_2 [9]. For that reason, D_{ij} is taken as the fuel, '*i*', diffusing into N_2 (denoted with the subscript j). This may hold true for hydrocarbons due to their high molar fuel-air ratio, but not for fuels that have low molar fuel-air ratio such as H_2, as underlined by Lapalme et al. [56]. Thus, as proposed by Wilke [60], the mixture-averaged coefficient of mass diffusion ($D_{i,mix}$) into the mixture was employed as defined in Equation 15:

$$D_{i,mix} = (1 - Y_{i.mix}) \left(\sum_{\substack{s=1 \\ s \neq i}}^{N} \frac{X_s}{D_{is}} \right)^{-1} \quad (15)$$

where Y is the mass fraction of the species '*i*' and '*X*' the molar fraction of each species '*s*' in the mixture; with details of the method available in [59]. In order to ensure the correct application of the method, the binary diffusion coefficients calculated in this work were compared with values generated employing the STANJAN transport calculator [61]. Differences were no greater than ±3% for binary blends containing CH_4, NH_3, O_2 and N_2, and up to 10% in the presence of H_2, in agreement with expected deviations [59], and thus the derived coefficients are deemed suitable for the purpose of this study.

5. Results and Discussion

5.1 Pure Fuels

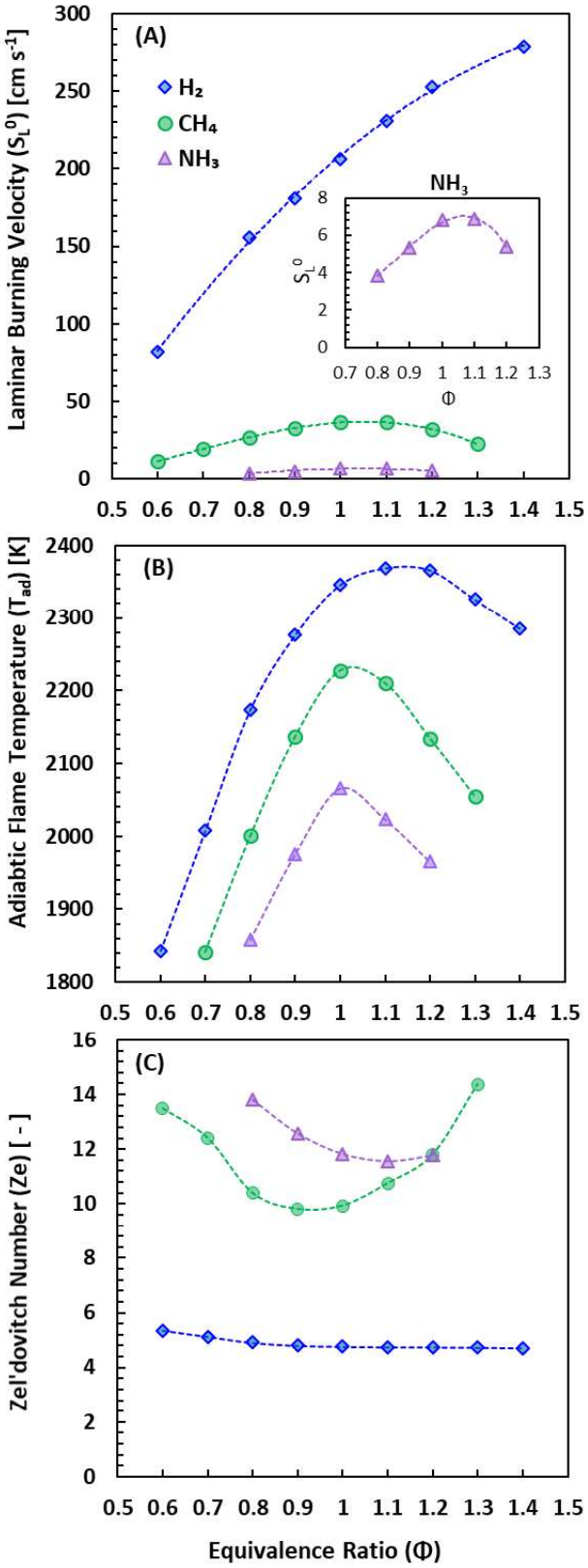

Figure 3 – Comparison of (a) laminar burning velocity, (b) Adiabatic flame temperature and (c) Zel'dovich number as a function of equivalence ratio for pure NH_3, CH_4, and H_2/air flames at 298 K & 0.1 MPa. S_L^0 data for H_2/air flames from [62].

The measured S_L^0 for the pure NH_3, CH_4 and H_2 /air flames are compared in Figure 3.a. NH_3/air flames display the slowest flame propagation rates, five to six times slower than those of CH_4/air flames; with a similar difference in flame speed magnitude between H_2/air and CH_4/air flames at stoichiometric conditions. It should be noted that the thermal diffusivity of these fuels decreases in the order of H_2, CH_4 and NH_3, analogous to the decreasing S_L^0 values. The adiabatic flame temperature and activation energy (represented by Ze) with respect to ϕ for the aforementioned pure fuels is illustrated in Fig. 3 (b) and (c), respectively. For CH_4 (and in general C_{1-4} alkanes), S_L^0 and T_{ad} peak at conditions slightly richer than stoichiometric conditions (ϕ~1.05 – 1.10), underlining the sensitivity of the flame propagation to the flame temperature. The fact that the minimum activation energy is located at similar conditions (ϕ~0.9), underlines the dictating influence of the flame temperature on the global activation energy. Due to flames temperatures peaking at around stoichiometric conditions, temperature-sensitive branching reactions are facilitated, thereby leading to overall faster reactions and reduced global activation energies, as highlighted by Jomaas et al. [49]. With respect to H_2, a similar trend in Ze is observed when plotted upon a much larger range of ϕ than that illustrated in Fig. 3 (c). Viewed across the total flammability range of H_2 a similar parabolic relationship analogous to that exhibited by CH_4 and NH_3 is apparent. Although H_2 flame temperature peaks at similar conditions to that of CH_4 (ϕ~1.1 – 1.2), both the maximum flame speed and minimum values of Ze are located at much richer conditions ($S_{L,max}^0$ for ϕ ~1.6-1.8, $Ze_{,min}$ for ϕ ~1.4 – 1.6). This shift in the flame speed to richer conditions (and by extension the reduced influence of flame temperature on S_L^0) has been attributed to the much larger value of the Lewis Number (Le >> 1 for ϕ >1.6), with flame acceleration, a consequence of preferential diffusion [49]. As a result, the minimum Ze witnesses a corresponding shift to richer conditions, since Ze is directly extracted from the flame speed (see Section 4). Thus, a transport mechanism (i.e. the thermo-diffusive response of the fuel for Le >> 1) generates a change in response in the flame speed, which subsequently impacts the flame property, highlighting the influence of transport on a supposedly chemical property [49]. This is of importance when attempting to understand behaviour of fuel blends which possess different transport properties (as it is the case here with H_2, CH_4 and NH_3) and the subsequent consequence on flame behaviour. On the other hand, for NH_3, S_L^0 and T_{ad} peak at approximately at the same equivalence ratio ranges (ϕ~1.0 – 1.10). The fact that the maximum flame speed, adiabatic flame temperature and minimum Ze all arise at nominally identical ϕ conditions underlines the equi-diffusive nature of NH_3, with Le close to unity, comparable to the preferential-diffusional properties of pure CH_4.

In premixed flames, instabilities can result from both preferential-diffusional and hydrodynamic (Darrieus-Landeau) instabilities. It should be highlighted that the Marsktein length (L_b) indicates the response of the flame to the stretch, it is also an indicator of the flame's propensity to instability and not the cause of the instability. Fig. 4 presents measured L_b for NH_3, CH_4 and H_2 / air flames from lean to rich conditions, from the present study and some other measurements available in literature at similar initial temperature (±5 K) and pressure conditions. To facilitate fair comparison, it is also indicated in the legend what methodology what used to extrapolate L_b (Linear or Non-Linear Model by Stretch (LMS) or (NMS); Linear Model based on Curvature, (LMC)). First, it should be highlighted that the values for CH_4 and H_2 are in a good agreement with previous data but for NH_3/air flame, the discrepancies are noticeable and can be partially attributed to the extrapolation methodology employed. All three fuels exhibit an increasing L_b as a function of ϕ increase from lean to rich conditions with the greatest change exhibited by NH_3, with negative value of L_b under lean conditions (comparable to that of H_2), and larger positive value than that of CH_4 and H_2 under rich conditions.

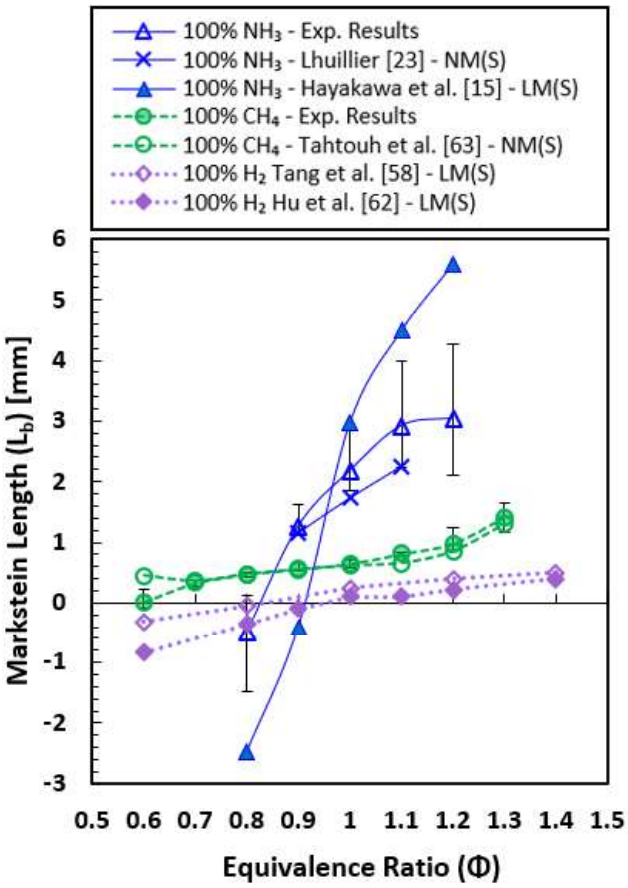

Figure 4 – Experimental values of L_b for pure NH_3, CH_4, H_2 as a function of ϕ (298 K, 0.1MPa). Data for NH_3 from [15] [23], CH_4 [63], H_2 [58] [62]

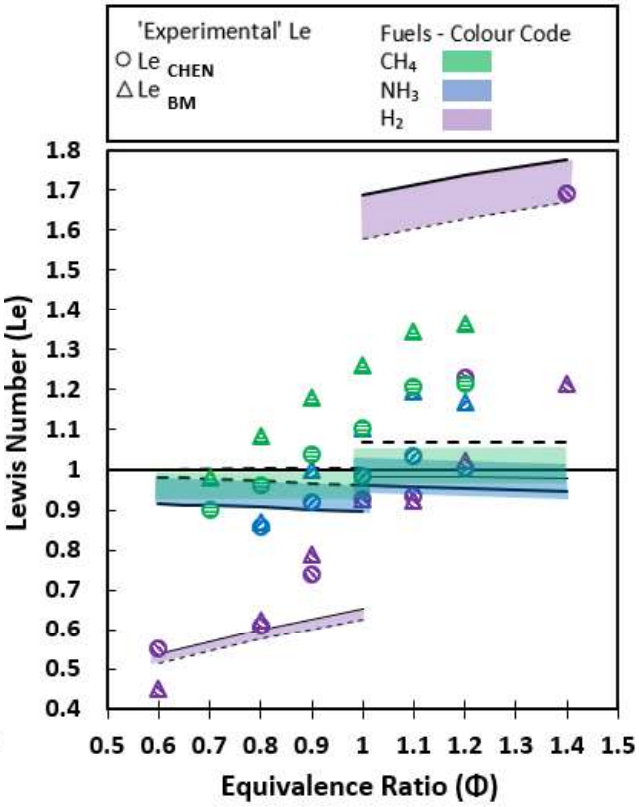

Figure 5 – Theoretical and experimental Le for NH_3, CH_4, H_2 as a function of ϕ (data for H_2 [75]). Full and dotted lines respectively reflect Hirschfelder and Wilke methods to evaluate D_{ij} (298 K, 0.1MPa)

To better understand the changes in the stretch response of pure fuels/air flames, the evolution of the corresponding Le is presented in Fig. 5, from lean to rich mixtures. 'Theoretical' Lewis numbers, estimated using the free-stream properties of the mixtures, are illustrated as colour bands with the upper and lower limits (represented by full and dashed lines) denoting the differences between either the Hirschfelder or Wilke method to evaluate the mass diffusion coefficient. While the correct Le is evaluated (Le ~ 1 for NH_3 and CH_4; Le << 1 at $\phi < 1$ and Le >> 1 at $\phi > 1$ for H_2), little variation is observable across the considered ϕ, aside from the transition from lean to rich conditions. Furthermore, it should be highlighted that minimum Le for NH_3 is just prior to stoichiometric conditions in agreement with [15], whilst for CH_4 and H_2, minimum Le is obtained at leanest conditions. Since Le was simply evaluated as a function of the mixture's thermal and mass diffusivity, variations in fundamental flame parameters such as the flame thickness, the activation energy and the expansion ratio [52] were not considered. As such, Le can be evaluated from the experimental L_b and these other properties affecting the flame, as recommended by Jomaas et al. [49], with the use of theoretical relationships established in literature (denoted as Le_{CHEN} and Le_{BM}, Eqn. 7 and 9, accordingly). Therefore, as it can be seen when comparing Figure 4 and 5, analogous L_b and Le evolution as a function of the fuel and the equivalence ratio is observable, regardless of the theoretical relationship relating L_b to Le. However, it is interesting to note that the greatest change in L_b magnitude is observed for NH_3, whilst exhibiting least change in Le, as noted by [8], potentially alluding that Le may not be the main driving factor behind the measured changes in stretch sensitivity for NH_3-based flames. Furthermore,

the transition from a negative to positive L_b for NH_3 obtained for ϕ ~ 0.8 – 1.0 is at comparable ϕ with the transition from Le < 1 to Le > 1 occurred.

5.2 Binary Fuel Mixtures

The influence of increasing fraction of either CH_4 or H_2 in NH_3/air mixture on S_L^0, across a wide range of ϕ is depicted in Figures 6 and 7 respectively. With respect to NH_3/H_2 blends, Otomo et al. [64], Shrestha et al. [65], Gotama et al. [66], Okafor et al., [18] and Stagni et al. [42] reaction mechanisms were all appraised by simulating a premixed 1-D adiabatic planar flame with the CHEMKIN-Pro package. A simulation of 10 cm was considered, with a total of 3000 grid points used with grid parameters GRID (0.025) and CURV (0.1), including multi-component diffusion and an assumed air composition of 79% N_2 – 21% O_2. However only the two latter mechanism are shown since they consistently gave best agreement with, respectively, all NH_3/CH_4 and NH_3/H_2 blends evaluated in this study.

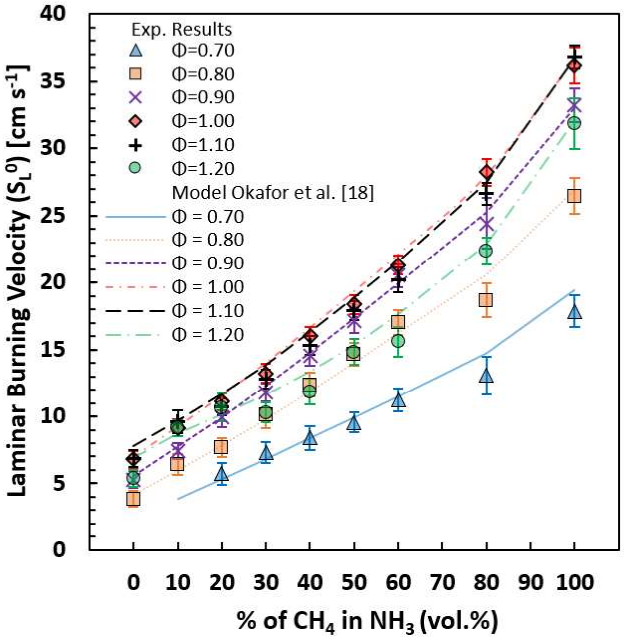

Figure 6 – S_L^0 for binary NH_3/CH_4 mixtures, comparison with simulated values with Okafor et al. kinetics model [18] (298 K, 0.1MPa)

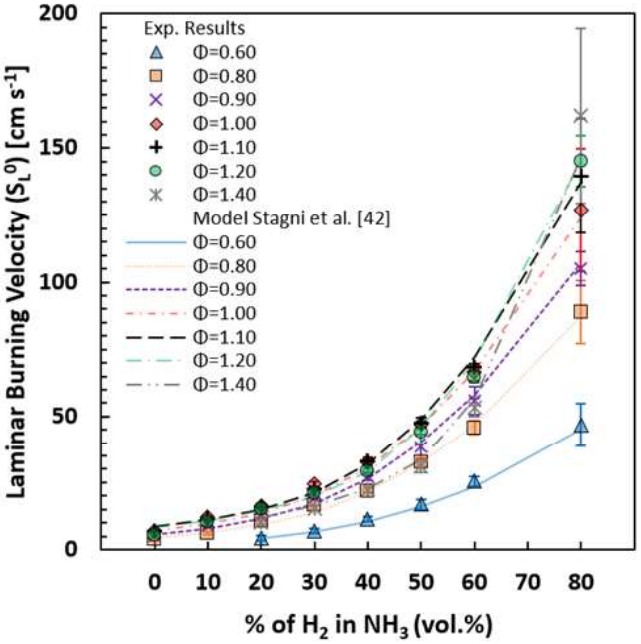

Figure 7 – S_L^0 for binary NH_3/H_2 mixtures, comparison with simulated values with Stagni et al. kinetics mechanism [42] (298 K, 0.1MPa)

As can be seen in Figure 6, irrespective of the ϕ, a quite linear increase in NH_3 laminar flame speed is observable upon CH_4 addition, with a very good prediction by Okafor et al. [18] mechanism. On the other hand, as illustrated in Figure 7, an increase in H_2 fraction results in an exponential increase in S_L^0, across the entire tested ϕ range, with also a very good prediction by Stagni et al. [42] mechanism, across all tested conditions. It is worth highlighting that ~ 10-20% addition (vol.%) of either CH_4 or H_2 results in a similar increase in NH_3 flame speed, with further increases resulting in very different flame speed behaviour. This increased reactivity of NH_3 based blends upon CH_4 and H_2 addition has been previously suitably reported [19] [67], with modelling work and sensitivity analysis suggesting that the flame speed, burning intensity (Q') and production of radicals, particularly O and H appear to be strongly correlated.

To investigate the stretch-related behaviour of NH_3/CH_4 and NH_3/H_2 flames, L_b is plotted as a function of either CH_4 or H_2 addition to NH_3 across a wide range of ϕ in Figure 8 and 9, respectively. Note that the evolutions of L_b as a function of ϕ are in SM3 and 4. For a $\phi \geq 0.9$, a linear decrease in L_b is observed with increasing CH_4 fraction. At $\phi = 0.80$, a negative value L_b is obtained for pure ammonia while 10% CH_4 addition results in L_b sign inversion (from negative to positive). As pure NH_3/air mixtures could not be ignited for $\phi < 0.8$, with this experimental apparatus, this tendency cannot be verified. Under rich conditions ($\phi \geq 1.1$), a decreasing stretch sensitivity is measured upon increasing H_2 fraction, similar in trend and magnitude to that observed for NH_3/CH_4 flames but for $\phi \geq 0.9$. However, interestingly for $\phi \leq 1.0$, an initial decrease in L_b is observed up to 30 – 40% H_2 addition, at which point any further addition of H_2 results in an increase in L_b, with non-linear behaviour accentuated as conditions get leaner. Similar non-monotonical variation in stretch-related behaviour was measured by Lhuillier [68] as well as by Ichikawa et al. [22], for NH_3/H_2 flames, at $\phi = 1.0$ and ostensibly identical experimental conditions (T_u = 298 K, P_u = 0.1 MPa), also plotted in Figure 9 for comparison purposes. As such, under lean conditions, NH_3/H_2 mixtures exhibit a greater negative L_b than that of pure H_2 flames. It should be highlighted that similar non-linear L_b behaviour was measured by Okafor et al. [24] for CH_4/H_2 flames, with an inflection point occurring upon ~ 70% H_2 addition. Similarly, Huang et al. [69] also reported similar behaviour for natural gas – hydrogen – air blends. As such, it may seem that this maybe a phenomenon attributable to the H_2 contribution, at least for NH_3 or CH_4 based flames, due to the strong and fast diffusivity of H_2 in the reactants. This stretch-sensitivity behaviour is of importance since the flames exhibiting negative L_b will be accelerated in highly stretched turbulent environments, whilst flames displaying a positive L_b will be weakened. This stretch-sensitivity response inevitably impacts the operation of practical combustion systems.

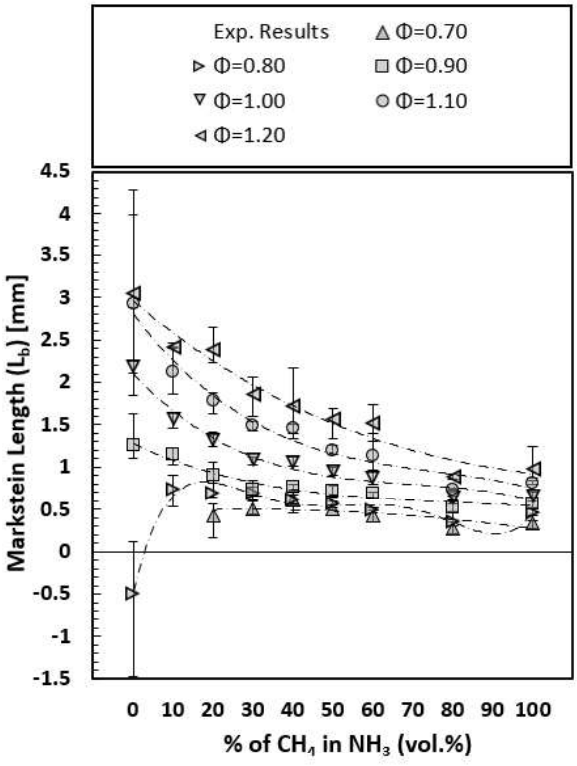

Figure 8 – L_b values of NH_3/CH_4 mixtures (298 K, 0.1 MPa)

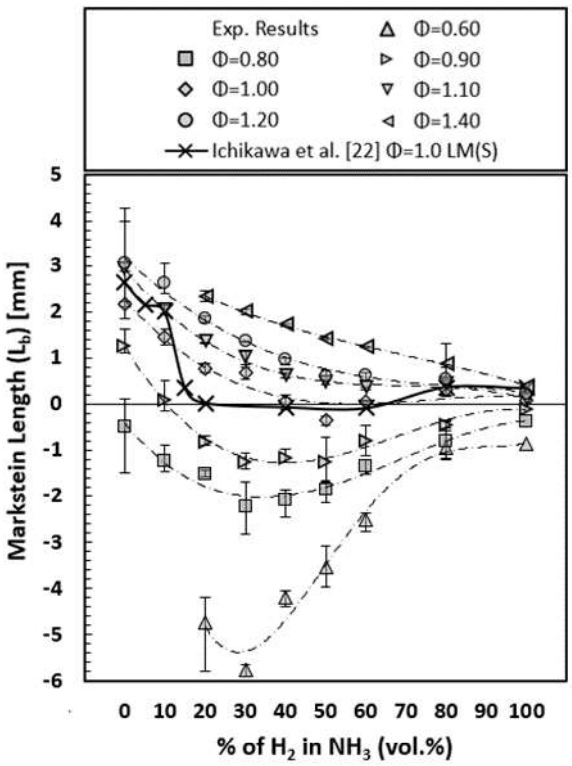

Figure 9 - L_b values of NH_3/H_2 mixtures (298 K, 0.1 MPa) 100% H_2 L_b values from [62]

For a better understanding of this change, a sensitivity analysis related to the contribution of major flame enhancing pathways (diffusive, thermal, kinetic) was undertaken. However, to correctly quantify the diffusive pathway, the most suitable Le formulation has to be considered. As such, the different Le_{eff} models (i.e. Le_V, Le_H, Le_D from Equations 12, 13 and 14 respectively) are used to yield to an estimate of L_b, by using the relationships proposed by Chen or Matalon and Bechtold, referred as L_b-Chen and L_b-BM, respectively. It should be noted that the purpose of such analysis is more qualitative than quantitative to validate which Le_{eff} model best captures the measured L_b behaviour of the tested blends.

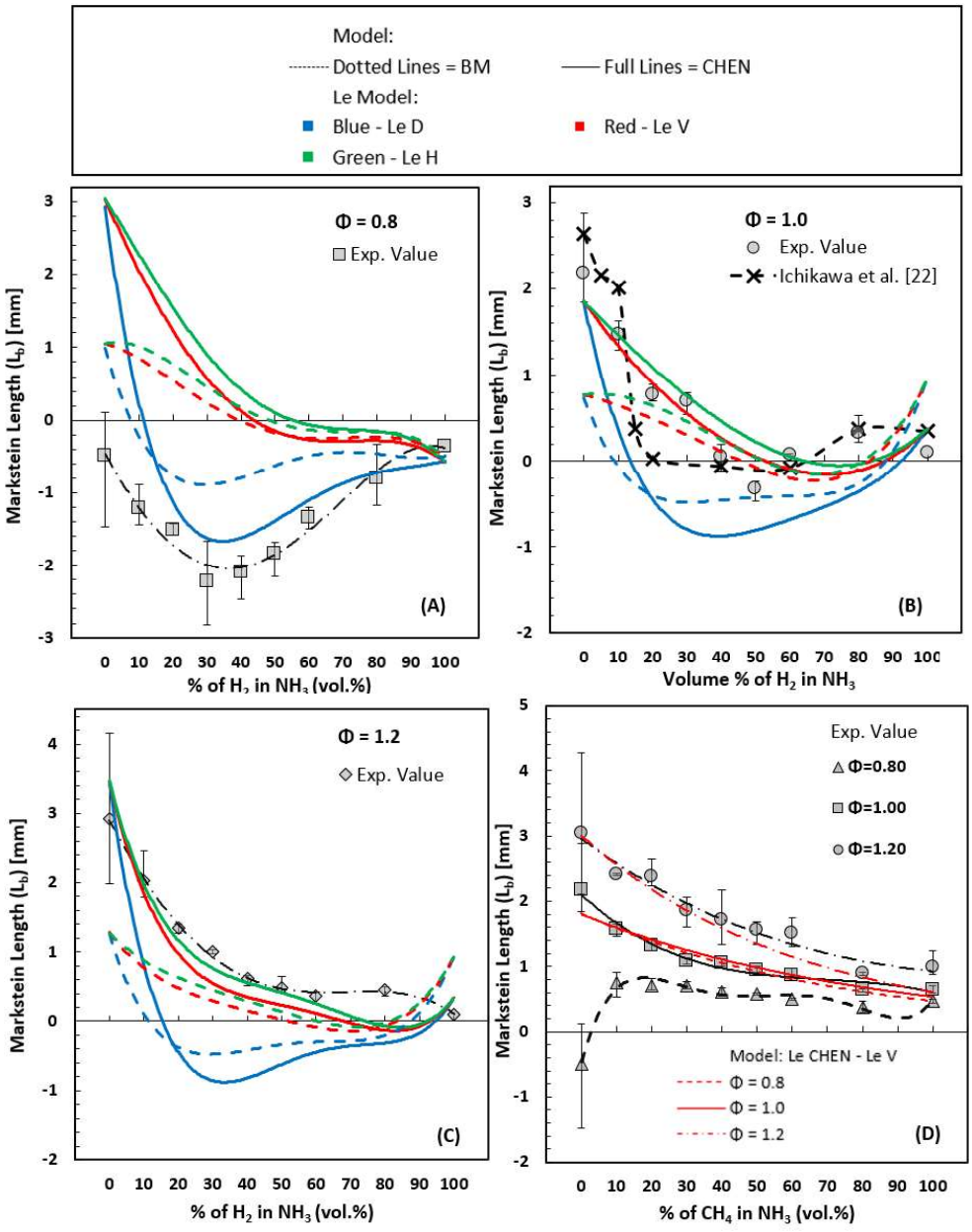

Figure 10 – Comparison of L_b-CHEN and L_b-BM estimates to the measured L_b for NH_3/H_2 flames (a) ϕ = 0.8 (b) ϕ = 1.0 (c) ϕ = 1.2 and for (d) NH_3/CH_4 flames

Figure 10 illustrates L_b-CHEN and L_b-BM for NH_3/H_2 blends, alongside experimentally measured L_b values. With respect to the CHEN formulation under lean H_2 condition (ϕ = 0.8, Fig. 10.a),

quantitative and qualitative agreements are observed with Le_D formulation, with the non-linear stretch behaviour well captured. Under H_2 richer condition (ϕ = 1.2, Fig.11.c), Le_D overpredicts the influence of H_2 on NH_3 with better agreement observed with a Le_V or Le_H model better reflecting the measured trend. Poor agreement is observed with the BM formulation, with again a Le_D best reflecting expected stretch behaviour under lean conditions, and Le_H exhibiting better agreement at richer conditions. Considering that the Le_D model was derived from the modelling of lean turbulent CH_4/H_2 flames [27], as well as that lean CH_4/H_2 appear to display similar non-linear stretch behaviour [24] to that of lean NH_3/H_2 flames, a better agreement was expected. Furthermore, this influence is due to the assumption that the flame curvature is dominant, hence the local enrichment of the most diffusive fuel at the flames leading edge is predicted. This concept appears to be valid under lean conditions, since H_2 and NH_3 have higher mass diffusivities than O_2. For richer conditions ($\phi \geq 1.0$), a model based on either volume or non-dimensional heat release appears to be more appropriate. With respect to NH_3/CH_4 flames, measured L_b and L_b-CHEN are compared in Fig. 10.d for ϕ = 0.8 – 1.2. It should be noted that since NH_3 and CH_4 display very similar preferential-diffusional behaviour (Le ~ 0.9 – 1.1), the application of either Le_{eff} models results in very similar values. Consequently, only the Le_V model is plotted on Figure 10.d. For the conditions greater than stoichiometry, a good quantitative and qualitative agreement is observed with the CHEN model, but under lean conditions, the CHEN model does not allow to verify the change from negative to positive L_b measured experimentally obtained upon 10% CH_4 addition to NH_3 (for only one equivalence ratio). In summary, for lean and rich NH_3/H_2 flames, the Le_D and Le_H formulation respectively, best captured changes in thermo-diffusive behaviour. With respect to NH_3/CH_4 flames, Le_V demonstrated the best agreement for all considered ϕ, with these conclusions maintained for the remainder of the analysis.

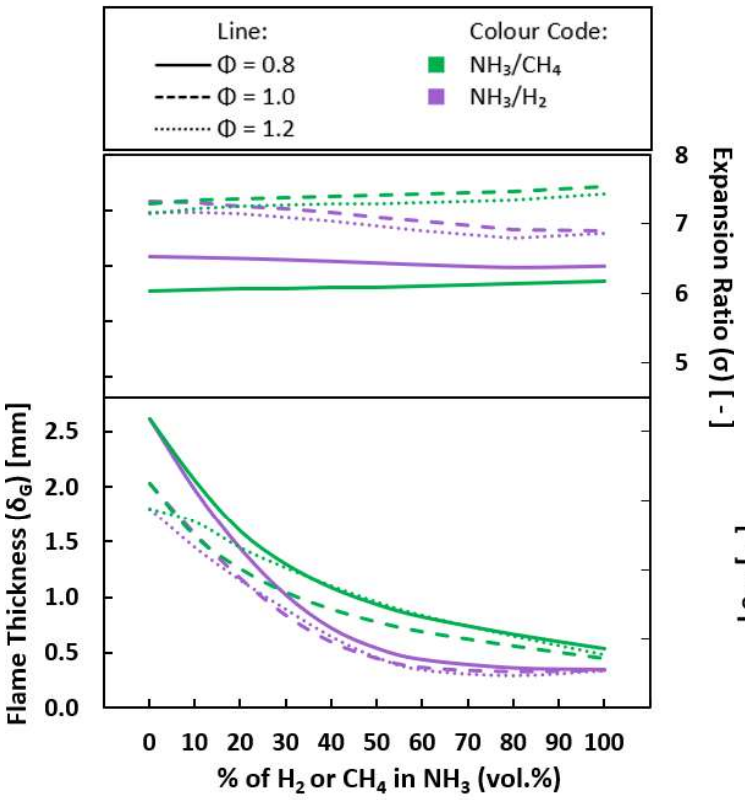

Figure 11 – Variation in δ_G and σ with addition of either CH_4 or H_2 to NH_3, ϕ = 0.8, 1.0, 1.2

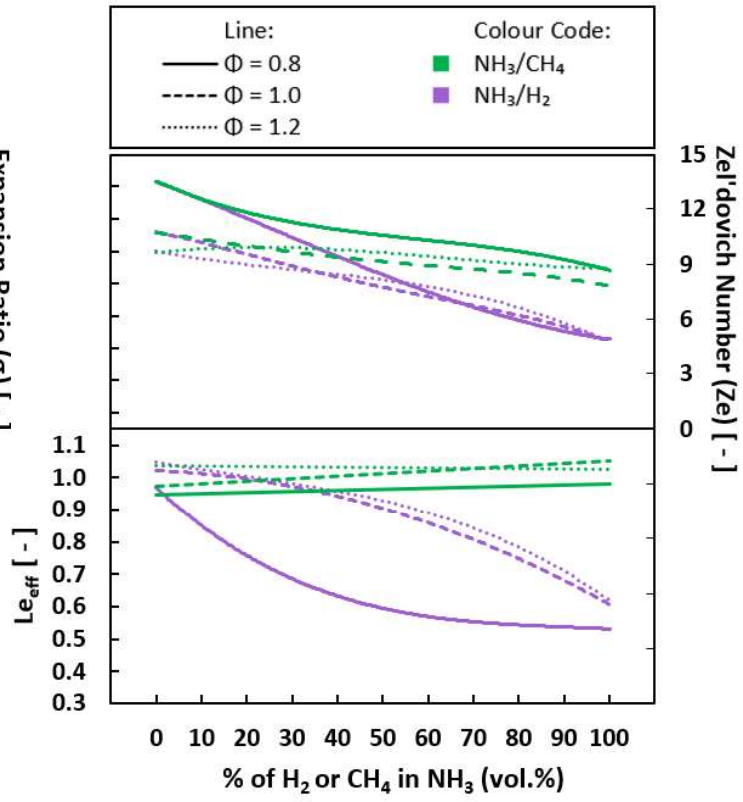

Figure 12 – Variation in Le_{eff} and Ze with addition of either CH_4 or H_2 to NH_3, ϕ = 0.8, 1.0, 1.2

As emphasised by Kwon et al. [70] and reviewed in [71], the fundamental parameters that induce hydrodynamic and diffusional-thermal instabilities are the thermal expansion, the flame thickness, the non-unity Le and the global activation energy (or equivalently Ze). Consistent with the hydrodynamic theory of Darrieus and Landau [9], the hydrodynamic instabilities arise from the thermal expansion of gases, with the density jump across the flame front proportional to the growth rate of hydrodynamic instability. In the case of an outwardly propagating spherical flame, the flame tends to be stabilised due to curvature induced positive stretch, consequently the flame thickness plays a significant role, since the thinner the flame the weaker the influence of curvature. Hence the risk of destabilisation is enhanced for thinner flames. It is interesting to note that addition of either CH_4 or H_2 to NH_3 does not really affect the thermal expansion, irrespective of ϕ, as shown in Figure 11. On the other hand, the flame thickness decreases strongly with increasing CH_4 or H_2 fractions, in effect promoting hydrodynamic instabilities to a similar extent. Nevertheless, the addition of either CH_4 or H_2 to NH_3 results in similar stretch-related behaviour under rich conditions, whilst exhibiting very different stretch-behaviour as conditions get leaner. The development of preferential-diffusional instabilities, characterised by Le, is the result of non-equi-diffusion. With respect to the NH_3/H_2 flames, the effects of preferential diffusion are a consequence of the higher mass diffusivity of H_2 and NH_3 compared to the O_2 molecule. As illustrated in Figure 12, Le decreases significantly with increasing H_2 fraction thereby promoting diffusional-thermal instabilities at ϕ = 0.8. Furthermore, as could be expected, the change in Le increases as the conditions get leaner, a consequence of each of the fuel's individual Le response. As underlined by Kwon et al. [70], considering that the development of preferential diffusional instabilities requires a modification of the flame front, it is thus reasonable to expect the global activation energy should also affect the development of diffusional-thermal instabilities. Accordingly, a lower E_a (illustrated as Ze in Figure 12) will tend to enhance instability of a diffusionally unstable flame such as lean NH_3/H_2 flame, with both Le and Ze decreasing with increasing H_2 concentration for all ϕ. The decrease in Ze is largely due to a decrease in the inner-layer temperature coupled with an increase in adiabatic flame temperature with increasing H_2 concentration for ϕ. For NH_3/H_2, the changes in measured L_b are thus potentially the result of competing hydrodynamic and thermo-diffusive instabilities, with the influence of the thermo-diffusional instabilities reducing as the ϕ increases. On the other hand, for NH_3/CH_4 flames, the addition of CH_4 to NH_3 results in little diffusional-thermal effects (Le ~ 1) across the entire considered ϕ range.

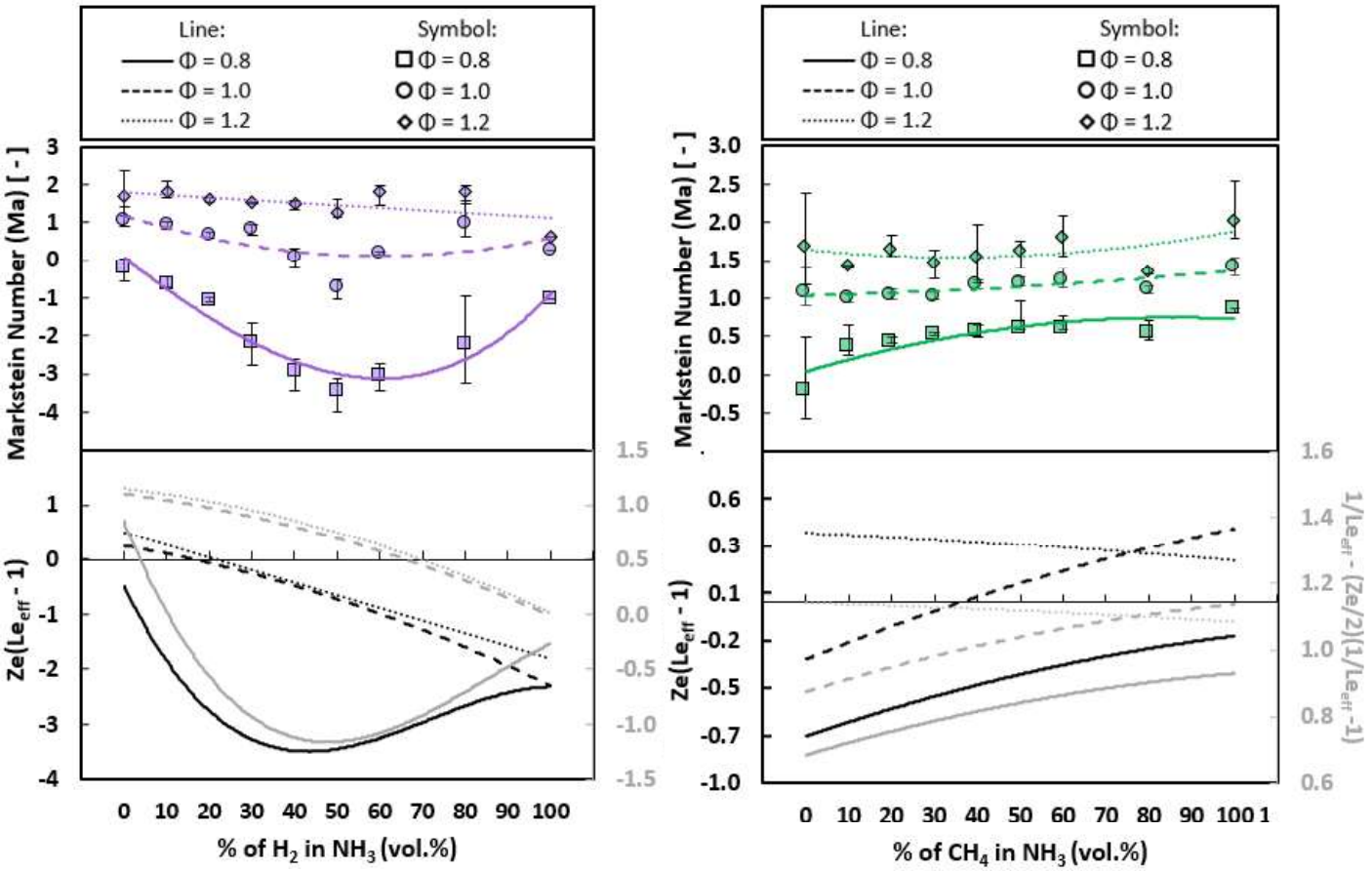

Figure 13 – Comparison of variation of $Ze(L_{eff} - 1)$ and $1/Le_{eff} - (Ze/2)(1/Le_{eff} -1)$ to measured Marsktein number as a function of (a) H_2 mole fraction, and (b) CH_4 mole fraction

From the analytical expression developed by Chen [38], [44], the equation 8 can be re-arranged to yield the Marsktein Number ($Ma = L_b/\delta$), resulting in $Ma = [\ 1/Le_{eff} - (Ze/2)(1/Le - 1)]\sigma$, where $1/Le_{eff} - (Ze/2)(1/Le_{eff} - 1)$ represents the thermo-diffusive effect. Similarly, the relationship linking L_b to Le developed by Matalon and Bechtold (Equation 9) can be re-arranged to evaluate Ma, in which the term $Ze(L_{eff} - 1)$ reflects the thermo-diffusive influence as underlined by Okafor et al. [24]. Figures 14.a and 14.b compare the experimental Ma to the trends in $1/Le_{eff} - (Ze/2)(1/Le - 1)$ and $Ze(L_{eff} - 1)$, for NH_3/H_2 and NH_3/CH_4 mixtures, respectively, at $\phi = 0.8 - 1.0 - 1.2$. First, as expected both $Ze(L_{eff} - 1)$ and $1/Le_{eff} - (Ze/2)(1/Le - 1)$ exhibit the same trends. For the lean NH_3/H_2 mixtures, the changes in measured Ma appear to be to a great extent the result, of changes in the thermo-diffusive properties, Le and Ze. At richer condition, slightly different trends are displayed between the experimental Ma and $Ze(L_{eff} - 1)$ and $1/Le_{eff} - (Ze/2)(1/Le - 1)$, potentially due to a greater change in the expansion ratio (see Figures 12) than under lean conditions. In relation to the NH_3/CH_4 mixtures (Figure 13.b), the measured Ma under lean and stoichiometric conditions yield matching trends to $Ze(L_{eff} - 1)$ and $1/Le_{eff} - (Ze/2)(1/Le - 1)$, potentially alluding that the Le and Ze are the driving forces behind the changes in stretch-related behaviour. At $\phi = 1.2$, a less good agreement is observed, potentially the consequence of nominal changes in Le and Ze, combined with an increasing expansion ratio. For lean NH_3/H_2 flames it seems that the changes in measured L_b are to a large extent the consequence of thermo-diffusive effects, with this influence reducing as conditions get richer. For the NH_3/CH_4 mixtures, the competition between thermo-diffusional and hydrodynamic instabilities yields to increasingly positive Ma values, resulting in propensity of flame stabilisation.

5.3 Flame Sensitivity Analysis

The enhancement of the flame propagation due to the addition of CH_4 or H_2 to NH_3 can be characterised as a combination of diffusive, thermal and kinetic effects [72], [73]. The individual pathway can be modelled as:

$$S_L^0 \sim \left(D_T \cdot Le_{eff}\right)^{1/2} exp(-T_a/2T_{ad}) \quad (16)$$

The first term on the right-hand side $(D_T \cdot Le_{eff})$ reflects the diffusive influence. The Arrhenius factor, which combines the relative influence of the global activation energy through the activation temperature ($T_a = E_a/R_u$), and the adiabatic flame temperature are represented in the second term $[exp(-T_a/2T_{ad})]$. These individually represent the thermal (T_{ad}) and kinetic (T_a) influences on the flame speed. Concerning the Le formulation, it was previously determined from Figure 11 that for lean and rich NH_3/H_2 flames, the Le_D and Le_H formulation respectively, best captured changes in thermo-diffusive behaviour. With respect to NH_3/CH_4 flames, Le_V demonstrated the best agreement for all considered ϕ. These conclusions are maintained regardless of the theoretical relationship relating L_b to Le, and hence applied for the following analysis. Equation 16 may be differentiated to determine the sensitivity of each individual pathway on the overall influence of the flame speed. Accordingly, the overall sensitivity coefficient can be expressed as per Equation 17 [72]:

$$\frac{1}{S_L^0} \cdot \frac{dS_L^0}{dx} = \frac{1}{2 \cdot D_T \cdot Le} \cdot \frac{d(D_T \cdot Le)}{dx} - \frac{1}{2 \cdot T_{ad}} \cdot \frac{2 \cdot T_a}{dx} + \frac{T_a}{2 \cdot T_{ad}^2} \frac{2 \cdot T_{ad}}{dx} \quad (17)$$

where *x*, the volume fraction of either CH_4 or H_2. Note that the three terms on the right-hand side denote the influence of the diffusive, kinetic, and thermal pathways, correspondingly. Sensitivity analysis is illustrated in Figure 14 for the blends and ϕ considered, with a positive and negative sensitivity factor representing flame speed enhancement and inhibition, respectively.

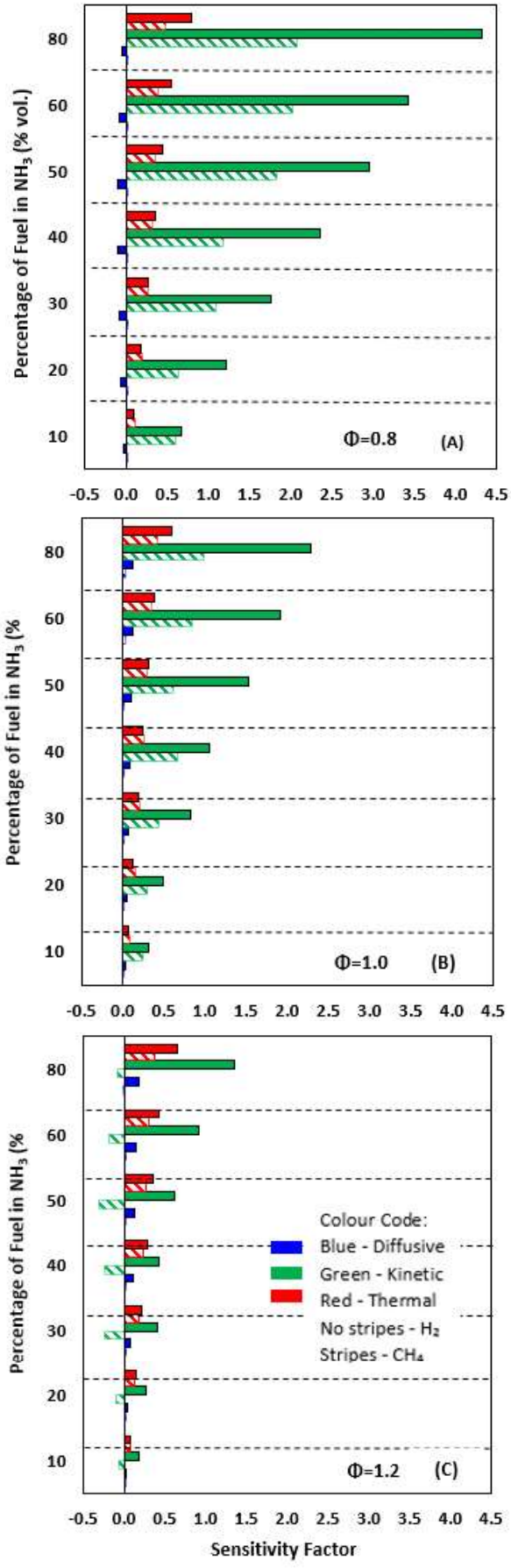

Figure 14 – Sensitivity Analysis of S_L^0 for NH_3/H_2 and NH_3/CH_4 blends, (a) ϕ = 0.8 (b) ϕ = 1.0 (c) ϕ = 1.2

As illustrated in Figure 14, the enhancement in flame speed of NH_3 based blends upon addition of either CH_4 or H_2 is predominantly an Arrhenius effect (kinetic), principally through the reduction of the overall activation energy and thus the activation temperature. For identical volumetric additions of up to 10% CH_4 or H_2 results in a similar reduction in E_a, leading to similar flame speeds, a trend well captured both experimentally and numerically. Any further addition of H_2 results in a significantly greater reduction in E_a than in the case of CH_4 addition, resulting in greater flame speeds. It should be noted that although remaining predominant for lean and stoichiometric conditions, the influence of the kinetic pathway reduces at richest conditions, particularly for CH_4 addition to NH_3, with a negative sensitivity at ϕ = 1.2. This agrees with the minor increase in E_a (represented by Ze, see Figure 12) at that condition, the consequence of the shifted minimum E_a to slightly richer conditions (ϕ = 1.1-1.2) of NH_3, as in Figure 3. The thermal pathway impact is lower than the kinetic effect, with the influence of the thermal pathway correlating well with modelled changes in adiabatic flame temperature. The addition of up to 60% of either CH_4 or H_2 results in changes of < 45 K, regardless of ϕ. With respect to the diffusive influence, it assumes negative sensitivity (or inhibiting effect) for lean NH_3/H_2 mixtures, and is negligible in comparison to other pathways. This is particularly the case for NH_3/CH_4, a consequence of the nominal changes in Le (Fig. 12) coupled with the limited change in thermal diffusivity of the mixture upon CH_4 addition, irrespective of the ϕ. It should be noted that even if the use of different kinetics mechanisms can induce different Arrhenius coefficients, the qualitative trends should remain valid, and thus performing such sensitivity analysis from first principles remains relevant providing useful insights.

6. Conclusions

The spherically expanding flame configuration was used to measure the unstretched laminar flame speeds and corresponding Markstein lengths in NH_3/H_2 and NH_3/CH_4 premixed flame across a wide range of compositions and equivalence ratio. A special attention was given to the estimate of Lewis number to analyse its influence on flame behaviour of NH_3, H_2 and CH_4 as well as for the blends. From this study, the following main outcomes can be made:

- Increasing H_2 and CH_4 fraction to NH_3-air laminar premixed flames results in an exponential and linear increase in flame speed, respectively. The greatest relative change in flame speed upon H_2 addition occurs under leanest and richest conditions while upon CH_4 addition, only under lean conditions. Stagni et al. and Okafor et al. mechanisms displayed the best agreement with experimental NH_3/H_2 and NH_3/CH_4 results, respectively.
- With respect to the stretch related behaviour, the addition of CH_4 to NH_3 results in a linear reduction in the stretch sensitivity for a fixed equivalence ratio. The volumetric based Lewis number yielded the best correlation with the measured Markstein lengths, for CH_4 addition to NH_3 resulting in nominal diffusional-thermal effects. For the stoichiometric and lean NH_3/H_2 flames, a non-monotonical variation in measured Markstein length was obtained, with a less and less linear behaviour as conditions get leaner. For NH_3/H_2, the changes in measured L_b were demonstrated to mainly be the result of thermo-diffusive effects (through the modelled changes in Le_{eff} and global activation energy) with the influence of the thermo-diffusional instabilities reducing as the equivalence ratio increases. For lean NH_3/H_2 mixtures, the diffusional-based Lewis number well captured the non-linear stretch behaviour as function of H_2 addition, whilst the heat release-based Lewis number resulted in better agreement at richer conditions.
- A sensitivity analysis related to the major flame enhancing pathways (diffusive, kinetic, thermal) has demonstrated that the enhanced flame propagation of NH_3/H_2 and NH_3/CH_4, is mainly due to the kinetic change, especially through the reduction of the activation temperature. The influence of the kinetic pathway reduces as conditions get richer,

particularly for CH_4 addition. The thermal pathway holds less influence in comparison to the kinetic pathway, with its influence showing good correlation with limited changes in adiabatic flame temperature of the considered blends. The diffusive pathway was negligible for all investigated mixtures, with a negative sensitivity for the lean NH_3/H_2 mixtures.

Declaration of Competing Interest

The authors declare that they have no known competing financial interest or personal relationships that could have appeared to influence the work reported in this paper.

Acknowledgements

This project has received funding from the European Union's Horizon 2020 Research and Innovation Program agreement No. 884157. http://flexnconfu.eu/

7. References

[1] T. Letcher, Climate Change: Observed Impacts on Planet Earth, 2nd ed., Elsevier, 2015.

[2] W. S. Chai, Y. Bao, P. Jin, G. Tang, L. Zhou, A review on ammonia, ammonia-hydrogen and ammonia-methane fuels, Renew. Sust. Energ. Rev. 147 (2021).

[3] H. Kobayashi, A. Hayakawa, K. A. Somarathne, E. C. Okafor, Science and technology of ammonia combustion, Proc. Combust. Inst. 37 109–133.

[4] N. A. Hussein, A. Valera-Medina, A. S. Alsaegh, Ammonia- hydrogen combustion in a swirl burner with reduction of NOx emissions, Enrgy. Proced. 158 (2019) 2305–2310.

[5] D. Pugh, J. Runyon, P. Bowen, A. Giles, A. Valera-Medina, R. Marsh, B. Goktepe, S. Hewlett., An investigation of ammonia primary flame combustor concepts for emissions reduction with OH*, NH2* and NH* chemiluminescence at elevated conditions, Proc. Combust. Inst. 38 (2021) 6451–6459.

[6] A. Hayakawa, Y. Arakawa, R. Mimoto, K. D. K. A. Somarathne, T. Kudo, H. Kobayashi, Experimental investigation of stabilization and emission characteristics of ammonia/air premixed flames in a swirl combustor, Int. J. Hydrogen Energy 42 (2017) 14010–14018.

[7] C. Lhuillier, P. Brequigny, F. Contino, C. Mounaïm-Rousselle, Experimental study on ammonia/hydrogen/air combustion in spark ignition engine conditions, Fuel 269 (2020) 117448.

[8] C. Lhuillier, P. Brequigny, F. Contino, C. Mounaïm-Rousselle, Experimental investigation on ammonia combustion behavior in a spark-ignition engine by means of laminar and turbulent expanding flames, Proc. Combust. Inst. 38 (2021) 6671–6678.

[9] C. K. Law, Combustion Physics, Cambridge: Cambridge University Press, 2006.

[10] C. K. Wu, C. K. Law, On the determination of laminar flame speeds from stretched flames, Symp. Combust. 20 (1985) 1941–1949.

[11] S. Ishizuka, C. K. Law, An experimental study on extinction and stability of stretched premixed flames, Symp. Combust. 19 (1982) 327–335.

[12] P. Clavin, Dynamic behavior of premixed flame fronts in laminar and turbulent flows, Prog.

Energy Combust. Sci. 11 (1985) 1–59.

[13] M. Matalon, On Flame Stretch, Combust. Sci. Technol. 31 (1983) 169–181.

[14] R. C. Aldredge, N. J. Killingsworth, Experimental evaluation of Markstein-number influence on thermoacoustic instability, Combust. Flame 137 (2004) 178–197.

[15] A. Hayakawa, T. Goto, R. Mimoto, Y. Arakawa, T. Kudo, H. Kobayashi, Laminar burning velocity and Markstein length of ammonia/air premixed flames at various pressures, Fuel 159 (2015) 98–106.

[16] R. Kanoshima, A. Hayakawa, T. Kudo, E.C. Okafor, S. Colson, A. Ichikawa, T. Kudo, H. Kobayahsi, Effects of initial mixture temperature and pressure on laminar burning velocity and Markstein length of ammonia/air premixed laminar flames, Fuel 310 (2022) 122149.

[17] E. C. Okafor, Y. Naito, S. Colson, A. Ichikawa, T. Kudo, A. Hayakawa, and H. Kobayashi, Experimental and numerical study of the laminar burning velocity of CH4–NH3–air premixed flames, Combust. Flame 187 (2018) 185–198.

[18] E. C. Okafor, Y. Naito, S. Colson, A. Ichikawa, T. Kudo, A. Hayakawa, H. Kobayashi, Measurement and modelling of the laminar burning velocity of methane-ammonia-air flames at high pressures using a reduced reaction mechanism, Combust. Flame 204 (2019) 162–175.

[19] T. Shu, Y. Xue, Z. Zhou, Z. Ren, An experimental study of laminar ammonia/methane/air premixed flames using expanding spherical flames, Fuel 290 (2021) 120003.

[20] J. H. Lee, S. I. Lee, O. C. Kwon, Effects of ammonia substitution on hydrogen/air flame propagation and emissions, Int. J. Hydrogen Energy 35 (2010) 11332–11341.

[21] J. H. Lee, J. H. Kim, J. H. Park, O. C. Kwon, Studies on properties of laminar premixed hydrogen-added ammonia/air flames for hydrogen production, Int. J. Hydrogen Energy 35 (2010) 1054–1064

[22] A. Ichikawa, A. Hayakawa, Y. Kitagawa, K. D. Kunkuma Amila Somarathne, T. Kudo, H. Kobayashi, Laminar burning velocity and Markstein length of ammonia/hydrogen/air premixed flames at elevated pressures, Int. J. Hydrogen Energy 40 (2015) 9570–9578.

[23] C. Lhuillier, P. Brequigny, N. Lamoureux, F. Contino, C. Mounaïm-Rousselle, Experimental investigation on laminar burning velocities of ammonia/hydrogen/air mixtures at elevated temperatures, Fuel 263 (2020) 116653.

[24] E. C. Okafor, A. Hayakawa, Y. Nagano, T. Kitagawa, Effects of hydrogen concentration on premixed laminar flames of hydrogen-methane-air, Int. J. Hydrogen Energy 39 (2014) 2409–2417.

[25] A. N. Lipatnikov, J. Chomiak, Molecular transport effects on turbulent flame propagation and structure, Prog. Energy Combust. Sci. 31 (2005) 1–73.

[26] S. P. R. Muppala, M. Nakahara, N. K. Aluri, H. Kido, J. X. Wen, M. V. Papalexandris, Experimental and analytical investigation of the turbulent burning velocity of two-component fuel mixtures of hydrogen, methane and propane, Int. J. Hydrogen Energy 34 (2009) 9258–9265.

[27] F. Dinkelacker, B. Manickam, S. P. R. Muppala, Modelling and simulation of lean premixed turbulent methane/hydrogen/air flames with an effective Lewis number approach, Combust. Flame 158 (2011) 1742–1749.

[28] M. Di Lorenzo, P. Brequigny, F. Foucher, C. Mounaim-Rousselle, Turbulent Flame Speed of a Gasoline surrogate in conditions representative of modern downsized Spark-Ignition engine,

Combust. Flame 240 (2022) 112041.

[29] J. B. Bell, R. K. Cheng, M. S. Day, I. G. Shepherd, Numerical simulation of Lewis number effects on lean premixed turbulent flames, Proc. Combust. Inst. 31 (2007) 1309–1317.

[30] N. Chakraborty, R. S. Cant, Effects of Lewis number on flame surface density transport in turbulent premixed combustion, Combust. Flame 158 (2011) 1768–1787.

[31] R. Ichimura, K. Hadi, N. Hashimoto, A. Hayakawa, H. Kobayashi, O. Fujita, Extinction limits of an ammonia/air flame propagating in a turbulent field, Fuel 246 (2019) 178–186.

[32] S. Zitouni, P. Brequigny, C. Mounaim-Rousselle, Turbulent Flame Speed and Morphology of Pure Ammonia flames and Blends with Methane or Hydrogen, Proc. Combust. Inst. (2022) doi: 10.1016/j.proci.2022.07.179.

[33] B. Galmiche, F. Halter, F. Foucher, Effects of high pressure, high temperature and dilution on laminar burning velocities and Markstein lengths of iso-octane/air mixtures, Combust. Flame 159 (2012) 3286–3299.

[34] S. Zitouni, D. Pugh, A. Crayford, P. J. Bowen, J. Runyon, Lewis number effects on lean premixed combustion characteristics of multi-component fuel blends, Combust. Flame 238 (2022) 111932.

[35] G. K. Giannakopoulos, A. Gatzoulis, C. E. Frouzakis, M. Matalon, A. G. Tomboulides, Consistent definitions of 'Flame Displacement Speed' and 'Markstein Length' for premixed flame propagation, Combust. Flame, 162 (2015) 1249–1264.

[36] P. Brequigny, F. Halter, C. Mounaïm-Rousselle, Lewis number and Markstein length effects on turbulent expanding flames in a spherical vessel, Exp. Therm. Fluid Sci. 73 (2016) 33–41.

[37] M. L. Frankel, G. I. Sivashinsky, On Effects Due To Thermal Expansion and Lewis Number in Spherical Flame Propagation, Combust. Sci. Technol. 31 (1983) 131–138.

[38] Z. Chen, On the extraction of laminar flame speed and Markstein length from outwardly propagating spherical flames, Combust. Flame, 158 (2011) 291–300.

[39] F. Wu, W. Liang, Z. Chen, Y. Ju, C. K. Law, Uncertainty in stretch extrapolation of laminar flame speed from expanding spherical flames, Proc. Combust. Inst. 35 (2015) 663–670.

[40] A. P. Kelley, C. K. Law, Nonlinear effects in the extraction of laminar flame speeds from expanding spherical flames, Combust. Flame 156 (2009) 1844–1851.

[41] F. Halter, T. Tahtouh, C. Mounaïm-Rousselle, Nonlinear effects of stretch on the flame front propagation, Combust. Flame 157 (2010) 1825–1832.

[42] A. Stagni, C. Cavallotti, S. Arunthanayothin, Y. Song, O. Herbinet, Fe. Battin-Leclerc and T. Faravelli, An experimental, theoretical and kinetic-modeling study of the gas-phase oxidation of ammonia, React. Chem. Eng. 5 (2020) 696–711.

[43] D. Bradley, P. H. Gaskell, X. J. Gu, Burning velocities, Markstein lengths, and flame quenching for spherical methane-air flames: A computational study, Combust. Flame 104 (1996) 176–198.

[44] Z. Chen, M. P. Burke, Y. Ju, Effects of Lewis number and ignition energy on the determination of laminar flame speed using propagating spherical flames, Proc. Combust. Inst. 32 (2009) 1253–1260.

[45] M. P. Burke, Z. Chen, Y. Ju, F. L. Dryer, Effect of cylindrical confinement on the determination of laminar flame speeds using outwardly propagating flames, Combust. Flame 156 (2009) 771–779.

[46] Z. Chen, On the accuracy of laminar flame speeds measured from outwardly propagating spherical flames: Methane/air at normal temperature and pressure, Combust. Flame 162 (2015) 2442–2453.

[47] X. Chen, Q. Liu, Q. Jing, Z. Mou, Y. Shen, J. Huang, H. Ma, Flame front evolution and laminar flame parameter evaluation of buoyancy-affected ammonia/air flames, Int. J. Hydrogen Energy 46(2021) 38504–38518.

[48] S. Verhelst, R. Woolley, M. Lawes, R. Sierens, Laminar and unstable burning velocities and Markstein lengths of hydrogen-air mixtures at engine-like conditions, Proc. Combust. Inst. 30, (2005) 209–216.

[49] G. Jomaas, C. K. Law, J. K. Bechtold, On transition to cellularity in expanding spherical flames, J. Fluid Mech. 583 (2007) 1–26.

[50] R. J. Moffat, Describing the uncertainties in experimental results, Exp. Therm. Fluid Sci. 1 (1988) 3–17.

[51] H. Yu, W. Han, J. Santner, X. Gou, C. Hoon Sohn, Y. Ju, Z. Chen, Radiation-induced uncertainty in laminar flame speed measured from propagating spherical flames, Combust. Flame 161 (2014) 2815–2824.

[52] J. K. Bechtold, M. Matalon, The dependence of the Markstein length on stoichiometry, Combust. Flame 127 (2001) 1906–1913.

[53] F. N. Egolfopoulos, C. K. Law, Chain mechanisms in the overall reaction orders in laminar flame propagation, Combust. Flame 80 (1990) 7–16.

[54] P. D. Ronney, G. I. Sivashinsky, A Theoretical Study of Propagation and Extinction of Nonsteady Spherical Flame Fronts, SIAM J. Appl. Math. 49 (1989) 1029–1046.

[55] N. Bouvet, F. Halter, C. Chauveau, Y. Yoon, On the effective Lewis number formulations for lean hydrogen/hydrocarbon/ air mixtures, Int. J. Hydrogen Energy 38 (2013) 5949–5960.

[56] D. Lapalme, R. Lemaire, P. Seers, Assessment of the method for calculating the Lewis number of H2/CO/CH4 mixtures and comparison with experimental results, Int. J. Hydrogen Energy 42 (2017) 8314–8328.

[57] C. K. Law, G. Jomaas, J. K. Bechtold, Cellular instabilities of expanding hydrogen/propane spherical flames at elevated pressures: Theory and experiment, Proc. Combust. Inst. 30 (2005) 159–167.

[58] C. Tang, Z. Huang, C. Jin, J. He, J. Wang, X. Wang, H. Miao, Laminar burning velocities and combustion characteristics of propane-hydrogen-air premixed flames, Int. J. Hydrogen Energy 33 (2008) 4906–4914.

[59] B. Poling, J. Prausnitz, J. O'Connell, The Properties of Gases and Liquids, 5th Ed., McGraw-Hill, 2001.

[60] D. F. Fairbanks, C. R. Wilke, Diffusion Coefficients in Multicomponent Gas Mixtures, Ind. Eng. Chem. 42 (1950) 471–475.

[61] D. Dandy, Transport Properties Calculator. https://navier.engr.colostate.edu/code/code-2/index.html (accessed Mar. 21, 2022).

[62] E. Hu, Z. Huang, J. He, H. Miao, Experimental and numerical study on laminar burning velocities and flame instabilities of hydrogen-air mixtures at elevated pressures and temperatures, Int. J. Hydrogen Energy 34 (2009) 8741–8755.

[63] T. Tahtouh, F. Halter, C. Mounaïm-Rousselle, Measurement of laminar burning speeds and Markstein lengths using a novel methodology, Combust. Flame 156 (2009) 1735–1743.

[64] J. Otomo, M. Koshi, T. Mitsumori, H. Iwasaki, K. Yamada, Chemical kinetic modeling of ammonia oxidation with improved reaction mechanism for ammonia/air and ammonia/hydrogen/air combustion, Int. J. Hydrogen Energy 43 (2018) 3004–3014.

[65] K. P. Shrestha, L. Seidel, T. Zeuch, F. Mauss, Detailed Kinetic Mechanism for the Oxidation of Ammonia Including the Formation and Reduction of Nitrogen Oxides, Energy and Fuels 32 (2018) 10202–10217.

[66] G. J. Gotama, A. Hayakawa, E.C. Okafor, R. Kanoshima, M. Hayashi, T. Kudo, H. Kobayashi, Measurement of the laminar burning velocity and kinetics study of the importance of the hydrogen recovery mechanism of ammonia/hydrogen/air premixed flames, Combust. Flame 236 (2022)111753.

[67] S. Zitouni, S. Mashruk, N. Mukundakumar, P. Brequigny, A. Zayoud, E. Pucci, S. Macchiavello, F. Contino, C. Rousselle, R. Bastiaans, A. Valera-Medina, Ammonia Blended Fuels-Energy Solutions for a Green Future, 10th Int. Gas Turbine Conf. IGTC21-62 (2021) [Online] Available: https://hal.archives-ouvertes.fr/hal-03519203.

[68] C. Lhuillier, Experimental and numerical investigation for the use of ammonia as hydrogen-carrying fuel for spark- ignition engines, 2020.

[69] Z. Huang, Y. Zhang, K. Zeng, B. Liu, Q. Wang, D. Jiang, Measurements of laminar burning velocities for natural gas-hydrogen-air mixtures, Combust. Flame 146 (2006) 302–311.

[70] O. C. Kwon, G. Rozenchan, C. K. Law, Cellular instabilities and self-acceleration of outwardly propagating spherical flames, Proc. Combust. Inst. 29 (2002) 1775–1783.

[71] F. Oppong, Z. Luo, X. Li, Y. Song, C. Xu, Intrinsic instability of different fuels spherically expanding flames: A review, Fuel Process. Technol. 234 (2022) 107325.

[72] S. Ravi, T. G. Sikes, A. Morones, C. L. Keesee, E. L. Petersen, Comparative study on the laminar flame speed enhancement of methane with ethane and ethylene addition, Proc. Combust. Inst. 35 (2015) 679–686.

[73] C. L. Tang, Z. H. Huang, C. K. Law, Determination, correlation, and mechanistic interpretation of effects of hydrogen addition on laminar flame speeds of hydrocarbon-air mixtures, Proc. Combust. Inst. 33 (2011) 921–928.

Influence of Hydrogen and Methane Addition in Laminar Ammonia Premixed Flame on Burning Velocity, Lewis Number and Markstein Length

Authors: Zitouni, S. (*), Brequigny P., Mounaïm-Rousselle C.,

Université Orléans, INSA-CVL, EA 4229 – PRISME, F-45072, France

(*) Corresponding Author Email:

seif-eddine.zitouni@univ-orleans.fr

Abstract:

The use of Ammonia (NH_3) and blends with either Methane (CH_4) or Hydrogen (H_2) obtained by in-situ NH_3 cracking, seem to be promising solutions to partially or fully decarbonise our energy systems. To strengthen understanding of fundamental combustion characteristics of these NH_3 blends, the outwardly propagating spherical flame configuration was employed to determine the flame speeds and Markstein lengths. The air/fuel mixtures were varied across a large range of compositions and equivalence ratios. In general addition of CH_4 or H_2 results in a linear and exponential increase in measured laminar burning velocity, respectively. Of the appraised mechanisms, Stagni and Okafor kinetics mechanisms yielded best agreement with NH_3/H_2 and NH_3/CH_4 flame speed measurements. With respect to measured Markstein length, for a fixed equivalence ratio, addition of CH_4 to NH_3 resulted in a linear reduction in stretch sensitivity for the tested conditions. For lean NH_3/H_2 flames, an initial decrease in Markstein length is observed up to 30 – 40% H_2 addition, at which point any further addition of H_2 results in an increase in Markstein Length, with a non-linear behaviour accentuated as conditions get leaner. Above stoichiometry similar stretch behaviour is observed to that of NH_3/CH_4. Different theoretical relationships between the Markstein length and Lewis Number were explored alongside effective Lewis Number formulations. For lean NH_3/H_2 mixtures, a diffusional based Lewis Number formulation yielded a favourable correlation, whilst a heat release model resulted in better agreement at richer conditions. For NH_3/CH_4 mixtures, a volumetric based Lewis Number formulation displayed best agreement for all evaluated equivalence ratios. For NH_3/H_2, changes in measured Markstein Length were demonstrated to potentially be the result of competing hydrodynamic and thermo-diffusive instabilities, with the influence of the thermo-diffusional instabilities reducing as the equivalence ratio increases. On the other hand, the addition of CH_4 to NH_3 results in the propensity of moderating hydrodynamic instabilities, resulting in a stabilising influence on the flame, reflected by increasing positive Markstein number values. Finally, a systematic analysis of the flame speed enhancements effects (kinetic, thermal, diffusive) of CH_4 and H_2 addition to NH_3 was undertaken. Augmented flame propagation of NH_3/CH_4 and NH_3/H_2 was demonstrated to be principally an Arrhenius effect, predominantly through the reduction of the associated activation energy.

Keywords: Ammonia-hydrogen, ammonia-methane, Laminar flame Speed, Lewis Number, Markstein Length

1. Introduction

The historical prevalence of hydrocarbon fuel usage to sustain our power and transport needs, and the associated greenhouse gas emissions produced, have resulted in important environmental and ecological adversities [1]. As such, in order to attain zero-carbon targets, the large-scale employment of renewable and carbon-free fuels within our energy systems is required to maintain a balanced trajectory between human development, progress and cohesion with the environment. In light of this context, Ammonia (NH_3) has emerged in recent years as an efficient zero-carbon hydrogen (H_2) carrier. Liquid NH_3 offers higher H_2 content than for example, ethanol, methanol and gasoline, in conjunction with exhibiting a higher volumetric energy density than that of liquid H_2 [2]. Due to NH_3 prevalent use in the agricultural industry, considerable storage and distribution infrastructure is already established [2]. Although NH_3 offers several advantages, there remains several practical combustion challenges, notably the control and reduction of pollutant emissions (NO_x and N_2O). Moreover, NH_3 exhibits slow burning velocities, often associated to low burning efficiency in engines, a narrow flammable range and high ignition energy, potentially yielding poor flame stabilisation and extinction characteristics resulting in local or global extinctions. To improve NH_3's combustion properties, blending NH_3 with methane (CH_4) (for a partial decarbonisation) or H_2 (from the possible 'in situ' cracking of ammonia) has been proposed, and has gained considerable recent attention, with comprehensive reviews of NH_3 related work undertaken [2], [3]. Successful demonstrations in both gas turbines [4]–[6] and internal combustion engines [7], [8] have been achieved at high temperatures and pressures. Nevertheless, studies remain limited, as such there seems to be a practical necessity to develop and strengthen understanding of fundamental combustion characteristics of blends containing NH_3, ultimately leading to the development of combustors offering greater flame stability and reduced pollutant emissions.

The unstretched laminar burning velocity (S_L^0), is one main fundamental physico-chemical property of any premixed air-fuel mixture, reflecting both the combustion process and mixture reactivity. As such, S_L^0 is a key parameter helping understand premixed operational instabilities, notably flashback, blow-off or extinction, and a central step in turbulent flame modelling [9]. Variations in fuel composition inherently introduce changes in transport and chemical properties, in turn influencing witnessed burning and reactivity characteristics of the fuel mixture. The Lewis number (Le), defined as the ratio of thermal to mass diffusivity of the deficient reactant, details the transport mechanisms of various species across the flame front [9]. Early experimental investigations [10],[11], supported by the development of asymptotic theories [12], [13], underline that preferential diffusion (i.e. Le deviating from unity), can strongly influence the burning rates of stretched flames – which undergo the combined effects of strain, curvature, and flame motion. Flames with Le > 1 exhibit greater relative thermal diffusivity, displaying a reduction in burning rate with increased stretch, due to heat loss to the unburned reactant. Conversely, flames with Le < 1 show a relative acceleration with increasing stretch [9]. The burnt gas Markstein length (L_b) is a measurable parameter which characterises the influence of Le on the flame response to the stretch rate. The Markstein number (Ma), defined as L_b divided by the laminar flame thickness (δ_L) – is an indicator of the propensity of a combustion system to be or not influenced by thermo-acoustic instability, and thus of interest to study [14].

Recent experimental studies have investigated S_L^0 and L_b characteristics of NH_3/air flames, notably by Hayakawa et al. [15], at atmospheric and 0.5 MPa of initial ambient pressure, and Kanoshima et al. [16], expanded on that work to include the influence of initial ambient temperature (400-500 K). Results from these studies underline that S_L^0 peaks at an equivalence ratio (ϕ) of ≈ 1.1, with an increase in pressure and temperature ensuing a decrease and increase in S_L^0, respectively. With respect to L_b, NH_3/air flames display an increasing L_b with increasing ϕ, a

similar trend to that of CH_4/air and H_2/air flames. It is noted that at normal temperature and pressure conditions (T=298K, P=0.1MPa) lean NH_3 flames exhibit negative L_b, with positive values recorded under rich conditions. Furthermore, L_b is observed to decrease with a rise in pressure and temperature, analogous behaviour to that of the flame thickness.

Okafor et al. [17], [18], investigated the influence of NH_3 on CH_4 based flames (up to ≈ 52% NH_3 by vol.%) across a wide range of ϕ and pressures (0.1 – 0.5 MPa), highlighting that S_L^0 decreases with increasing NH_3 fraction and pressure, developing a detailed and reduced kinetic mechanism. Experimental results of Shu et al. [19] on NH_3/CH_4 flames (298 K, 0.1 MPa), demonstrated similar tendency but with a uniform decrease in the flame flammability limits with NH_3 increase. They also highlighted the important role played by the H and OH radicals in NH_3/CH_4 flame propagation. In relation to flame stretch sensitivity of CH_4/NH_3 flames, Okafor et al. [17] emphasize the shift from a linear to a non-linear flame speed-stretch rate relationship exhibited with increasing ϕ and NH_3 fraction. It should be noted that this is unusual for fuels displaying Le values close to 1 (as is the case for pure CH_4 and NH_3), with this behaviour mainly attributed to an increase in the preheating zone thickness.

Lee et al. [20], [21] and more recently, Ichikawa et al. [22] and Lhuillier et al. [23] investigated the influence of H_2 upon NH_3 based flames. Ichikawa et al., demonstrated that at stoichiometric conditions (ϕ=1), S_L^0 increases non-linearly with increasing H_2 fraction, and decreases with increasing pressure. Lhuillier et al. reported an exponential increase in S_L^0 upon addition of H_2 at various initial conditions (298-473K, ϕ = 0.8 – 1.4, H_2 = 60% vol. max). With respect to the flame stretch sensitivity, Ichikawa et al.[22] reported a non-monotonic variation, with an initial substantial decrease in L_b with increasing H_2, prior to a minor increase in L_b upon further H_2 addition. Interestingly, this stretch behaviour dampens at higher pressures, with minimal variation in recorded L_b of NH_3 flames upon H_2 enrichment. Noteworthily, similar stretch-related non-monotonic trends have been observed for lean CH_4/H_2 flames [24].

Table 1: Summary of Literature Review

All references below employed the spherically expanding flame configuration

Fuel Mixture (vol.%)	Equivalence Ratio (ϕ)	T_u (K)	P_u (MPa)	Radiation Corrected	Ref
100% NH_3	0.7 – 1.3	298	0.1 – 0.3 – 0.5	No	[15]
100% NH_3	0.8 – 1.2	400 - 500	0.1 – 0.3 – 0.5	Yes	[16]
CH_4/NH_3 (up to 52% NH_3)	0.8 – 1.3	298	0.1	Yes	[17]
CH_4/NH_3 (up to 52% NH_3)	0.8 – 1.3	298	0.3 – 0.5	Yes	[18]
CH_4/NH_3 (NH_3; 10, 30, 50,70, 90%)	0.6 – 1.4	298	0.1 – 0.5	No	[19]
H_2/NH_3 (up to 30% H_2)	0.8, 1.0, 1.67	298	0.1	No	[20]
H_2/NH_3 (H_2; 10, 30,50%)	0.6, 0.8, 1.0, 1.25, 1.67	298	0.1	No	[21]
H_2/NH_3 (H_2; 0,5,10,15,20,40,60,80,100%)	1.0	298	0.1 – 0.3 – 0.5	No	[22]
H_2/NH_3 (H_2; 0,5,30,40,50,60%)	0.8 – 1.4	298 – 473	0.1	Yes	[23]

The importance of flame stretch sensitivity and Le goes clearly beyond the laminar flame regime. Lipatnikov and Chomiak [25], in their extensive review of molecular transport effects on flame propagation, highlighted that preferential diffusional instabilities affect both weak and strong

turbulent combustion. The influence of Le on turbulent flames has been reported in the course of experimental studies [26]–[28] as well as in direct numerical simulations [29], [30]. Although limited in scale, emerging studies focusing on turbulence-flame interaction for NH_3 and its blends with either H_2 and CH_4 underlined the potential role of preferential-diffusion and flame-stretch interaction upon turbulent flame characteristics. For example, Ichimura et al. [31] investigated NH_3/air flames at various turbulent intensities, underlining that although S_L^0 of NH_3/air is greatest at $\phi \approx 1.1$, lean mixtures exhibited better resistance to turbulence induced extinction than richer conditions, due to the potential thermo-diffusive accelerating effects of lean NH_3/air mixtures, displaying Le < 1. Similarly, Lhuillier et al. [8] investigated NH_3/H_2 and NH_3/CH_4 (15% vol. of H_2 or CH_4) turbulent flame propagation under engine related operating conditions (445K, 0.54 MPa). They reported a decreasing and increasing turbulent to laminar flame speed ratio upon CH_4 and H_2 addition, respectively, induced by the different thermo-diffusive properties and stretch-related behaviour of these ammonia blends.

Clearly, although emerging, the experimental study on the addition of H_2 or CH_4 to NH_3-based flames remains scarce. Furthermore, recent turbulent combustion experiments underlined the potential influence of preferential-diffusional instabilities upon NH_3-based flames [8], [31], [32], hence, the aim of this work is to investigate in detail the influence of Le change on flame behaviour. NH_3/CH_4 and NH_3/H_2 mixtures were varied across a large range of blend composition and equivalence ratio, representative of the prospective demands of fuel-flexible combustors widely employed for power generation. The addition of either CH_4 or H_2 to a given NH_3/air mixture increases flame temperature, reactivity, mixture flame speed but changes the thermo-diffusive behaviour, which is studied in-detail throughout this work.

2. Experimental set-up and specifications

Laminar flame speed measurements were performed using a constant-volume spherical vessel. Details of the apparatus and post-processing techniques can be found in [33], updated for NH_3 specifications in [23], and thus only a brief summary is presented herein. The spherical vessel is equipped with four orthogonal 70 mm quartz viewing windows and has a nominal internal volume of 4.2 L. Thermal mass flow controllers (Brooks 5850S (± 1%)) were employed to introduce the reactants into the vessel. Mole fractions of all species were determined as a function of temperature (T), initial pressure (P) and fuel-air equivalence ratio. A piezo-electric pressure transducer and a type-K thermocouple were employed to check respectively the pressure and temperature prior to ignition. The maximum deviation between the effective initial pressure inside the chamber and the required initial pressure was no more than 1%. A vacuum-pump was used to empty the combustion chamber twice between tests ensuring a residual pressure of no more than 0.009 bar, with the remaining air compensated within the equivalence ratio calculation. Pre-mixing was achieved using an internal fan. A capacitor-discharge ignition was achieved via fine tungsten electrodes mounted at 90° to the measurement plane. After quiescence is attained, simultaneous TTL signal to the data-acquisition and ignition systems trigger the experiments. High speed Schlieren imaging of flame propagation was accomplished using a CMOS high speed camera (Phantom V1210) set to a suitable frame capture rate (3000 – 12000 fps), facilitating a spatial resolution of ~0.10 mm per pixel. Edge-detection algorithms written in a bespoke MATLAB script were employed to calculate flame propagation rates. A minimum of 3 to 5 repeats were conducted per experimental condition.

3. Experimental specifications and theory

Measurements were performed at initial conditions of 298 K (± 3 K) and 0.1 MPa (± 1 x 10^{-3} MPa), with high-purity fuels (NH_3 (99.95%), CH_4 (>99.995%) and H_2 (99.999%)) and dry-zero compressed air (AirLiquide, 20.9% O_2). To investigate the influence of CH_4 and H_2 on NH_3 flame speed and stretch-related behaviour, molar ratios were varied form 0 – 100% for CH_4; and 0 – 80% for H_2, in incremental

steps across a wide range of equivalence ratios (ϕ= 0.7 – 1.2 and 0.6 – 1.4 respectively), with Table 2 summarising the experimental conditions.

Table 2: Experimental conditions ; T_u = 298 K (± 3 K), P_u = 0.1 MPa (± 1 x 10^{-3} MPa).

Equivalence Ratio (ϕ)	Percentage of Fuel in NH_3 (vol.%)	
	CH_4	H_2
0.6	/	20,30,40,50,60,80
0.7	20,30,40,50,60,80,100	/
0.8	0,10,20,30,40,50,60,80,100	0,10,20,30,40,50,60,80
0.9	0,10,20,30,40,50,60,80,100	0,10,20,30,40,50,60,80
1.0	0,10,20,30,40,50,60,80,100	0,10,20,30,40,50,60,80
1.1	0,10,20,30,40,50,60,80,100	0,10,20,30,40,50,60,80
1.2	0,10,20,30,40,50,60,80,100	0,10,20,30,40,50,60,80
1.4	/	20,30,40,50,60,80

Schlieren images were undertaken as in [17], [23], [34], with the shadowed edge considered as the burnt gas isotherm, which as discussed by Giannakopoulos et al. [35], is critical for characterising the influence of flame stretch. The laminar burning velocity and L_b relative to the burnt side were experimentally determined employing the same procedure as in previous studies [34], [36]. For an outwardly spherically propagating flame, the stretched flame speed (S_b) is expressed as the temporal derivative of the Schlieren flame radius (r_{sch}) as in Equation 1:

$$S_b = \frac{dr_{sch}}{dt} \quad (1)$$

The flame stretch rate (K) is defined as the change in flame area (A) gradient and calculated for a propagating spherical flame as shown in Equation 2:

$$K = \frac{1}{A} \cdot \frac{dA}{dt} = \frac{2}{r_{sch}} \cdot \frac{dr_{sch}}{dt} \quad (2)$$

Various correlations between S_b and K have been proposed, allowing the estimation of the unstretched flame speed (S_b^0). Wu et Law [10], proposed a linear relationship, based upon the assumption the flame is weakly stretched and that thermal and mass diffusion are near equal (Le≈1) and suggest that the flame speed and K are related as per Equation 3:

$$S_b = S_b^0 - L_b \cdot K \quad (3)$$

Hence, according to the theoretical model given by Equation 3, S_b^0 can be subsequently derived by extrapolation of the relationship to a corresponding intercept value (K = 0), equivalent to a flame radius of infinite radius. It may also be noted that L_b characterises the influence of stretch upon flame propagation, with the magnitude and sign of L_b related to Le. This linear model has been the most commonly employed for flame speed measurements using expanding spherical flames, however, as highlighted by Wu et al. [37], it is a first order correction of the stretch effect and hence some degree of uncertainty is the flame speed extrapolation is to be expected. In this work, this methodology will be referenced as LMS (i.e. Linear Model based on flame Stretch).

The second model is attributed to Frankel and Sivashinsky [38], first proposed by Markstein [39], is based upon the assumption of large flame radii. Frankel and Sivashinsky analysed spherically expanding flames considering the effects of thermal expansion and Le, obtaining the following relationship in Equation 4:

$$S_b = S_b^0 - S_b^0 \cdot L_b \cdot \frac{2}{r_{fsch}} \quad (4)$$

Equation 4 shows that the flame curvature ($\kappa_{curv}=2/r_{fsch}$) and S_b vary linearly, hence allowing the evaluation of S_b^0 and L_b from the linear extrapolation of S_b and $2/r_{fsch}$ [37], [40]. This method has not received widespread use [19], [34], [40], and here is referenced as LMC (i.e. Linear Model based on Curvature).

The third extrapolation method, attributed to Kelley and Law [41], is a non-linear model that allows for arbitrary Le and takes into account the deviations in adiabatic and planar assumptions, prominent in flames which are heavily influenced by stretch such as lean H_2-based flames. This non-linear model is expressed as in Equation 5:

$$\left(\frac{S_b}{S_b^0}\right) \cdot In\left(\frac{S_b}{S_b^0}\right)^2 = -\frac{2 \cdot L_b \cdot K}{S_b^0} \quad (5)$$

A quasi-steady nonlinear association between S_b and K is employed – rearranged with the error used for least squares regression – to obtain an extrapolated unstretched flame speed. This model has been used frequently over the last decade, improving accuracy [37], [42], and will be referenced here as the NMS (i.e. Non-Linear Model based on Stretch).

Chen [40] and Wu et al. [37] underline that the accuracy of different extrapolation techniques is related to the Le of the fuel-air mixture. Chen [40] demonstrated that LMS is only suitable for fuel/air mixtures that exhibit weak stretch and Le close to unity. Chen [40] showed that it is preferable to employ LMC for mixtures exhibiting positive L_b and NMS for negative L_b, due to the non-linear relationship between S_b and K; with these recommendations adopted in this study. Moreover, Wu et al. [37], quantified the uncertainty in extrapolation through the limitation of exploitable data range in relation to Markstein and Karlovitz numbers ($Ma_{lin}Ka_{mid}$); all data presented in this work fall within the recommended values of -0.05 – 0.15 range.

Irrespective of the extrapolation methodology employed, to obtain representative values of laminar flame speed, the burned gas expansion factor has to be used as $S_L^0 = S_b^0 \cdot (\rho_b/\rho_u)$ with adiabatic equilibrium densities calculated using CHEMKIN-Pro, employing the PREMIX software and using Stagni et al. [43] and Okafor et al. [18] kinetics reaction mechanisms, for NH_3/H_2 and NH_3/CH_4, respectively. The selection of these mechanisms is discussed later in section 5.2.

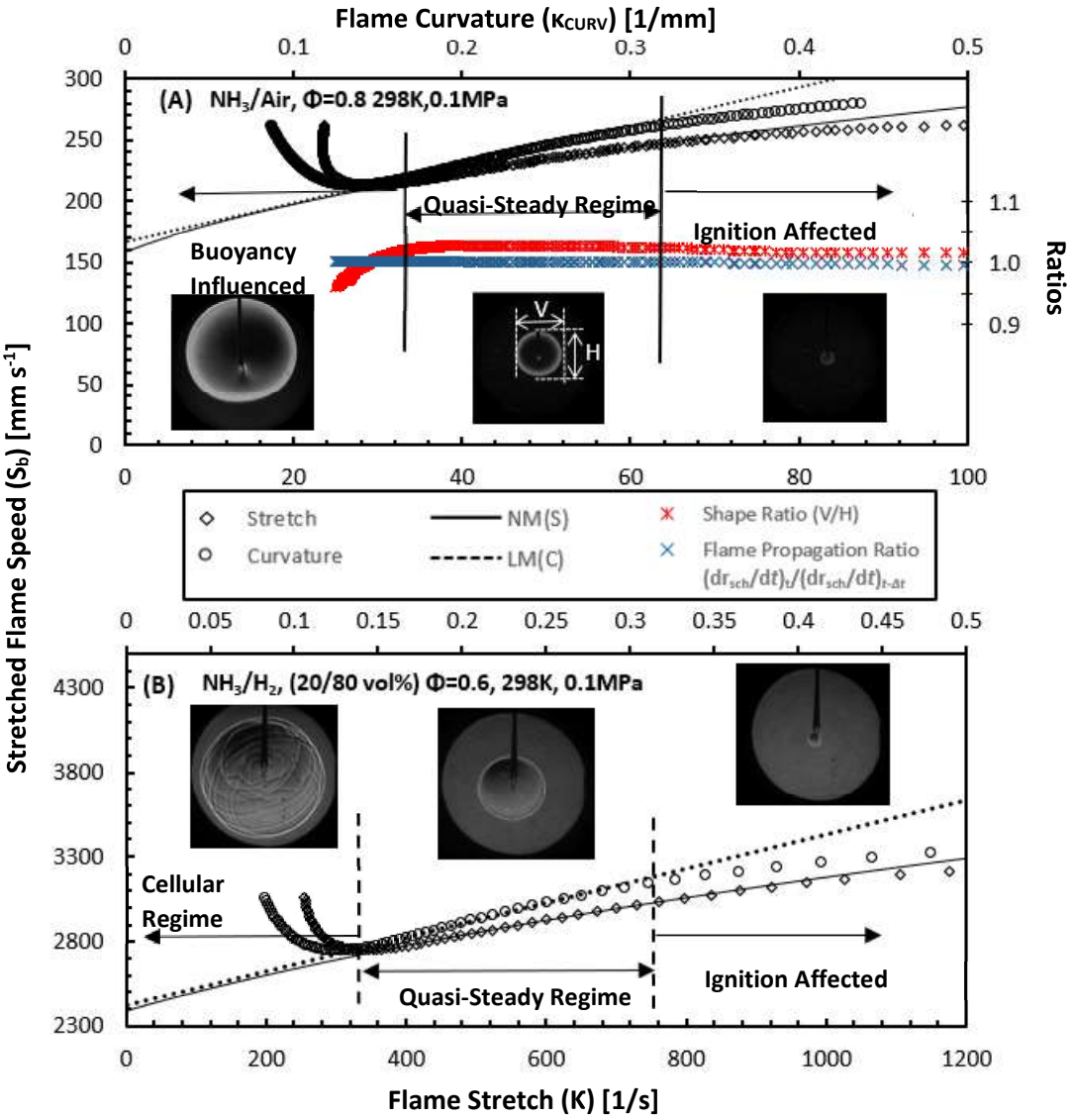

Figure. 1 – Stretched flame speed vs stretch rate (K) and curvature (κ_{CURV}) for (a) pure NH_3/air and (b) NH_3/H_2 (20/80 vol.%) (T_u – 298 K, P – 0.1 MPa)

Limits were set on the range of exploitable radii to minimise the influence of the spark, the buoyancy or the cellularity, and the confinement during the flame growth, ensuring measurements were restricted within the quasi-steady regime. Bradley et al. [44] suggest a spark affected radius up to 6 mm for CH_4/air flames, however Chen et al. [45] demonstrate this critical radius value to be dependent of Le. The capacitor-discharge ignition energy was varied in order to minimise the influence of the spark upon flame propagation. Preliminary investigation related to the influence of ignition energy demonstrated minimal variation in results derived from data above 7 mm. Consequently, for all data presented here, 8 mm was chosen as the minimum radius. To limit pressure effects a maximum radius of 25 mm was considered, within the 30% of chamber radius as proposed by Burke et al. [46]. Extrapolation methods used to yield flame speed and the corresponding L_b rely on a sufficiently large stable quasi-steady flame propagation regime. In the present study, pure NH_3/air flames, or blends containing less than 10% of CH_4 or H_2 (vol.%) at leanest and richest conditions were observed to be heavily influenced by the buoyancy, a consequence of their very low burning rate. As a result these flames were observed to lose sphericity, morphing in an ellipsoidal expanding flame, as noted by Hayakawa et al. [15] and Chen et al. [47] for identical initial conditions (298 K, 0.1 MPa). For such flames, the methodology proposed by Hayakawa et al. [15] in delimiting the transition between

ignition influenced, quasi-steady and buoyancy influenced propagation regimes was followed. The aforementioned regimes are determined based upon the flame shape and propagation ratio, defined as the vertical and horizontal radius of the flame ($r_{sch,V}/r_{sch,H}$) and $(dr_{sch}/dt)_t/(dr_{sch}/dt)_{t-\Delta t}$ (where dr_{sch}/dt denoting the flame propagation speed at time t), respectively. Figure 1.a illustrates the change in flame shape ratio and moving average of the flame propagation ratio against stretch for a lean NH_3/air flame (ϕ=0.80); with the relationship of stretched flame speed with stretch and curvature superimposed. As can be seen in Figure 1.a, a quasi-steady propagation regime is clearly identifiable, as such the point at which the flame shape ratio considerably changed (± 3%) was taken to represent the maximum flame radius limit. It should be noted that the upward motion of the growing flame kernel does not yield a significant influence upon the propagation speed, since change in the stretched flame speed still maintained proportionality to both flame-stretch and curvature until the transition point was attained. Under other conditions, minor modifications in useable flame radius selection were also required due to known instability issues associated with lean combustion of H_2-containing fuels. Lean H_2-based flames are particularly unstable with regard to diffusive effects, a consequence of their low Le (Le << 1), resulting in flame acceleration at low stretch and curvature rates [48], as illustrated in Figure 1.b, with an example case of a lean NH_3/H_2 (20/80 vol.%, ϕ=0.6) flame. Under the tested experimental conditions, it was noted that no flames developed a cellular surface composed of cells of comparable size. However, large cracks of a permanent nature appeared at leanest conditions (ϕ=0.60) for flames containing ≥ 40% H_2, with further H_2 enrichment enhancing surface cracking, as illustrated in Figure 2. As underlined by Jomaas et al. [49], these large-scale cracks are most probably the result of large-amplitude initial disturbances, most probably triggered by the ignition event, and not a consequence of preferential diffusion. Nevertheless, using a suitably fast frame capture rate, a minimum of 30 acquired radii was obtained even for the fastest flames, from which flame speed data were estimated.

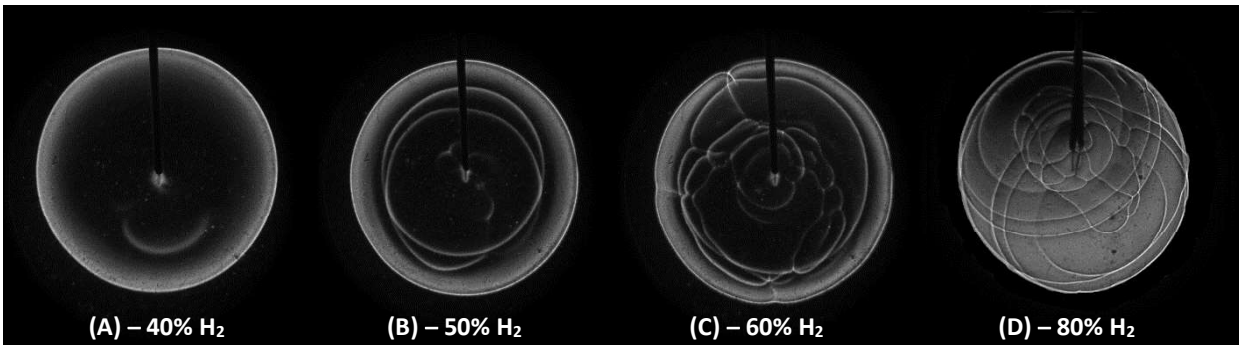

Figure 2 – Schlieren images illustrating the development of flame surface cracking as a function of H_2 fraction for NH_3/H_2 flames (T_u – 298 K, P – 0.1 MPa, ϕ=0.60)

The measurements of laminar flame speed are an essential step in order to improve the accuracy of reaction mechanisms [50]. Therefore, the quantification of the measurement uncertainties is required. For this study, uncertainty quantification relies upon the methods outlined by Moffat [51], employing a combination of the experimental facility specifications and accuracy of the processing techniques employed. It should be noted that the uncertainty is quantified for the unstretched flame speed (S_b^0), and not for S_L^0, since this is the parameter measured, here named as $U_{S_b^0}$.The total uncertainty estimate is given by Equation 6, where $B_{S_b^0}$ represents the total bias uncertainty, $t_{M\text{-}1.95}$ the student's value at 95% confidence interval and M-1 degrees of freedom, $\sigma_{S_b^0}$ the standard deviation of the repeated experiments, and M the number of experimental repeats at each condition;

$$U_{S_b^0} = \sqrt{B_{S_b^0}^2 + \left(\frac{t_{M-1,95}\sigma_{S_b^0}}{\sqrt{M}}\right)^2} \quad (6)$$

The total bias uncertainty, given by Equation 7, relating changes in S_b^0 with respect to an independent influential variable, (v_i, i.e. temperature, ambient pressure, ϕ, optical system, gas mixture quality) and the fixed error linked to that variable, y_i,

$$B_{S_b^0} = \sqrt{\sum_{i=1}^{n} \left(\frac{\partial S_b^0(v_i)}{\partial v_i} y_i\right)^2} \quad (7)$$

In order to determine $B_{S_b^0}$ by Equation 7, the relationships between S_b^0 and each independent variable must be established. As applied in [23], the potential changes in S_b^0 from several parameters are calculated as a function of ϕ; such as temperature (±3 K) and pressure (±1 x 10^{-3} MPa) by using data modelling with CHEMKIN-PRO. Uncertainty resulting from the mixture preparation was estimated to be ± 0.01%, that of the optical system was evaluated from the summated fractional error of both the spatial resolution of the system (±0.05/25mm) and camera (± 1.5-7.5/3000-15000 fps). Losses due to radiation influence measured flame burning speed, through the combined effect on the flame propagation itself and the calculated density ratio, with radiation-induced uncertainty particularly significant for slow propagating flames (< 12 cm s^{-1}) [52]. Lhuillier et al. [23] investigated the dependence of errors resulting from radiation for NH_3/air flames, concluding that the correlation proposed by Yu et al. [52] was applicable, with this recommendation applied for this study. For the experimental results in this study, the greatest radiation-induced error (~23%) was related to leanest NH_3/air flame measured (ϕ = 0.80), indicating that the laminar flame speed was underestimated by ~ 0.56 cm/s. Finally, error bars on all subsequent plots illustrating laminar flame speed measurements (S_L^0) are derived from Equation 6 and 7, with the error for $U_{S_b^0}$ scaled with respect to the density ratio.

4. Evaluation of Fundamental Parameters

Chen and Ju [40], [45] and Matalon and Bechtold [53], have proposed theoretical relationships relating the Markstein length (L_b) and Lewis Number (Le), requiring the evaluation of various fundamental flame parameters. The Zel'dovich number, was evaluated using the expression $Ze = (E_a/R_u) \cdot [(T_{ad} - T_u)/(T_{ad}^2)]$ with R_u the universal gas constant, T_u and T_{ad}, the temperature of the unburnt mixture and the adiabatic flame temperature, respectively. The activation energy, E_a, is defined as the slope of the mass burning flux (m^0) and the inverse adiabatic flame temperature at constant ϕ and pressure, empirically determined using the expression $E_a = -2R_u\{\partial[\ln(m^0)]/\partial[1/T_{ad}]\}$, where the mass burning flux can be replaced by $m^0 = (\rho_u \cdot S_L^0)$, as recommended by Egolfopoulos and Law [54]. It should be noted that this method is only valid for sufficiently off-stoichiometric conditions, with interpolation required for E_a values for mixtures near stoichiometry [55]. For the flame thickness, two definitions can be considered [9]. The first, commonly termed as the kinetic (or diffusion) flame thickness (δ_K), is defined as $\delta_K = \lambda/(\rho_u \cdot c_p \cdot S_L^0)$, where λ represents the thermal conductivity and c_p the specific heat at constant pressure. The second, referenced as the 'gradient' flame thickness (δ_G) can be expressed as $\delta_G = (T_{ad} - T_u)/(dT/dx)_{max}$.

4.1 Relationships of Le and L_b

For the purpose of this work, the relationships relating Le to L_b, proposed by Chen [40], [45] and Matalon and Bechtold [53] are considered. The first formulation based on spherically expanding flames is derived from the analytical developments done by Chen and Ju, and then used by Bouvet et al. [56], Lapalme et al. [57] and Zitouni et al. [34] in their studies on preferential-diffusion effects upon

multi-component fuels. It should be noted that the 'kinetic' flame thickness is consistent with the approach detailed by Chen [40], [45]. This estimate of Le is referenced herein as Le_{CHEN} and can be expressed per Equation 8:

$$Le_{CHEN} = \left[\frac{L_b}{\sigma \cdot \delta_K} - \frac{Ze}{2}\right]^{-1}\left[1 - \frac{Ze}{2}\right] \tag{8}$$

With $\sigma = \rho_b/\rho_u$, the expansion ratio. From Equation 8, the retrieval of L_b is possible as in Equation 9.

$$L_{b-CHEN} = \left[\frac{1}{Le} - \left(\frac{Ze}{2}\right)\left(\frac{1}{Le} - 1\right)\right]\sigma \cdot \delta_K \tag{9}$$

A second formulation by Bechtold and Matalon, was derived from theoretical analysis on the dependence of L_b on stoichiometry. This formulation was considered by Jomaas et al. [49] in the case of acetylene (C_2H_2), Lapalme et al. [57] for H_2/CO and Zitouni et al. [34], for CH_4 blended with H_2 or C_3H_8. Lapalme et al. [57], on their assessment of the method of calculating Le and comparison with experimental results, demonstrate that employing the kinetic flame thickness definition with the Bechtold and Matalon relationship results in much higher values of Le than plausible. Similar conclusions are drawn by Zitouni [58], hence the 'gradient' flame thickness is employed. This estimate of Le is denoted in following as Le_{BM}, and is expressed per Equation 10:

$$Le_{BM} = 1 + \left[\frac{L_b}{\delta_G} - \frac{2}{\sqrt{\sigma}+1}\right]\left[\frac{2 \cdot Ze}{\sigma - 1}\left\{\sqrt{\sigma} - 1 - In\left(\frac{1}{2}\left(\sqrt{\sigma}+1\right)\right)\right\}\right]^{-1} \tag{10}$$

Which provides $L_{b\text{-}BM}$ as per Equation 11:

$$L_{b-BM} = \delta_G\left[\frac{\gamma_1}{\sigma} - \left\{\frac{Ze}{2}(Le-1)\gamma_2\right\}\right] \tag{11}$$

where γ_1 and γ_2 are functions of the expansion ratio given in Equation 12:

$$\gamma_1 = \frac{2 \cdot \sigma}{\left(\sqrt{\sigma}+1\right)}\ ; \quad \gamma_2 = \left[\frac{4}{\sigma - 1}\right]\left[\sqrt{\sigma} - 1 - In\left(\frac{\sqrt{\sigma}+1}{2}\right)\right] \tag{12}$$

4.2 Lewis Number evaluation of multi-component fuels

Whilst the definition of the Lewis Number for single-fuel mixtures is relatively straightforward, no clear consensus on the correct formulation of Le for multi-fuel mixtures seems to exist [56]. The challenge arising from the fact that the diffusivity of each fuel must be considered. This is particularly applicable when the transport diffusion mechanisms are different as is the case for H_2, NH_3 or any alkanes. Bouvet et al. [56] identified three 'effective' Le formulations. The first formulation is based upon a volumetric fraction weighted average, resulting from Muppala et al. [26] computational study of turbulent $CH_4 - H_2/C_3H_8$ flames. At low-turbulence, this formulation results in reasonable agreement between modelled and experimental burning velocities; whilst at higher turbulent intensity modelled burning rates significantly underpredicted measurements. This volume weighted formulation will be referenced in this work as Le_V, and is expressed per Equation 13:

$$Le_V = \sum_{i=1}^{f} x_i \cdot Le_i \tag{13}$$

where x_i, is the fuel volumetric or mol fraction of the species i.

The second Le formulation is derived by Law et al. [59] from the asymptotic analysis of high pressure H_2/C_3H_8 laminar spherical flames. This formulation has been widely employed to discuss the thermo-

diffusive behaviour of mostly binary and tertiary blends of hydrocarbons and hydrogen [27], [60]. This formulation is based upon the weighted average of the fuels' nondimensional heat release (q_i), referenced in this work as Le_H, and expressed as per Equation 14:

$$Le_H = 1 + \frac{\sum_{i=1}^{f} q_i (Le_i - 1)}{\sum_{i=1}^{f} q_i} \quad (14a)$$

where

$$q_i = \frac{Q \cdot Y_{i,unburnt}}{c_p \cdot T_u} \quad (14b)$$

with Q representing the overall heat of reaction, Y_i, the mass fraction of species i.

The third one is related to the work conducted by Dinkelacker et al. [27] on lean H_2/CH_4 flames. It is assumed that if the flame curvature is dominant, then the local enrichment of the most diffusive fuel at the flames leading edge can be expected. This overall reaction-rate enhancement is translated into a volumetric-weighted average of the fuel diffusivities. This diffusion weighted formulation will be referenced in this work as Le_D, and expressed per Equation 15:

$$Le_D = \frac{D_T}{\sum_{I=1}^{F} x_i \cdot D_{ij}} \quad (15)$$

where D_T is the mixture's thermal diffusivity and D_{ij} are the binary mass diffusion coefficients. Several methods have been proposed to estimate the binary mass diffusion coefficients at moderate ambient pressure (<10 bar), with empirical constants based upon experimental data [61]. The method of Wilke as well as that of Hirschfelder, Bird and Spot, detailed in [61], is used in this study. Once the binary coefficients for the combinations of gases are estimated, an effective formulation of the deficient species in the mixture must be designated. For lean fuel-air mixtures, the deficient reactant is scarce compared to the surrounding N_2 [9]. For that reason, D_{ij} is taken as the fuel, '*i*', diffusing into N_2 (denoted with the subscript j). This may hold true for hydrocarbons due to their high molar fuel-air ratio, but not for fuels that have low molar fuel-air ratio such as H_2, as underlined by Lapalme et al. [57]. Thus, as proposed by Wilke [62], the mixture-averaged coefficient of mass diffusion ($D_{i,mix}$) into the mixture was employed as defined in Equation 16:

$$D_{i,mix} = (1 - Y_{i.mix}) \left(\sum_{\substack{s=1 \\ s \neq i}}^{N} \frac{X_s}{D_{is}} \right)^{-1} \quad (16)$$

where Y is the mass fraction of the species '*i*' and '*X*' the molar fraction of each species '*s*' in the mixture; with details of the method available in [61]. In order to ensure the correct application of the method, the binary diffusion coefficients calculated in this work were compared with values generated employing the STANJAN transport calculator [63]. Differences were no greater than ±3% for binary blends containing CH_4, NH_3, O_2 and N_2, and up to 10% in the presence of H_2, in agreement with expected deviations [61]. This would translate to a maximum difference of < 3% upon the theoretical Le for H_2 air/flames, and < 1% for blends containing CH_4 and NH_3, and thus the derived coefficients are deemed suitable for the purpose of this study.

Irrespective of the Lewis Number formulation employed, the thermal diffusivity $D_T = \lambda / (\rho_u \cdot c_p)$ has to be evaluated. The calculation of ρ_u and c_p (specific heat capacity at constant pressure) were

based on the ideal gas theory and are relatively straightforward. The evaluation of the thermal conductivity for each individual species (λ_i) was calculated based upon the Chung et al. [64] method and outlined by Poling et al. [61]. This calculation procedure uses a predictive method to estimate λ_i, and requires only the critical temperature (T_c), volume (V_c) and pressure (P_c) as inputs, available in [61]. This correlation has been compared to extensive testing with experimental data and demonstrated to be robust, with deviations of expected λ_i < 6% [65]. For multi-component fuels, the mixed average thermal conductivities (λ_{mix}) were calculated using Mathur et al.'s [66] suggestion:

$$\lambda_{mix} = \frac{1}{2}\left(\sum_{i=1}^{N} x_i\lambda_i + \frac{1}{\sum_{k=1}^{N}\frac{x_i}{\lambda_i}}\right) \quad (17)$$

Where (x_i) and (λ_i) are the mole fraction and thermal conductivity of the 'ith' species, respectively. This method has previously been employed by Bouvet et al. [56], in their study of Le for multi-component fuel mixtures. To ensure the validity and correct application of the methodologies employed to calculate the thermal diffusivity, evaluated vales were compared to values calculated using the STANJAN transport calculator [63] for single and binary mixtures. Differences are less than ± 3%, irrespective of the number of fuels composing the blend, thereby validating the robustness of the methodologies selected, and thus deemed suitable for the purpose of this work.

5. Results and Discussion

5.1 Pure Fuels

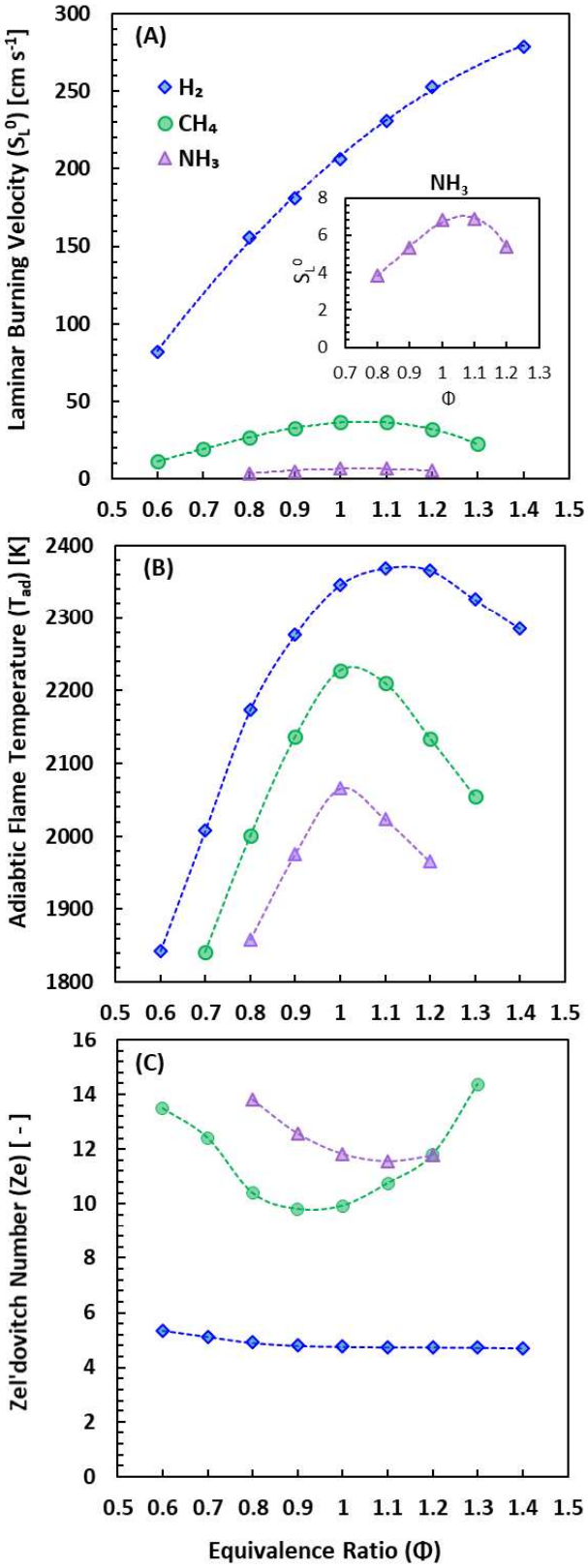

Figure 3 – Comparison of (a) laminar burning velocity, (b) Adiabatic flame temperature and (c) Zel'dovich number as a function of equivalence ratio for pure NH_3, CH_4, and H_2/air flames at 298 K & 0.1 MPa. S_L^0 data for H_2/air flames from [67].

The measured S_L^0 for the pure NH_3, CH_4 and H_2 /air flames are compared in Figure 3.a. NH_3/air flames display the slowest flame propagation rates, five to six times slower than those of CH_4/air flames; with a similar difference in flame speed magnitude between H_2/air and CH_4/air flames at stoichiometric conditions. It should be noted that the thermal diffusivity of these fuels decreases in the order of H_2, CH_4 and NH_3, analogous to the decreasing S_L^0 values. Comparison of the measured pure fuel flame speeds for CH_4/air and NH_3/air with other peer-reviewed datasets [17], [68]–[73], alongside values attained numerically, are located in the supplementary materials (SM). With respect to CH_4/air (SM.1), excellent agreement is displayed with selected literature [17], [68],[69], particularly with datasets from [17], [68], both employing the NM(S), with the Okafor et al. [18] reaction mechanism exhibiting excellent agreement with measured results in this study. With respect to NH_3/air (SM.2), measurements of S_L^0 remain limited. Good agreement is observed with Hayakawa et al. [15] and Lhuillier et al. [23], who both employed the spherically expanding flame method. Very good agreement is also observed with the dataset of Han et al. [71], who employed the Heat Flux Method. However, overall relatively large scatter is observable between the various datasets, with relative differences close to ~30% and 25% under rich (ϕ=1.2) and lean conditions (ϕ=0.9). These differences may potentially be attributable in part to the different experimental methods employed, as well as the fact that not all the datasets compared have taken into account losses due to radiation, with radiation-induced uncertainty particularly significant for slow propagating flames (< 12 cm s^{-1}) [52]. With respect to the appraised reaction mechanisms, all reaction mechanisms greatly over-predict NH_3/air S_L^0 at leanest conditions (ϕ=0.8) and under rich conditions (ϕ>1.1). Overall, good agreement is observed only at ϕ=0.9 – 1.0 with Okafor et al. [18] and Stagni et al. [43] reaction mechanisms, with best agreement overall with Okafor et al. [18].

The adiabatic flame temperature and activation energy (represented by Ze) with respect to ϕ for the aforementioned pure fuels is illustrated in Figure 3 (b) and (c), respectively. For CH_4 (and in general C_{1-4} alkanes), S_L^0 and T_{ad} peak at conditions slightly richer than stoichiometric conditions (ϕ~1.05 – 1.10), underlining the sensitivity of the flame propagation to the flame temperature. The fact that the minimum activation energy is located at similar conditions (ϕ~0.9), underlines the dictating influence of the flame temperature on the global activation energy. Due to flames temperatures peaking at around stoichiometric conditions, temperature-sensitive branching reactions are facilitated, thereby leading to overall faster reactions and reduced global activation energies, as highlighted by Jomaas et al. [49]. With respect to H_2, a similar trend in Ze is observed when plotted upon a much larger range of ϕ than that illustrated in Figure 3 (c). Viewed across the total flammability range of H_2 a similar parabolic relationship analogous to that exhibited by CH_4 and NH_3 is apparent. Although H_2 flame temperature peaks at similar conditions to that of CH_4 (ϕ~1.1 – 1.2), both the maximum flame speed and minimum values of Ze are located at much richer conditions ($S_{L,max}^0$ for ϕ ~1.6-1.8 [74], $Ze_{,min}$ for ϕ ~1.4 – 1.6). This shift in the flame speed to richer conditions (and by extension the reduced influence of flame temperature on S_L^0) has been attributed to the much larger value of the Lewis Number (Le >> 1 for ϕ >1.6), with flame acceleration, a consequence of preferential diffusion [49]. As a result, the minimum Ze witnesses a corresponding shift to richer conditions, since Ze is directly extracted from the flame speed (see Section 4). Thus, a transport mechanism (i.e. the thermo-diffusive response of the fuel for Le >> 1) generates a change in response in the flame speed, which subsequently impacts the flame property, highlighting the influence of transport on a supposedly chemical property [49]. This is of importance when attempting to understand behaviour of fuel blends which possess different transport properties (as it is the case here with H_2, CH_4 and NH_3) and the subsequent consequence on flame behaviour. On the other hand, for NH_3, S_L^0 and T_{ad} peak at approximately at the same equivalence ratio ranges (ϕ~1.0 – 1.10). The fact that the maximum flame speed, adiabatic flame temperature and minimum Ze all arise at nominally identical ϕ conditions

underlines the equi-diffusive nature of NH_3, with Le close to unity, comparable to the preferential-diffusional properties of pure CH_4.

In premixed flames, instabilities can result from both preferential-diffusional and hydrodynamic (Darrieus-Landeau) instabilities. It should be highlighted that the Marsktein length (L_b) indicates the response of the flame to the stretch, it is also an indicator of the flame's propensity to instability and not the cause of the instability. Figure 4 presents measured L_b from the present study as well as some other measurements available in literature, at similar initial temperature (±5 K) and pressure conditions, for NH_3 [15], [70], CH_4 [17], [68], [75] and H_2 [60], [67] flames from lean to rich conditions. To facilitate fair comparison, it is also indicated in the legend what methodology was used to extrapolate L_b (Linear or Non-Linear Model by Stretch (LMS) or (NMS); Linear Model based on Curvature, (LMC)). First, it should be noted that there exist very limited experimental L_b datasets for NH_3. At first there appears to be relatively large scatter between the various datasets, particularly for NH_3 and rich CH_4 flames. However, good agreement is observed between datasets when the same or a similar extrapolation method are compared, irrespective of the fuel evaluated. For example, good agreement is observed between our measured L_b values for NH_3 and CH_4 when employing LM(S) and those of Hayakawa et al. [15] and Gu et al. [17] respectively, who also employed LM(S). Similarly, when employing LM(C) and comparing results to research groups that employed NM(S), excellent agreement is also observed, irrespective of the fuel, with results from both extrapolation models expected to be similar, as highlighted by Chen [40]. The above highlights the influence that the extrapolation models have on the Markstein Length. All three fuels exhibit an increasing L_b as a function of ϕ increase from lean to rich conditions with the greatest change exhibited by NH_3, with negative value of L_b under lean conditions (comparable to that of H_2), and larger positive value than that of CH_4 and H_2 under rich conditions.

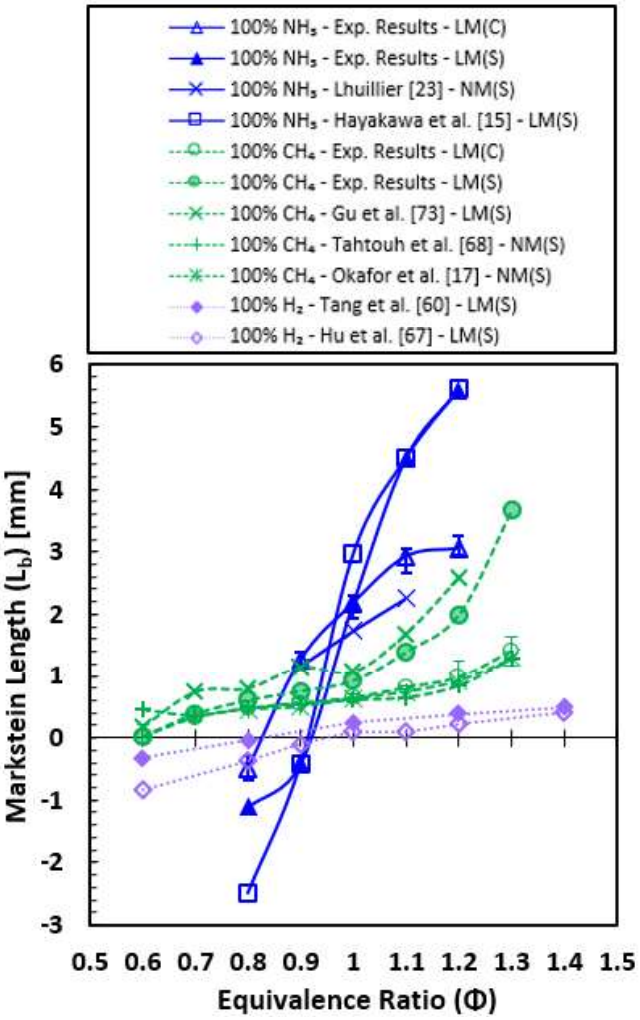

Figure 4 – Experimental values of L_b for pure NH_3, CH_4, H_2 as a function of ϕ (298 K, 0.1MPa).

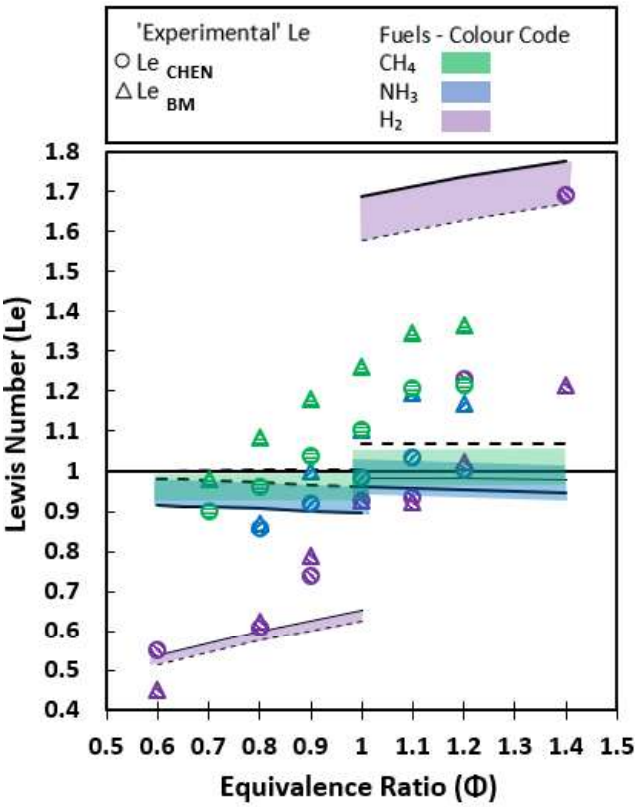

Figure 5 – Theoretical and experimental Le for NH_3, CH_4, H_2 as a function of ϕ (data for H_2 [67]). Full and dotted lines respectively reflect Hirschfelder and Wilke methods to evaluate D_{ij} (298 K, 0.1MPa)

To better understand the changes in the stretch response of pure fuels/air flames, the evolution of the corresponding Le is presented in Figure 5, from lean to rich mixtures. 'Theoretical' Lewis numbers, estimated using the free-stream properties of the mixtures, are illustrated as colour bands with the upper and lower limits (represented by full and dashed lines) denoting the differences between either the Hirschfelder or Wilke method to evaluate the mass diffusion coefficient. While the correct Le is evaluated (Le ~ 1 for NH_3 and CH_4; Le << 1 at $\phi < 1$ and Le >> 1 at $\phi > 1$ for H_2), little variation is observable across the considered ϕ, aside from the transition from lean to rich conditions. Furthermore, it should be highlighted that minimum Le for NH_3 is just prior to stoichiometric conditions in agreement with [15], whilst for CH_4 and H_2, minimum Le is obtained at leanest conditions. Since Le was simply evaluated as a function of the mixture's thermal and mass diffusivity, variations in fundamental flame parameters such as the flame thickness, the activation energy and the expansion ratio [53] were not considered. As such, Le can be evaluated from the experimental L_b and these other properties affecting the flame, as recommended by Jomaas et al. [49], with the use of theoretical relationships established in literature (denoted as Le_{CHEN} and Le_{BM}, Eqn. 8 and 10, accordingly). Therefore, as it can be seen when comparing Figure 4 and 5, analogous L_b and Le evolution as a function

of the fuel and the equivalence ratio is observable, regardless of the theoretical relationship relating L_b to Le. However, it is interesting to note that the greatest change in L_b magnitude is observed for NH_3, whilst exhibiting least change in Le, as noted by [8], potentially alluding that Le may not be the main driving factor behind the measured changes in stretch sensitivity for NH_3-based flames. Furthermore, the transition from a negative to positive L_b for NH_3 obtained for $\phi \sim 0.8 - 1.0$ is at comparable ϕ with the transition from Le < 1 to Le > 1 occurred.

In order to assess how well the considered formulations captured Le behaviour the lean and rich limits of Le for each fuel was evaluated. The Le limits bound the minimum (lean) and maximum (rich) plausible Le values for ultra-lean and ultra-rich mixtures. To estimate those limits the upper and lower flammability limits of the fuels were utilised. With respect to CH_4, lean and rich limits were evaluated to be 0.93 and 1.07, respectively, marginally smaller than those reported previously, namely 0.955 [27] and 1.10 [57], underlining the equi-diffusive nature of CH_4. As can be seen from Figure 5, Le_{CHEN} best respects these limits, particularly at richest conditions, in agreement with similar conducted by Lapalme et al. [57] and Zitouni et al. [34]. For H_2, Le lean and rich limits were estimated to be 0.34 and 2.02, respectively. On the lean side, this is in good agreement with literature, 0.29 [57], whilst on the rich side, Le limits evaluated in this work (2.02) are smaller than other reported values, 2.32 [76] and 2.58 [57], potentially due to the underestimation of the H_2 binary mass diffusion coefficients, as underlined previously (Section 4.2). Nevertheless, good agreement is attained by all formulations for H_2. With respect to NH_3, with lean and rich limits of 0.89 and 1.08, respectively, similar in scale to those of CH_4. Although no sources were found to compare the Le limits of NH_3, Hayakawa et al. [15] evaluated an Le of 0.95 and 1.09, for NH_3/air mixtures under lean (Φ = 0.7) and rich (Φ = 1.3) conditions, respectively (flammability limits of NH_3; $\Phi_{min} \sim 0.63$ and $\Phi_{max} \sim 1.4$). Overall, Le_{CHEN} best captures expected thermo-diffusive behaviour of NH_3.

5.2 Binary Fuel Mixtures

The influence of increasing fraction of either CH_4 or H_2 on NH_3/air S_L^0, across a wide range of Φ is depicted in Figure 6 and 7 respectively, alongside values attained numerically. With respect to NH_3/H_2 blends, the Tian et al. [77], Shrestha et al. [78], Gotama et al. [79], Okafor et al., [18] and Stagni et al. [43] reaction mechanisms were all appraised, however only the latter is illustrated since it consistently gave best agreement with all NH_3/H_2 blends evaluated in this study. Similarly, with respect to NH_3/CH_4 blends, only the Okafor et al. [18] is depicted since it consistently yielded best agreement with the evaluated blends.

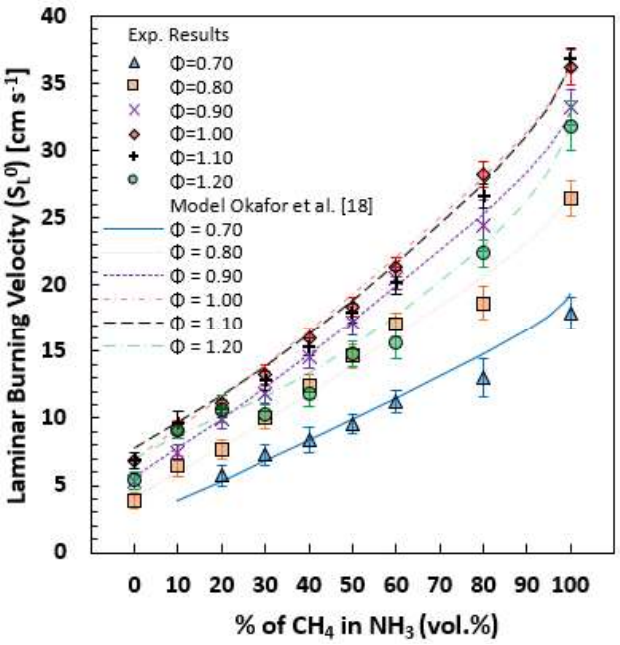

Figure 6 – S_L^0 for binary NH_3/CH_4 mixtures, comparison with simulated values with Okafor et al. kinetics model [18] (298 K, 0.1MPa)

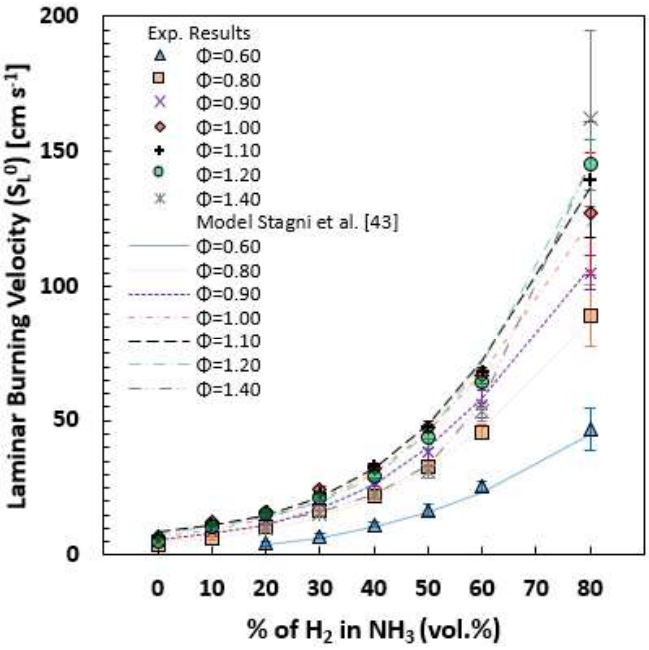

Figure 7 – S_L^0 for binary NH_3/H_2 mixtures, comparison with simulated values with Stagni et al. kinetics mechanism [42] (298 K, 0.1MPa)

As can be seen in Figure 6, irrespective of the Φ, a fairly linear increase in NH_3 flame speed is observable upon CH_4 addition, with the Okafor et al. [18] mechanism exhibiting very good agreement with measured results. On the other hand, as illustrated in Figure 7, an increase in H_2 addition results in an exponential increase in S_L^0 of NH_3 based flames, across the entire tested ϕ range. The Stagni et al. [43] mechanism best captured this exponential increase in flame speed, showing excellent agreement with experimental values from this study, across all tested conditions. It is worth highlighting that ~ 10-20% addition (vol.%) of either CH_4 or H_2 results in a similar increase in NH_3 flame speed, with further increases resulting in very different flame speed behaviour. This increased reactivity of NH_3 based blends upon CH_4 and H_2 addition has been previously suitably reported [19] [80], with modelling work and sensitivity analysis suggesting that the flame speed, burning intensity (Q') and production of radicals, particularly O and H appear to be strongly correlated.

To investigate the stretch-related behaviour of NH_3/CH_4 and NH_3/H_2 flames, L_b is plotted as a function of either CH_4 or H_2 addition to NH_3 across a wide range of ϕ in Figure 8 and 9, respectively. Note that the evolutions of L_b as a function of ϕ are in SM3 and 4. For a $\phi \geq 0.9$, a linear decrease in L_b is observed with increasing CH_4 fraction. At $\phi = 0.80$, a negative value L_b is obtained for pure ammonia while 10% CH_4 addition results in L_b sign inversion (from negative to positive). As pure NH_3/air mixtures could not be ignited for $\phi < 0.8$, with this experimental apparatus, this tendency cannot be verified. Under rich conditions ($\phi \geq 1.1$), a decreasing stretch sensitivity is measured upon increasing H_2 fraction, similar in trend and magnitude to that observed for NH_3/CH_4 flames but for $\phi \geq 0.9$. However, interestingly for $\phi \leq 1.0$, an initial decrease in L_b is observed up to 30 – 40% H_2 addition, at which point any further addition of H_2 results in an increase in L_b, with non-linear behaviour accentuated as conditions get leaner. Similar non-monotonical variation in stretch-related behaviour was measured by Lhuillier [70] as well as by Ichikawa et al. [22], for NH_3/H_2 flames, at $\phi = 1.0$ and ostensibly identical experimental conditions (T_u = 298 K, P_u = 0.1 MPa), also plotted in Figure 9 for comparison purposes. As such, under lean conditions, NH_3/H_2 mixtures exhibit a greater negative L_b than that of pure H_2

flames. It should be highlighted that similar non-linear L_b behaviour was measured by Okafor et al. [24] for CH_4/H_2 flames, with an inflection point occurring upon ~ 70% H_2 addition. Similarly, Huang et al. [81] also reported similar behaviour for natural gas – hydrogen – air blends. As such, it may seem that this maybe a phenomenon attributable to the H_2 contribution, at least for NH_3 or CH_4 based flames, due to the strong and fast diffusivity of H_2 in the reactants. This stretch-sensitivity behaviour is of importance since the flames exhibiting negative L_b will be accelerated in highly stretched turbulent environments, whilst flames displaying a positive L_b will be weakened. This stretch-sensitivity response inevitably impacts the operation of practical combustion systems.

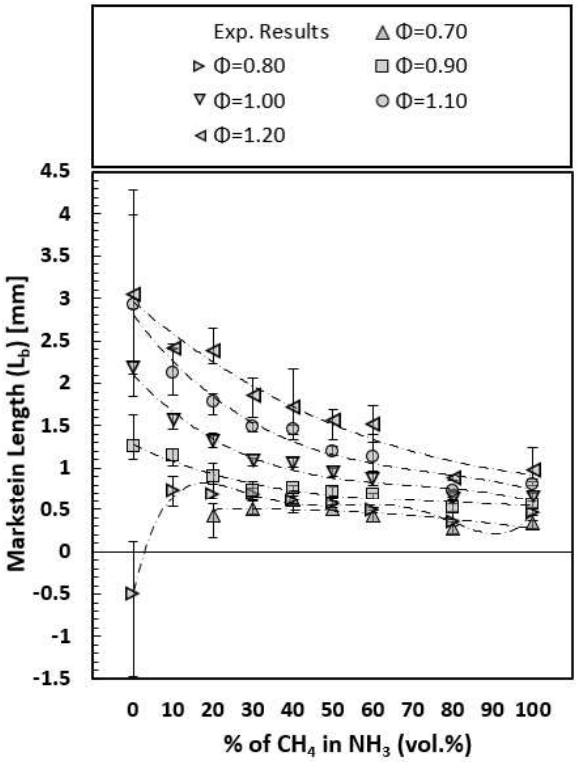

Figure 8 – L_b values of NH_3/CH_4 mixtures (298 K, 0.1 MPa)

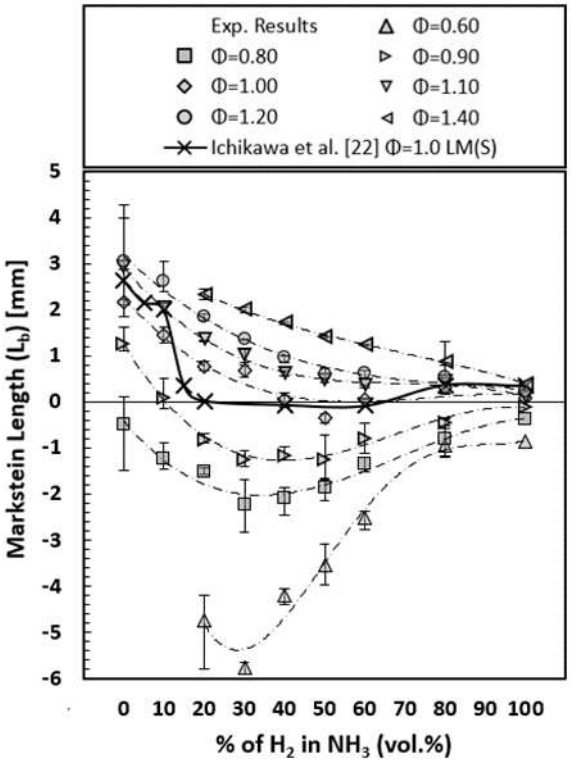

Figure 9 - L_b values of NH_3/H_2 mixtures (298 K, 0.1 MPa) 100% H_2 L_b values from [62]

For a better understanding of this change, a sensitivity analysis related to the contribution of major flame enhancing pathways (diffusive, thermal, kinetic) was undertaken. However, to correctly quantify the diffusive pathway, the most suitable Le formulation has to be considered. As such, the different Le_{eff} models (i.e. Le_V, Le_H, Le_D from Equations 12, 13 and 14 respectively) are used to yield to an estimate of L_b, by using the relationships proposed by Chen or Matalon and Bechtold, referred as L_b-Chen and L_b-BM, respectively. It should be noted that the purpose of such analysis is more qualitative than quantitative to validate which Le_{eff} model best captures the measured L_b behaviour of the tested blends.

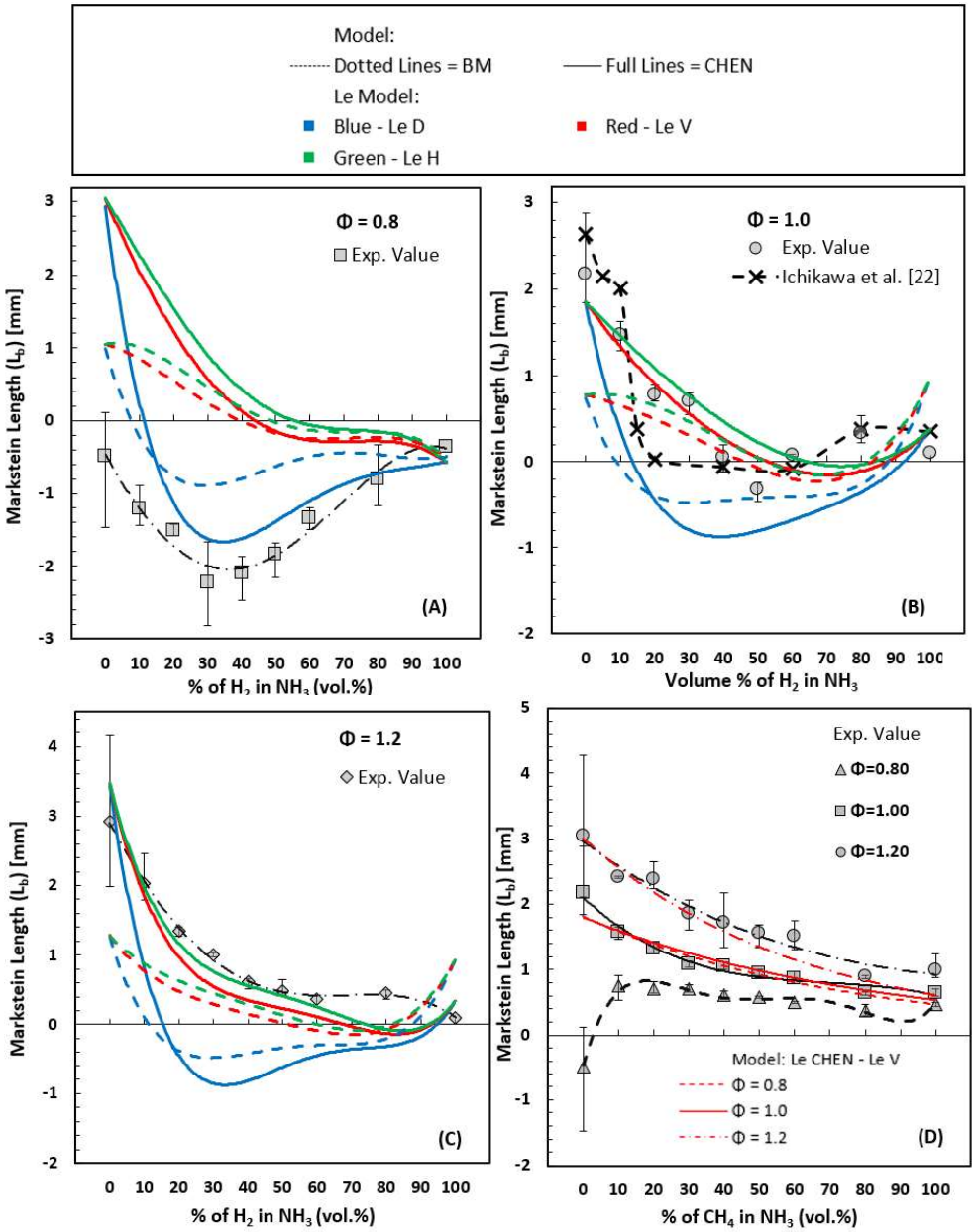

Figure 10 – Comparison of L_b-CHEN and L_b-BM estimates to the measured L_b for NH_3/H_2 flames (a) ϕ = 0.8 (b) ϕ = 1.0 (c) ϕ = 1.2 and for (d) NH_3/CH_4 flames

Figure 10 illustrates L_b-CHEN and L_b-BM for NH_3/H_2 blends, alongside experimentally measured L_b values. With respect to the CHEN formulation under lean H_2 condition (ϕ = 0.8, Figure 10.a), quantitative and qualitative agreements are observed with Le_D formulation, with the non-linear stretch behaviour well captured. Under H_2 richer condition (ϕ = 1.2, Figure 11.c), Le_D overpredicts the influence of H_2 on NH_3 with better agreement observed with a Le_V or Le_H model better reflecting the measured trend. Poor agreement is observed with the BM formulation, with again a Le_D best reflecting expected stretch behaviour under lean conditions, and Le_H exhibiting better agreement at richer conditions. Considering that the Le_D model was derived from the modelling of lean turbulent CH_4/H_2 flames [27], as well as that lean CH_4/H_2 appear to display similar non-linear stretch behaviour [24] to that of lean NH_3/H_2 flames, a better agreement was expected. Furthermore, this influence is due to the assumption that the flame curvature is dominant, hence the local enrichment of the most diffusive fuel at the flames leading edge is predicted. This concept appears to be valid under lean conditions, since H_2 and

NH_3 have higher mass diffusivities than O_2. For richer conditions ($\phi \geq 1.0$), a model based on either volume or non-dimensional heat release appears to be more appropriate. With respect to NH_3/CH_4 flames, measured L_b and L_b-CHEN are compared in Figure 10.d for $\phi = 0.8 - 1.2$. It should be noted that since NH_3 and CH_4 display very similar preferential-diffusional behaviour (Le ~ 0.9 – 1.1), the application of either Le_{eff} models results in very similar values. Consequently, only the Le_V model is plotted on Figure 10.d. For the conditions greater than stoichiometry, a good quantitative and qualitative agreement is observed with the CHEN model, but under lean conditions, the CHEN model does not allow to verify the change from negative to positive L_b measured experimentally obtained upon 10% CH_4 addition to NH_3 (for only one equivalence ratio). In summary, for lean and rich NH_3/H_2 flames, the Le_D and Le_H formulation respectively, best captured changes in thermo-diffusive behaviour. With respect to NH_3/CH_4 flames, Le_V demonstrated the best agreement for all considered ϕ, with these conclusions maintained for the remainder of the analysis.

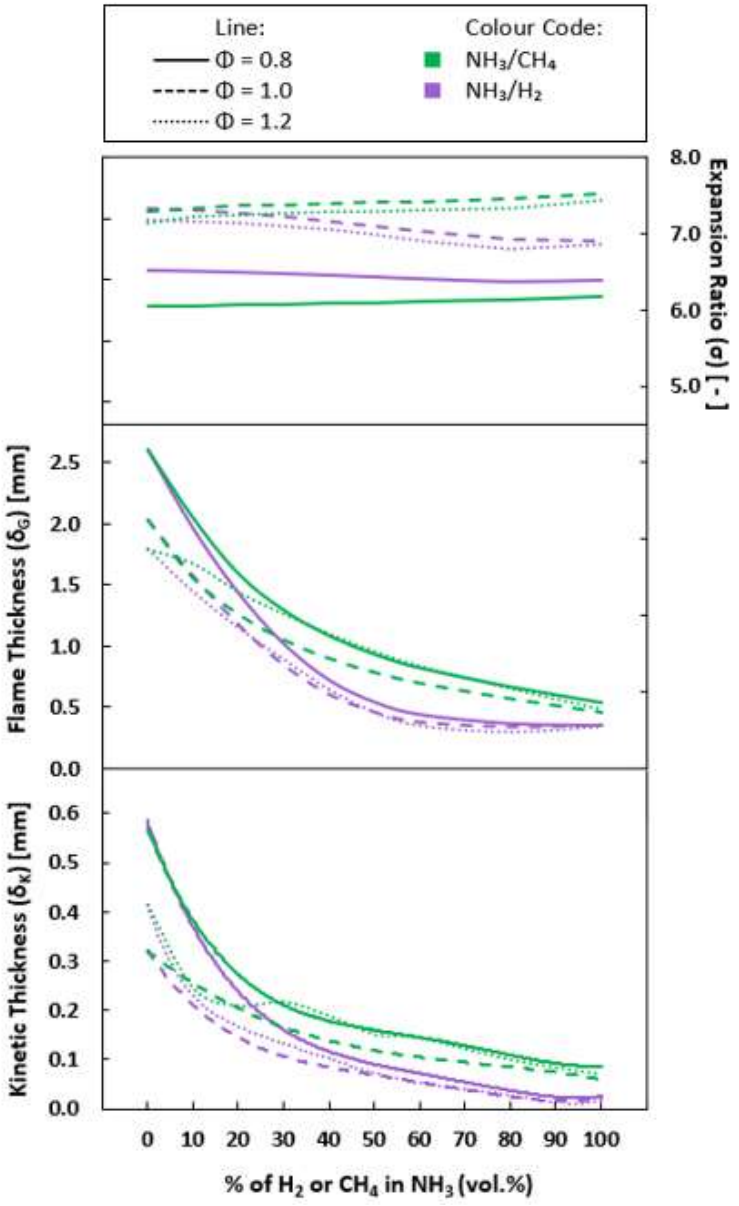

Figure 11 – Variation in δ_K, δ_G and σ with addition of either CH_4 or H_2 to NH_3, ϕ = 0.8, 1.0, 1.2

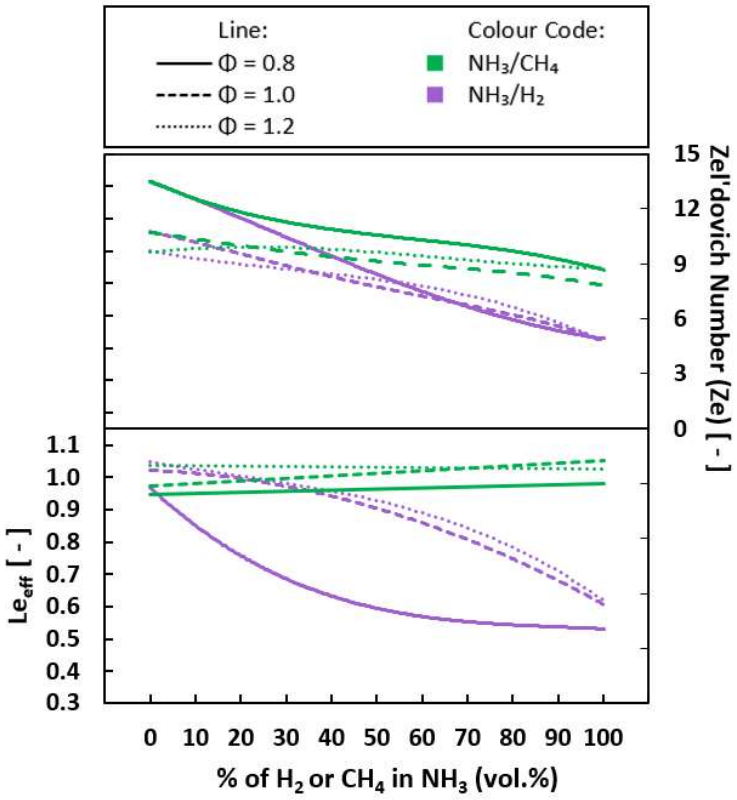

Figure 12 – Variation in Le_{eff} and Ze with addition of either CH_4 or H_2 to NH_3, ϕ = 0.8, 1.0, 1.2

As emphasised by Kwon et al. [82] and reviewed in [83], the fundamental parameters that induce hydrodynamic and diffusional-thermal instabilities are the thermal expansion, the flame thickness, the non-unity Le and the global activation energy (or equivalently Ze). Consistent with the hydrodynamic theory of Darrieus and Landau [9], the hydrodynamic instabilities arise from the thermal expansion of gases, with the density jump across the flame front proportional to the growth rate of hydrodynamic instability. In the case of an outwardly propagating spherical flame, the flame tends to be stabilised due to curvature induced positive stretch, consequently the flame thickness plays a significant role, since the thinner the flame the weaker the influence of curvature. Hence the risk of destabilisation is enhanced for thinner flames. It is interesting to note that addition of either CH_4 or H_2 to NH_3 does not really affect the thermal expansion, irrespective of ϕ, as shown in Figure 11. On the other hand, the flame thickness decreases strongly with increasing CH_4 or H_2 fractions, in effect promoting hydrodynamic instabilities to a similar extent. Nevertheless, the addition of either CH_4 or H_2 to NH_3 results in similar stretch-related behaviour under rich conditions, whilst exhibiting very different stretch-behaviour as conditions get leaner. The development of preferential-diffusional instabilities, characterised by Le, is the result of non-equi-diffusion. With respect to the NH_3/H_2 flames, the effects of preferential diffusion are a consequence of the higher mass diffusivity of H_2 and NH_3 compared to the O_2 molecule. As illustrated in Figure 12, Le decreases significantly with increasing H_2 fraction thereby promoting diffusional-thermal instabilities at ϕ = 0.8. Furthermore, as could be expected, the change in Le increases as the conditions get leaner, a consequence of each of the fuel's individual Le response. As underlined by Kwon et al. [82], considering that the development of preferential diffusional instabilities requires a modification of the flame front, it is thus reasonable to expect the global activation energy should also affect the development of diffusional-thermal instabilities. Accordingly, a lower E_a (illustrated as Ze in Figure 12) will tend to enhance instability of a diffusionally unstable flame such as lean NH_3/H_2 flame, with both Le and Ze decreasing with increasing H_2 concentration for all ϕ. The decrease in Ze is largely due to a decrease in the inner-layer temperature coupled with an increase in adiabatic flame temperature with increasing H_2 concentration for ϕ. For NH_3/H_2, the changes in measured L_b are thus potentially the result of competing hydrodynamic and thermo-diffusive instabilities, with the influence of the thermo-diffusional instabilities reducing as the ϕ increases. On the other hand, for NH_3/CH_4 flames, the addition of CH_4 to NH_3 results in little diffusional-thermal effects (Le ~ 1) across the entire considered ϕ range.

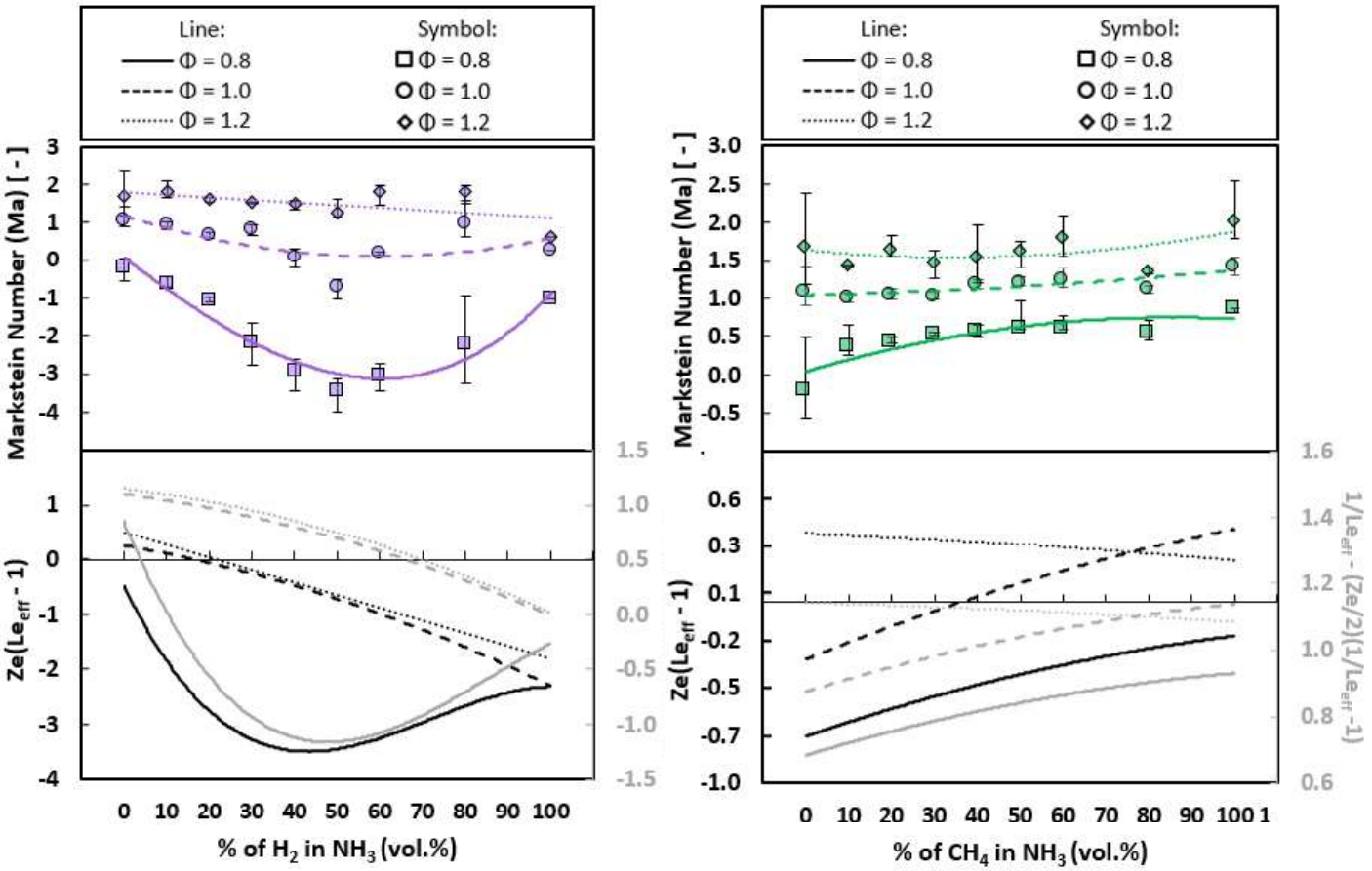

Figure 13 – Comparison of variation of $Ze(L_{eff} - 1)$ and $1/Le_{eff} - (Ze/2)(1/Le_{eff} - 1)$ to measured Marsktein number as a function of (a) H_2 mole fraction, and (b) CH_4 mole fraction

From the analytical expression developed by Chen [40], [45], the equation 9 can be re-arranged to yield the Marsktein Number ($Ma = L_b/\delta$), resulting in $Ma = [\ 1/Le_{eff} - (Ze/2)(1/Le - 1)]\sigma$, where $1/Le_{eff} - (Ze/2)(1/Le_{eff} - 1)$ represents the thermo-diffusive effect. Similarly, the relationship linking L_b to Le developed by Matalon and Bechtold (Equation 10) can be re-arranged to evaluate Ma, in which the term $Ze(L_{eff} - 1)$ reflects the thermo-diffusive influence as underlined by Okafor et al. [24]. Figures 13.a and 13.b compare the experimental Ma to the trends in $1/Le_{eff} - (Ze/2)(1/Le - 1)$ and $Ze(L_{eff} - 1)$, for NH_3/H_2 and NH_3/CH_4 mixtures, respectively, at $\phi = 0.8 - 1.0 - 1.2$. First, as expected both $Ze(L_{eff} - 1)$ and $1/Le_{eff} - (Ze/2)(1/Le - 1)$ exhibit the same trends. For the lean NH_3/H_2 mixtures, the changes in measured Ma appear to be to a great extent the result, of changes in the thermo-diffusive properties, Le and Ze. At richer condition, slightly different trends are displayed between the experimental Ma and $Ze(L_{eff} - 1)$ and $1/Le_{eff} - (Ze/2)(1/Le - 1)$, potentially due to a greater change in the expansion ratio (see Figures 12) than under lean conditions. In relation to the NH_3/CH_4 mixtures (Figure 13.b), the measured Ma under lean and stoichiometric conditions yield matching trends to $Ze(L_{eff} - 1)$ and $1/Le_{eff} - (Ze/2)(1/Le - 1)$, potentially alluding that the Le and Ze are the driving forces behind the changes in stretch-related behaviour. At $\phi = 1.2$, a less good agreement is observed, potentially the consequence of nominal changes in Le and Ze, combined with an increasing expansion ratio. For lean NH_3/H_2 flames it seems that the changes in measured L_b are to a large extent the consequence of thermo-diffusive effects, with this influence reducing as conditions get richer. For the NH_3/CH_4 mixtures, the competition between thermo-diffusional and hydrodynamic instabilities yields to increasingly positive Ma values, resulting in propensity of flame stabilisation.

5.3 Flame Sensitivity Analysis

The enhancement of the flame propagation due to the addition of CH_4 or H_2 to NH_3 can be characterised as a combination of diffusive, thermal and kinetic effects [84], [85]. The individual pathway can be modelled as:

$$S_L^0 \sim \left(D_T \cdot Le_{eff}\right)^{1/2} exp(-T_a/2T_{ad}) \quad (18)$$

The first term on the right-hand side $(D_T \cdot Le_{eff})$ reflects the diffusive influence. The Arrhenius factor, which combines the relative influence of the global activation energy through the activation temperature ($T_a = E_a/R_u$), and the adiabatic flame temperature are represented in the second term $[exp(-T_a/2T_{ad})]$. These individually represent the thermal (T_{ad}) and kinetic (T_a) influences on the flame speed. Concerning the Le formulation, it was previously determined from Figure 10 that for lean and rich NH_3/H_2 flames, the Le_D and Le_H formulation respectively, best captured changes in thermo-diffusive behaviour. With respect to NH_3/CH_4 flames, Le_V demonstrated the best agreement for all considered ϕ. These conclusions are maintained regardless of the theoretical relationship relating L_b to Le, and hence applied for the following analysis. Equation 18 may be differentiated to determine the sensitivity of each individual pathway on the overall influence of the flame speed. Accordingly, the overall sensitivity coefficient can be expressed as per Equation 19 [84]:

$$\frac{1}{S_L^0} \cdot \frac{dS_L^0}{dx} = \frac{1}{2 \cdot D_T \cdot Le} \cdot \frac{d(D_T \cdot Le)}{dx} - \frac{1}{2 \cdot T_{ad}} \cdot \frac{2 \cdot T_a}{dx} + \frac{T_a}{2 \cdot T_{ad}^2} \frac{2 \cdot T_{ad}}{dx} \quad (19)$$

where *x*, the volume fraction of either CH_4 or H_2. Note that the three terms on the right-hand side denote the influence of the diffusive, kinetic, and thermal pathways, correspondingly. Sensitivity analysis is illustrated in Figure 14 for the blends and ϕ considered, with a positive and negative sensitivity factor representing flame speed enhancement and inhibition, respectively.

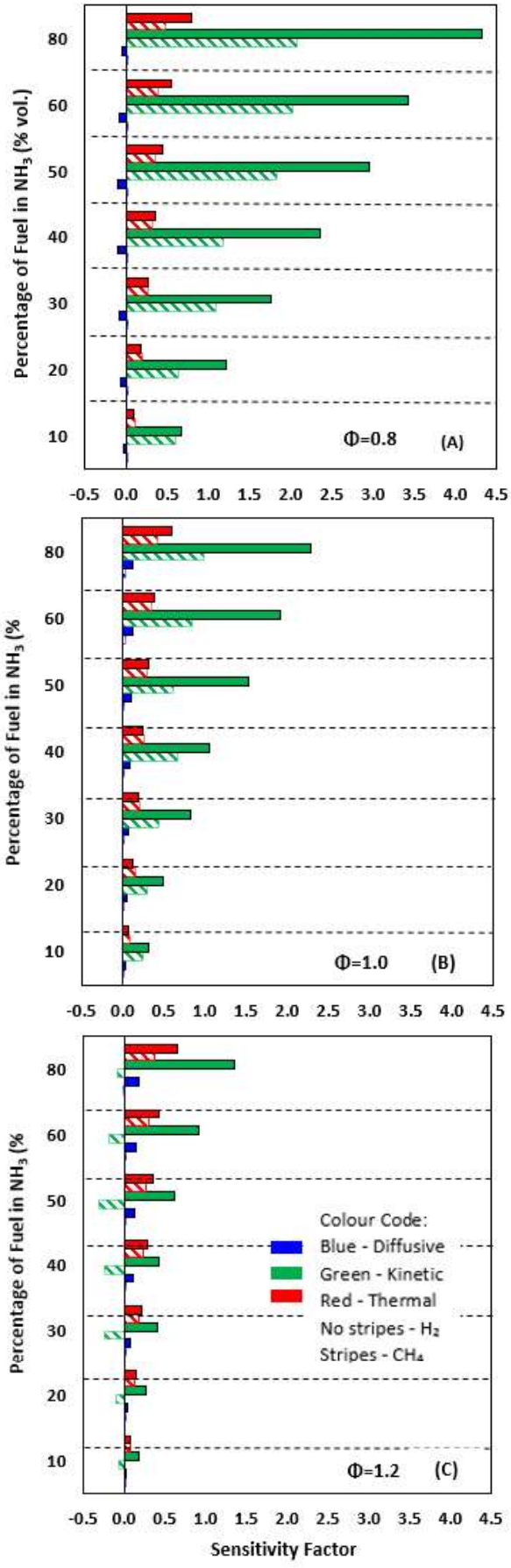

Figure 14 – Sensitivity Analysis of S_L^0 for NH_3/H_2 and NH_3/CH_4 blends, (a) ϕ = 0.8 (b) ϕ = 1.0 (c) ϕ = 1.2

As illustrated in Figure 14, the enhancement in flame speed of NH_3 based blends upon addition of either CH_4 or H_2 is predominantly an Arrhenius effect (kinetic), principally through the reduction of the overall activation energy and thus the activation temperature. For identical volumetric additions of up to 10% CH_4 or H_2 results in a similar reduction in E_a, leading to similar flame speeds, a trend well captured both experimentally and numerically. Any further addition of H_2 results in a significantly greater reduction in E_a than in the case of CH_4 addition, resulting in greater flame speeds. It should be noted that although remaining predominant for lean and stoichiometric conditions, the influence of the kinetic pathway reduces at richest conditions, particularly for CH_4 addition to NH_3, with a negative sensitivity at ϕ = 1.2. This agrees with the minor increase in E_a (represented by Ze, see Figure 12) at that condition, the consequence of the shifted minimum E_a to slightly richer conditions (ϕ = 1.1-1.2) of NH_3, as in Figure 3. The thermal pathway impact is lower than the kinetic effect, with the influence of the thermal pathway correlating well with modelled changes in adiabatic flame temperature. The addition of up to 60% of either CH_4 or H_2 results in changes of < 45 K, regardless of ϕ. With respect to the diffusive influence, it assumes negative sensitivity (or inhibiting effect) for lean NH_3/H_2 mixtures, and is negligible in comparison to other pathways. This is particularly the case for NH_3/CH_4, a consequence of the nominal changes in Le (Fig. 12) coupled with the limited change in thermal diffusivity of the mixture upon CH_4 addition, irrespective of the ϕ. It should be noted that even if the use of different kinetics mechanisms can induce different Arrhenius coefficients, the qualitative trends should remain valid, and thus performing such sensitivity analysis from first principles remains relevant providing useful insights.

6. Conclusions

The spherically expanding flame configuration was used to measure the unstretched laminar flame speeds and corresponding Markstein lengths in NH_3/H_2 and NH_3/CH_4 premixed flame across a wide range of compositions and equivalence ratio. A special attention was given to the estimate of Lewis number to analyse its influence on flame behaviour of NH_3, H_2 and CH_4 as well as for the blends. From this study, the following main outcomes can be made:

- Increasing H_2 and CH_4 fraction to NH_3-air laminar premixed flames results in an exponential and linear increase in flame speed, respectively. The greatest relative change in flame speed upon H_2 addition occurs under leanest and richest conditions while upon CH_4 addition, only under lean conditions. Stagni et al. and Okafor et al. mechanisms displayed the best agreement with experimental NH_3/H_2 and NH_3/CH_4 results, respectively.
- With respect to the stretch related behaviour, the addition of CH_4 to NH_3 results in a linear reduction in the stretch sensitivity for a fixed equivalence ratio. The volumetric based Lewis number yielded the best correlation with the measured Markstein lengths, for CH_4 addition to NH_3 resulting in nominal diffusional-thermal effects. For the stoichiometric and lean NH_3/H_2 flames, a non-monotonical variation in measured Markstein length was obtained, with a less and less linear behaviour as conditions get leaner. For NH_3/H_2, the changes in measured L_b were demonstrated to mainly be the result of thermo-diffusive effects (through the modelled changes in Le_{eff} and global activation energy) with the influence of the thermo-diffusional instabilities reducing as the equivalence ratio increases. For lean NH_3/H_2 mixtures, the diffusional-based Lewis number well captured the non-linear stretch behaviour as function of H_2 addition, whilst the heat release-based Lewis number resulted in better agreement at richer conditions.
- A sensitivity analysis related to the major flame enhancing pathways (diffusive, kinetic, thermal) has demonstrated that the enhanced flame propagation of NH_3/H_2 and NH_3/CH_4, is mainly due to the kinetic change, especially through the reduction of the activation temperature. The influence of the kinetic pathway reduces as conditions get richer,

particularly for CH_4 addition. The thermal pathway holds less influence in comparison to the kinetic pathway, with its influence showing good correlation with limited changes in adiabatic flame temperature of the considered blends. The diffusive pathway was negligible for all investigated mixtures, with a negative sensitivity for the lean NH_3/H_2 mixtures.

Declaration of Competing Interest

The authors declare that they have no known competing financial interest or personal relationships that could have appeared to influence the work reported in this paper.

Acknowledgements

This project has received funding from the European Union's Horizon 2020 Research and Innovation Program agreement No. 884157. http://flexnconfu.eu/

7. References

[1] T. Letcher, Climate Change: Observed Impacts on Planet Earth, 2nd ed., Elsevier, 2015.

[2] W. S. Chai, Y. Bao, P. Jin, G. Tang, L. Zhou, A review on ammonia, ammonia-hydrogen and ammonia-methane fuels, Renew. Sust. Energ. Rev. 147 (2021).

[3] H. Kobayashi, A. Hayakawa, K. A. Somarathne, E. C. Okafor, Science and technology of ammonia combustion, Proc. Combust. Inst. 37 109–133.

[4] N. A. Hussein, A. Valera-Medina, A. S. Alsaegh, Ammonia- hydrogen combustion in a swirl burner with reduction of NOx emissions, Enrgy. Proced. 158 (2019) 2305–2310.

[5] D. Pugh, J. Runyon, P. Bowen, A. Giles, A. Valera-Medina, R. Marsh, B. Goktepe, S. Hewlett., An investigation of ammonia primary flame combustor concepts for emissions reduction with OH*, NH2* and NH* chemiluminescence at elevated conditions, Proc. Combust. Inst. 38 (2021) 6451–6459.

[6] A. Hayakawa, Y. Arakawa, R. Mimoto, K. D. K. A. Somarathne, T. Kudo, H. Kobayashi, Experimental investigation of stabilization and emission characteristics of ammonia/air premixed flames in a swirl combustor, Int. J. Hydrogen Energy 42 (2017) 14010–14018.

[7] C. Lhuillier, P. Brequigny, F. Contino, C. Mounaïm-Rousselle, Experimental study on ammonia/hydrogen/air combustion in spark ignition engine conditions, Fuel 269 (2020) 117448.

[8] C. Lhuillier, P. Brequigny, F. Contino, C. Mounaïm-Rousselle, Experimental investigation on ammonia combustion behavior in a spark-ignition engine by means of laminar and turbulent expanding flames, Proc. Combust. Inst. 38 (2021) 6671–6678.

[9] C. K. Law, Combustion Physics, Cambridge: Cambridge University Press, 2006.

[10] C. K. Wu, C. K. Law, On the determination of laminar flame speeds from stretched flames, Symp. Combust. 20 (1985) 1941–1949.

[11] S. Ishizuka, C. K. Law, An experimental study on extinction and stability of stretched premixed flames, Symp. Combust. 19 (1982) 327–335.

[12] P. Clavin, Dynamic behavior of premixed flame fronts in laminar and turbulent flows, Prog.

Energy Combust. Sci. 11 (1985) 1–59.

[13] M. Matalon, On Flame Stretch, Combust. Sci. Technol. 31 (1983) 169–181.

[14] R. C. Aldredge, N. J. Killingsworth, Experimental evaluation of Markstein-number influence on thermoacoustic instability, Combust. Flame 137 (2004) 178–197.

[15] A. Hayakawa, T. Goto, R. Mimoto, Y. Arakawa, T. Kudo, H. Kobayashi, Laminar burning velocity and Markstein length of ammonia/air premixed flames at various pressures, Fuel 159 (2015) 98–106.

[16] R. Kanoshima, A. Hayakawa, T. Kudo, E.C. Okafor, S. Colson, A. Ichikawa, T. Kudo, H. Kobayahsi, Effects of initial mixture temperature and pressure on laminar burning velocity and Markstein length of ammonia/air premixed laminar flames, Fuel 310 (2022) 122149.

[17] E. C. Okafor, Y. Naito, S. Colson, A. Ichikawa, T. Kudo, A. Hayakawa, and H. Kobayashi, Experimental and numerical study of the laminar burning velocity of CH4–NH3–air premixed flames, Combust. Flame 187 (2018) 185–198.

[18] E. C. Okafor, Y. Naito, S. Colson, A. Ichikawa, T. Kudo, A. Hayakawa, H. Kobayashi, Measurement and modelling of the laminar burning velocity of methane-ammonia-air flames at high pressures using a reduced reaction mechanism, Combust. Flame 204 (2019) 162–175.

[19] T. Shu, Y. Xue, Z. Zhou, Z. Ren, An experimental study of laminar ammonia/methane/air premixed flames using expanding spherical flames, Fuel 290 (2021) 120003.

[20] J. H. Lee, S. I. Lee, O. C. Kwon, Effects of ammonia substitution on hydrogen/air flame propagation and emissions, Int. J. Hydrogen Energy 35 (2010) 11332–11341.

[21] J. H. Lee, J. H. Kim, J. H. Park, O. C. Kwon, Studies on properties of laminar premixed hydrogen-added ammonia/air flames for hydrogen production, Int. J. Hydrogen Energy 35 (2010) 1054–1064

[22] A. Ichikawa, A. Hayakawa, Y. Kitagawa, K. D. Kunkuma Amila Somarathne, T. Kudo, H. Kobayashi, Laminar burning velocity and Markstein length of ammonia/hydrogen/air premixed flames at elevated pressures, Int. J. Hydrogen Energy 40 (2015) 9570–9578.

[23] C. Lhuillier, P. Brequigny, N. Lamoureux, F. Contino, C. Mounaïm-Rousselle, Experimental investigation on laminar burning velocities of ammonia/hydrogen/air mixtures at elevated temperatures, Fuel 263 (2020) 116653.

[24] E. C. Okafor, A. Hayakawa, Y. Nagano, T. Kitagawa, Effects of hydrogen concentration on premixed laminar flames of hydrogen-methane-air, Int. J. Hydrogen Energy 39 (2014) 2409–2417.

[25] A. N. Lipatnikov, J. Chomiak, Molecular transport effects on turbulent flame propagation and structure, Prog. Energy Combust. Sci. 31 (2005) 1–73.

[26] S. P. R. Muppala, M. Nakahara, N. K. Aluri, H. Kido, J. X. Wen, M. V. Papalexandris, Experimental and analytical investigation of the turbulent burning velocity of two-component fuel mixtures of hydrogen, methane and propane, Int. J. Hydrogen Energy 34 (2009) 9258–9265.

[27] F. Dinkelacker, B. Manickam, S. P. R. Muppala, Modelling and simulation of lean premixed turbulent methane/hydrogen/air flames with an effective Lewis number approach, Combust. Flame 158 (2011) 1742–1749.

[28] M. Di Lorenzo, P. Brequigny, F. Foucher, C. Mounaim-Rousselle, Turbulent Flame Speed of a Gasoline surrogate in conditions representative of modern downsized Spark-Ignition engine,

Combust. Flame 240 (2022) 112041.

[29] J. B. Bell, R. K. Cheng, M. S. Day, I. G. Shepherd, Numerical simulation of Lewis number effects on lean premixed turbulent flames, Proc. Combust. Inst. 31 (2007) 1309–1317.

[30] N. Chakraborty, R. S. Cant, Effects of Lewis number on flame surface density transport in turbulent premixed combustion, Combust. Flame 158 (2011) 1768–1787.

[31] R. Ichimura, K. Hadi, N. Hashimoto, A. Hayakawa, H. Kobayashi, O. Fujita, Extinction limits of an ammonia/air flame propagating in a turbulent field, Fuel 246 (2019) 178–186.

[32] S. Zitouni, P. Brequigny, C. Mounaim-Rousselle, Turbulent Flame Speed and Morphology of Pure Ammonia flames and Blends with Methane or Hydrogen, Proc. Combust. Inst. (2022) doi: 10.1016/j.proci.2022.07.179.

[33] B. Galmiche, F. Halter, F. Foucher, Effects of high pressure, high temperature and dilution on laminar burning velocities and Markstein lengths of iso-octane/air mixtures, Combust. Flame 159 (2012) 3286–3299.

[34] S. Zitouni, D. Pugh, A. Crayford, P. J. Bowen, J. Runyon, Lewis number effects on lean premixed combustion characteristics of multi-component fuel blends, Combust. Flame 238 (2022) 111932.

[35] G. K. Giannakopoulos, A. Gatzoulis, C. E. Frouzakis, M. Matalon, A. G. Tomboulides, Consistent definitions of 'Flame Displacement Speed' and 'Markstein Length' for premixed flame propagation, Combust. Flame, 162 (2015) 1249–1264.

[36] P. Brequigny, F. Halter, C. Mounaïm-Rousselle, Lewis number and Markstein length effects on turbulent expanding flames in a spherical vessel, Exp. Therm. Fluid Sci. 73 (2016) 33–41.

[37] F. Wu, W. Liang, Z. Chen, Y. Ju, C. K. Law, Uncertainty in stretch extrapolation of laminar flame speed from expanding spherical flames, Proc. Combust. Inst. 35 (2015) 663–670.

[38] M. L. Frankel, G. I. Sivashinsky, On Effects Due To Thermal Expansion and Lewis Number in Spherical Flame Propagation, Combust. Sci. Technol. 31 (1983) 131–138.

[39] G. H. Markstein, Experimental and Theoretical Studies of Flame-Front Stability, J. Aeronaut. Sci. 18, (1951) 199–209.

[40] Z. Chen, On the extraction of laminar flame speed and Markstein length from outwardly propagating spherical flames, Combust. Flame, 158 (2011) 291–300.

[41] A. P. Kelley, C. K. Law, Nonlinear effects in the extraction of laminar flame speeds from expanding spherical flames, Combust. Flame 156 (2009) 1844–1851.

[42] F. Halter, T. Tahtouh, C. Mounaïm-Rousselle, Nonlinear effects of stretch on the flame front propagation, Combust. Flame 157 (2010) 1825–1832.

[43] A. Stagni, C. Cavallotti, S. Arunthanayothin, Y. Song, O. Herbinet, Fe. Battin-Leclerc, T. Faravelli, An experimental, theoretical and kinetic-modeling study of the gas-phase oxidation of ammonia, React. Chem. Eng. 5 (2020) 696–711.

[44] D. Bradley, P. H. Gaskell, X. J. Gu, Burning velocities, Markstein lengths, and flame quenching for spherical methane-air flames: A computational study, Combust. Flame 104 (1996) 176–198.

[45] Z. Chen, M. P. Burke, Y. Ju, Effects of Lewis number and ignition energy on the determination of laminar flame speed using propagating spherical flames, Proc. Combust. Inst. 32 (2009) 1253–1260.

[46] M. P. Burke, Z. Chen, Y. Ju, F. L. Dryer, Effect of cylindrical confinement on the determination of laminar flame speeds using outwardly propagating flames, Combust. Flame 156 (2009) 771–779.

[47] X. Chen, Q. Liu, Q. Jing, Z. Mou, Y. Shen, J. Huang, H. Ma, Flame front evolution and laminar flame parameter evaluation of buoyancy-affected ammonia/air flames, Int. J. Hydrogen Energy 46(2021) 38504–38518.

[48] S. Verhelst, R. Woolley, M. Lawes, R. Sierens, Laminar and unstable burning velocities and Markstein lengths of hydrogen-air mixtures at engine-like conditions, Proc. Combust. Inst. 30, (2005) 209–216.

[49] G. Jomaas, C. K. Law, J. K. Bechtold, On transition to cellularity in expanding spherical flames, J. Fluid Mech. 583 (2007) 1–26.

[50] Z. Chen, On the accuracy of laminar flame speeds measured from outwardly propagating spherical flames: Methane/air at normal temperature and pressure, Combust. Flame 162 (2015) 2442–2453.

[51] R. J. Moffat, Describing the uncertainties in experimental results, Exp. Therm. Fluid Sci. 1 (1988) 3–17.

[52] H. Yu, W. Han, J. Santner, X. Gou, C. Hoon Sohn, Y. Ju, Z. Chen, Radiation-induced uncertainty in laminar flame speed measured from propagating spherical flames, Combust. Flame 161 (2014) 2815–2824.

[53] J. K. Bechtold, M. Matalon, The dependence of the Markstein length on stoichiometry, Combust. Flame 127 (2001) 1906–1913.

[54] F. N. Egolfopoulos, C. K. Law, Chain mechanisms in the overall reaction orders in laminar flame propagation, Combust. Flame 80 (1990) 7–16.

[55] P. D. Ronney, G. I. Sivashinsky, A Theoretical Study of Propagation and Extinction of Nonsteady Spherical Flame Fronts, SIAM J. Appl. Math. 49 (1989) 1029–1046.

[56] N. Bouvet, F. Halter, C. Chauveau, Y. Yoon, On the effective Lewis number formulations for lean hydrogen/hydrocarbon/ air mixtures, Int. J. Hydrogen Energy 38 (2013) 5949–5960.

[57] D. Lapalme, R. Lemaire, P. Seers, Assessment of the method for calculating the Lewis number of H2/CO/CH4 mixtures and comparison with experimental results, Int. J. Hydrogen Energy 42 (2017) 8314–8328.

[58] S.E.M. Zitouni, Combustion Characteristics of Lean Premixed Methane/Higher Hydrocarbon/Hydrogen Flames, PhD Thesis, Cardiff University, 2020.

[59] C. K. Law, G. Jomaas, J. K. Bechtold, Cellular instabilities of expanding hydrogen/propane spherical flames at elevated pressures: Theory and experiment, Proc. Combust. Inst. 30 (2005) 159–167.

[60] C. Tang, Z. Huang, C. Jin, J. He, J. Wang, X. Wang, H. Miao, Laminar burning velocities and combustion characteristics of propane-hydrogen-air premixed flames, Int. J. Hydrogen Energy 33 (2008) 4906–4914.

[61] B. Poling, J. Prausnitz, J. O'Connell, The Properties of Gases and Liquids, 5th Ed., McGraw-Hill, 2001.

[62] D. F. Fairbanks, C. R. Wilke, Diffusion Coefficients in Multicomponent Gas Mixtures, Ind. Eng. Chem. 42 (1950) 471–475.

[63] D. Dandy, Transport Properties Calculator. https://navier.engr.colostate.edu/code/code-2/index.html (accessed Mar. 21, 2022).

[64] T.-H. Chung, L. L. Lee, K. E. Starling, Applications of kinetic gas theories and multiparameter correlation for prediction of dilute gas visosity and thermal conductivity, Ind. Eng. Chem. Fundam. (1984) 8–13.

[65] T.-H. Chung, M. Ajlan, L. L. Lee, K. E. Starling, Multiparameter Transport Correlation for Nonpolar and Polar Fluid Transport Properties, Ind. Eng. Chem Res. 27 (1988) 671–679.

[66] S. Mathur, P. Tondon, S. C. Saxena, Thermal conductivity of binary, ternary and quaternary mixtures of rare gases, Mol. Phys. 12 (1967) 569–579.

[67] E. Hu, Z. Huang, J. He, H. Miao, Experimental and numerical study on laminar burning velocities and flame instabilities of hydrogen-air mixtures at elevated pressures and temperatures, Int. J. Hydrogen Energy 34 (2009) 8741–8755.

[68] T. Tahtouh, F. Halter, C. Mounaïm-Rousselle, Measurement of laminar burning speeds and Markstein lengths using a novel methodology, Combust. Flame 156 (2009) 1735–1743.

[69] W. Lowry, J. de Vries, M. Krejci, E. Petersen, Z. Serinyel, W. Metcalfe, H. Curran, G. Bourque, Laminar flame speed measurements and modeling of pure alkanes and alkane blends at elevated pressures, J. Eng. Gas Turbines Power 133 (2011) 1–9.

[70] C. Lhuillier, Experimental and numerical investigation for the use of ammonia as hydrogen-carrying fuel for spark- ignition engines, PhD Thesis, University of Orleans and Vrije Universiteit Brussel, 2020.

[71] X. Han, Z. Wang, M. Costa, Z. Sun, Y. He, K. Cen, Experimental and kinetic modeling study of laminar burning velocities of NH3/air, NH3/H2/air, NH3/CO/air and NH3/CH4/air premixed flames, Combust. Flame 206 (219) 214–226.

[72] B. Mei, X. Zhang, S. Ma, M. Cui, H. Guo, Z. Cao, Y. Li, Experimental and kinetic modeling investigation on the laminar flame propagation of ammonia under oxygen enrichment and elevated pressure conditions, Combust. Flame 210 (2019) 236–246.

[73] K. Takizawa, A. Takahashi, K. Tokuhashi, S. Kondo, A. Sekiya, Burning velocity measurements of nitrogen-containing compounds, J. Hazard. Mater. 155 (2008) 144–152.

[74] W. Han, P. Dai, X. Gou, Z. Chen, A review of laminar flame speeds of hydrogen and syngas measured from propagating spherical flames, Appl. Energy Combust. Sci. 1–4 (2020).

[75] X. J. Gu, M. Z. Haq, M. Lawes, R. Woolley, Laminar burning velocity and Markstein lengths of methane-air mixtures, Combust. Flame 121 (2000) 41–58.

[76] C. K. Law, C. J. Sung, Structure, aerodynamics, and geometry of premixed flamelets, Prog. Energy Combust. Sci. 26,(2000) 459–505.

[77] Z. Tian, L. Zhang, Y. Li, T. Yuan, F. Qi, An experimental and kinetic modeling study of a premixed nitromethane flame at low pressure, Proc. Combust. Inst. 32(2009) 311–318.

[78] K. P. Shrestha, L. Seidel, T. Zeuch, F. Mauss, Detailed Kinetic Mechanism for the Oxidation of Ammonia Including the Formation and Reduction of Nitrogen Oxides, Energy and Fuels 32 (2018) 10202–10217.

[79] G. J. Gotama, A. Hayakawa, E.C. Okafor, R. Kanoshima, M. Hayashi, T. Kudo, H. Kobayashi, Measurement of the laminar burning velocity and kinetics study of the importance of the hydrogen recovery mechanism of ammonia/hydrogen/air premixed flames, Combust. Flame

236 (2022) 111753.

[80] S. Zitouni, S. Mashruk, N. Mukundakumar, P. Brequigny, A. Zayoud, E. Pucci, S. Macchiavello, F. Contino, C. Rousselle, R. Bastiaans, A. Valera-Medina, Ammonia Blended Fuels-Energy Solutions for a Green Future, 10th Int. Gas Turbine Conf. IGTC21-62 (2021) [Online] Available: https://hal.archives-ouvertes.fr/hal-03519203.

[81] Z. Huang, Y. Zhang, K. Zeng, B. Liu, Q. Wang, D. Jiang, Measurements of laminar burning velocities for natural gas-hydrogen-air mixtures, Combust. Flame 146 (2006) 302–311.

[82] O. C. Kwon, G. Rozenchan, C. K. Law, Cellular instabilities and self-acceleration of outwardly propagating spherical flames, Proc. Combust. Inst. 29 (2002) 1775–1783.

[83] F. Oppong, Z. Luo, X. Li, Y. Song, C. Xu, Intrinsic instability of different fuels spherically expanding flames: A review, Fuel Process. Technol. 234 (2022) 107325.

[84] S. Ravi, T. G. Sikes, A. Morones, C. L. Keesee, E. L. Petersen, Comparative study on the laminar flame speed enhancement of methane with ethane and ethylene addition, Proc. Combust. Inst. 35 (2015) 679–686.

[85] C. L. Tang, Z. H. Huang, C. K. Law, Determination, correlation, and mechanistic interpretation of effects of hydrogen addition on laminar flame speeds of hydrocarbon-air mixtures, Proc. Combust. Inst. 33 (2011) 921–928.